PLK1 AS A PROMISING TARGET IN THE CANCER TREATMENT

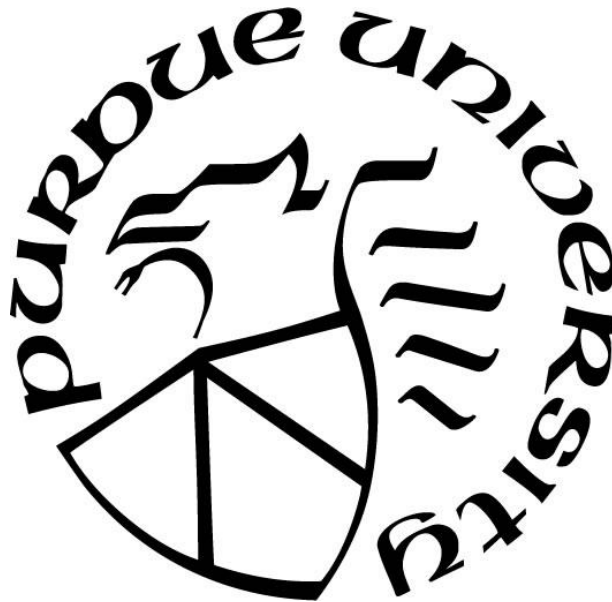by

Fengyi Mao

A Dissertation

Submitted to the Faculty of Purdue University

In Partial Fulfillment of the Requirements for the degree of

Doctor of Philosophy

Animal Sciences

West Lafayette, Indiana

December 2020

THE PURDUE UNIVERSITY GRADUATE SCHOOL
STATEMENT OF COMMITTEE APPROVAL

Dr. Shihuan Kuang, Chair

College of Agriculture

Dr. Xiaoqi Liu

College of Medicine, University of Kentucky

Dr. Ourania M. Andrisani

College of Veterinary Medicine

Dr. Ryan Cabot

College of Agriculture

Approved by:

Dr. Zoltan Machaty

Dedicated to my parents

ACKNOWLEDGMENTS

Firstly, I would like to express my sincere gratitude to my advisor Dr. Xiaoqi Liu, for his continuous support of my study and research, for his education, patience, and motivation. His guidance helped me all the time during my study, and none of these would achieve without his mentoring.

I also want to express my great appreciation to Dr. Shihuan Kuang for his generous support and guidance. Without his help and recommendation, it would be impossible for me to start my Ph.D. study at Purdue, and my research would be much tougher as well.

I would like to thank my thesis committee: Dr. Ourania M. Andrisani and Dr. Ryan Cabot, for their insightful comments and encouragement, also for their advice to widen my research from various perspectives.

My thankfulness is also to my fellow labmates for the stimulating discussions, patient and generous help, and all the fun we have had in the last five years.

Last but not the least, I would like to thank my parents for their support throughout my life.

TABLE OF CONTENTS

LIST OF TABLES

LIST OF FIGURES

LIST OF ABBREVIATIONS

2-NBDG:	2-(N-(7-Nitrobenz-2-oxa-1,3-diazol-4-yl)Amino)-2-Deoxyglucose)
53BP1:	P53-Binding Protein 1
ADT:	Androgen Deprivation Therapy
APC/C:	Anaphase-Promoting Complex
AR:	Androgen Receptor
ATM:	Ataxia Telangiectasia Mutated
ATR:	Ataxia Telangiectasia And Rad3-Related Protein
BET:	Bromodomain And Extraterminal Domain
BRCA1:	Breast Cancer Type 1 Susceptibility Protein
BRD4:	Bromodomain-Containing Protein 4
Cdc25C:	Cell Division Cycle 25c
CDE/CHR:	Cell Cycle-Dependent Element/Cell Cycle Genes Homology Region
CDF-1:	CDE-CHR Binding Factor-1
CDK1:	Cyclin-Dependent Kinase 1
CEP55:	Centrosomal Protein Of 55 kDa
Chfr:	Checkpoint With Forkhead And Ring Finger Domains
CHIP:	C-Terminal Hsc70-Interacting Protein
CHK1:	Checkpoint Kinase 1
CHK2:	Checkpoint Kinase 2
C-Nap1:	Centrosomal Nek2-Associated Protein 1
CRPC:	Castration-Resistant Prostate Cancer
CUL3:	Cullin 3

KLHL22:   Kelch Like Family Member 22

DAPI: 4′,6-diamidino-2-phenylindole

DMEM: Dulbecco's Modified Eagle's Medium

DREAM complex: Dimerization Partner, RB-Like, E2F And Multi-Vulval Class B

E2F1:   E2F Transcription Factor 1

E2F3:   E2F Transcription Factor 3

E2F4:   E2F Transcription Factor 4

EMI1:   Early Mitotic Inhibitor 1

FKH-TFs: Forkhead Transcription Factors

FoxM1:   Forkhead Box M1

FRET: Fluorescence Resonance Energy Transfer

GTSE1:   G2 And S-Phase-Expressed 1

HR: Homologous Recombination

IDL: Interdomina Linker

KD: Kinase Domain

KT-MT: Kinetochore–Microtubule

MCC: Mitotic Checkpoint Complex

MKLP2:   Mitotic Kinesin-Like Protein2

MMB complex: Myb-Muvb Complex

MPS1:   Monopolar Spindle 1

Mst2:   Serine/Threonine Kinase 3

MTT: 3-(4,5-dimethylthiazol-2-yl)-2,5-diphenyltetrazolium bromide

MYPT1:   Myosin Phosphatase Target Subunit 1

NEBD: Nuclear Envelope Breakdown

Nek2A:	NIMA Related Kinase 2
NF-Y/CBF:	CCAAT-Binding Factor
NFκB:	Nuclear Factor Kappa-Light-Chain-Enhancer Of Activated B Cells
NLP:	Ninein-Like Protein
NUDC:	Nuclear Distribution Gene C
PBD:	Polo-Box Domain
PCa:	Prostate Cancer
PDX:	Patient-Derived Xenograft
PI:	Propidium Iodide
PLK1:	Polo-like Kinase 1
PP1B:	Protein Phosphatase 1 Catalytic Subunit Beta
PP1C:	Protein Phosphatase 1 Catalytic Subunit Gamma
PP2A:	Protein Phosphatase 2 Phosphatase Activator
PRC1:	Protein Regulator Of Cytokinesis 1
RB:	Retinoblastoma Tumor Suppressor
RSF1:	Remodeling And Spacing Factor 1
SAC:	Spindle Assembly Checkpoint
Sas-4:	Spindle Assembly Abnormal 4
SP-1:	Specificity Protein 1
SUMOs:	Small Ubiquitin-like Modifiers
TCF3:	Transcription Factor 3
Topors:	Topoisomerase I-Binding Protein
USP16:	Ubiquitin Specific Peptidase 16
γ-TuRCs:	γ-Tubulin Ring Complexes

ABSTRACT

Polo-like kinase 1 (PLK1) is a critical cell cycle regulator and overexpressed in multiple cancer types. As previously reported, PLK1 is tightly related to patient survival and cancer progression. Prostate cancer (PCa) is the most frequently diagnosed cancer in men and the second leading cause of cancer-associated death in the US. Once PCa patients develop resistance toward initial androgen deprivation therapy (ADT), the castration-resistant prostate cancer (CRPC) will occur and become lethal. Thus, a novel therapeutic strategy to treat CRPC patients is urgently required. Herein, we have identified a novel combination therapy that PLK1 inhibitor GSK461364A and BRD4 inhibitor JQ1 cooperate to treat CRPC both *in vitro* and *in vivo*. GSK461364A and JQ1 act synergistically to inhibit cell proliferation and induce cell apoptosis through regulating c-MYC and AR signaling and dramatically impact cell metabolism as well.

Furthermore, the progression of malignant melanoma, the most aggressive and deadly skin cancers, also firmly correlates with the PLK1 expression level in patients. In this study, we have utilized the mouse melanoma model $Braf^{CA/+} / Pten^{loxp/loxp}$ to investigate the role of Plk1 in melanoma progression and metastasis. Elevated expression of *Plk1* significantly shortened the survival period, promoted proliferation, induced metastasis, and impacted metabolism in mouse melanoma models. Intriguingly, PLK1 also contributes to the drug resistance toward PLX-4032, which is the FDA-approved drug to treat metastatic melanoma patients harboring BRAF V600E mutation. Therefore, the efficacy of combining PLX-4032 and PLK1 inhibitor BI6727 has been tested in human melanoma cell lines and the xenograft model, showing a strong synergy between the two drugs. To conclude, we have demonstrated that PLK1 functions as an oncogene in cancer development, and targeting PLK1 would be a promising therapeutic strategy in clinic.

CHAPTER. 1   PLK1, FUNCTION IN MITOSIS

1.1   Introduction

The polo-like kinase (PLK) was first discovered in *Drosophila* in 1988, and its essential role in regulating cell division has been well demonstrated since then (1, 2). Currently, five members of the PLK family (PLK1-PLK5) have been investigated in human, which function as serine-threonine kinases to regulate multiple intracellular processes, such as DNA replication, mitosis, and DNA damage response (3, 4). PLK1 is the best-studied family member, involving in DNA damage response and cell cycle progression (5, 6). PLK1 harbors two structural domains, the polo-box domain (PBD), related to substrates binding and subcellular distribution, and the kinase domain (KD), which could be regulated by upstream activating kinases (7-9). Because of its crucial role in mitosis, the expression and activity of PLK1 are precisely and tightly controlled throughout the whole cell cycle. It has been well established that PLK1 is low in interphase, gradually increases during S and G2 phase, and reaches a peak during mitosis, which is conserved with the cell cycle progression (10-13). Notably, PLK1 overexpresses in cancerous tissues and associates with the survival of cancer patients in numerous cancer types, including lung cancer, breast cancer, liver cancer, colon cancer, stomach cancer, and melanoma (14). The disease-free survival and overall survival period remarkably shorten in patients with higher PLK1 expression level, in comparison to those with lower expression of PLK1, suggesting PLK1 as a potential and promising target for cancer therapy (14). In this review, we will briefly discuss how PLK1 is regulated in both mRNA and protein levels during the cell cycle. The biological roles of PLK1 in cell cycle progression and DNA damage will be introduced as well.

1.2   Regulating PLK1 in cell cycle

1.2.1   Transcriptional regulation

It has been well established that the promoter region of Plk1, located 5' to the translation start site, is sufficient and crucial for mouse and human Plk1 expression (13, 15, 16). There are three positive regulatory elements found between nucleotides -35 and -95, which could significantly induce Plk1 expression during G2/M (16). Based on the consensus sequence motifs, several transcription

factors have been identified to regulate Plk1 during the cell cycle, containing TCF3, AP1, AP2, SP-1, NF-Y/CBF, NFκB (15), E2F1 (17), and E2F3 as well (18). Moreover, FKH-TFs (forkhead transcription factors), regulators of the mitotic program, could also bind directly to the Plk1 promoter *in vivo* and lead to its activation (19). Most importantly, Forkhead Box M1 (FoxM1) could dramatically stimulate Plk1 in a G2-specific manner (20), thus contributing to a cell-cycle dependent regulation of Plk1. In agreement, the deletion of FoxM1 or Plk1 in cells will result in similar pleiotropic mitotic defects, exhibiting unstable chromosome and inaccurate chromosome segregation (20, 21).

Compared to the transcriptional activation, the repression of Plk1 in the cell cycle is better studied. A bipartite repressor element, termed as CDE/CHR (cell cycle-dependent element/cell cycle genes homology region), has been identified as a crucial factor in the Plk1 repression (16). The CDE/CHR element is a central regulator in cell cycle progression and presents at the promoter region of other G2/M related genes as well, including cyclin B1, cyclin A, CDK1, Aurora A, or Cdc25C (22, 23). The mutations in the CDE/CHR element could dramatically diminish the cell cycle-specific regulation of the Plk1 transcription (16). Several transcription factors have been demonstrated to mediate the activity of CDE/CHR element, such as CDF-1 (CDE-CHR binding factor-1) (24), the DREAM (DP, RB-like, E2F4, and MuvB) complex (25), and the MMB (Myb-MuvB) complex (25). Besides, RB and its related pocket proteins p107/p130 have been reported to suppress the expression of Plk1 (26). E2F4 cooperates with p107/p130 and recruits SWI/SNF complex to the Plk1 promoter region, thus leading to the histone deacetylation and gene repression (26). Furthermore, due to the role of PLK1 in the DNA damage response, PLK1 is tightly regulated by the DNA damage repair signaling pathway. DNA damage activates cell cycle checkpoints and allows DNA repair before mitotic entry through ATM, ATR, and their downstream CHK1 and CHK2 kinase (27-29), leading to the inhibition of Plk1 activity via both transcriptional regulation and protein modification (30, 31). BRCA1 and its downstream CHK1 have been proven as a suppressor of Plk1 expression after ionizing radiation in breast cancer (32). Most importantly, p53 could suppress Plk1 expression either by directly binding to the Plk1 promoter (33) or through its downstream p21 (34). In response to DNA damage, p53 could bind to the Plk1 promoter region, then recruit histone deacetylases to inhibit Plk1 expression (33). In parallel, as a mediator of the p53 repressive function, p21 could promote the switch from the MMB complex to the DREAM

complex on the CHR element of the Plk1 promoter to block its transcription (34, 35). Moreover, p53 also inhibits the transcription activity of FOXM1 and E2F1, thereby further diminish the transcription of PLK1 (36, 37).

Along with the development of epigenetics, it has been revealed that the modification of DNA and histones tightly correlates with cell cycle regulation (38). According to the previous publications, the methylation status in PLK1's promoter region varies in response to the environmental stimulus in cancer cells (39, 40). However, the knowledge of how PLK1 is modulated by the epigenetic network at the transcription level is still limited and requires further investigation.

1.2.2 Post-translational regulation

Based on the biochemical studies, the PBD of PLK1 binds to its KD, thus inhibits its catalytic activity (41, 42). Deletion or mutations of PBD could dramatically increase the activity of KD during the G2 phase, suggesting the autoinhibitory machinery in the regulation of PLK1 activity (41, 42). Later, its autoinhibitory state has been further understood and confirmed through analyzing the crystal structure of zPlk1. The binding of PBD and KD could either reduce the flexibility of the hinge region or sequestrate the activation loop, leading to the inhibition of kinase activity (43).

In contrast, the phosphorylation of T210 or S137 by Aurora A/Bora and other activating kinases could interrupt the intermolecular interaction and fully activate PLK1 during mitosis (9, 43-45). During mitosis, mass spectrometry analysis has identified T210 as a main post-translational modification of PLK1 (9, 46, 47), which has been considered as the first step to initiate PLK1's activity (48). Compared to wild type PLK1, the substitution of aspartate for T210 results in constitutive activation, while the replacement of alanine or valine reduces its activity significantly (47, 48). It has been well established that Aurora A cooperates with Bora to control the G2/M transition and mitotic entry, as well as activate PLK1 in the G2 phase (44, 45). Bora, as a known cofactor of Aurora A, binds directly to PLK1 and increases the accessibility of the activation loop on PLK1, thus facilitates Aurora A to phosphorylate T210 before mitotic entry (44, 45). Although Aurora A and Bora accumulate in the late G2 phase, they degrade and decrease drastically by proteasomes in mitosis, leaving the question of how PLK1 remains activated during mitosis (49,

50). A study has demonstrated that once PLK1 is fully activated, minimal amounts of Aurora A/Bora complex could maintain PLK1's activity until the end of mitosis (49). Interestingly, during mitosis, the proteolysis of Bora requires phosphorylation by PLK1, which could enhance its interaction with SCF-β-TrCP and promote degradation (50). Once the PLK1 phosphorylation site is mutated, Bora would be stabilized in the mitosis, leading to prolonged metaphase and delayed anaphase in cell division (50). Apart from T210, phosphorylation at S137 is another important post-translational modification found in PLK1, regarded as the prerequisite for the appropriate mitotic progression. Unlike T210, the phosphorylation of S137 occurs in late mitosis (51). Expression of S137D in cells results in improper activation of APC/C (anaphase-promoting complex) and eventually leads to mitotic catastrophe (51). However, further investigation is indispensable to validate and understand the role of S137 in PLK1's function. Moreover, Pak1 (p21-Activated kinase1) has been reported to phosphorylate PLK1 at S49, which is essential for the establishment of a functional bipolar spindle and maintenance of proper spindle tension (52). Besides, another study based on mass spectrometry has identified additional phosphorylation sites on the catalytic domain of PLK1 showing a robust induction during mitosis, while the regulator and function of which are still unclear (46). Distinct from phosphorylation, the study of how phosphatases control PLK1 spatiotemporal activity is limited. MYPT1/PP1C and MYPT1/PP1β could bind to PLK1 to diminish its phosphorylation at T210, thus tightly control PLK's activity during mitosis as previously demonstrated (53, 54). Besides, cyclin A/ CDK1 could negatively modulate the activity of PLK1 in prometaphase by priming its binding with MYPT1, which destabilizes the KT-MT attachment and ensures faithful chromosome segregation (55). Moreover, PP2A binding with different regulatory subunits could dephosphorylate PLK1 in distinct stages and exhibit divergent effects. PP2A / B56 regulates PLK1 to maintain the balance of kinetochore-microtubule attachments during mitosis (56), whereas PP2A/B55α associates with PLK1 to regulate checkpoint recovery after DNA damage (57).

Similar to phosphorylation, ubiquitination is a reversible protein modification to regulate the spatially and temporally activity of PLK1 (58). During the G2/M transition, PLK1 would be ubiquitinated by the checkpoint protein Chfr and finally subject to degradation under the mitotic stress, therefore prevent Cdc25C from activation and delay the mitotic entry (59). On the contrary, once cells proceed to normal G2/M transition, USP16 (ubiquitin-specific peptidase 16) would

deubiquitinate PLK1 to ensure its recruitment and activity on kinetochores. Consequently, proper kinetochore-microtubule (KT-MT) attachment and accurate chromosome alignment could be established and guaranteed in the metaphase (60). Interestingly, cullin3 (CUL3) based E3 ligase antagonizes to USP16 and contributes to PLK1's dynamic cellular localization instead of degradation (61). Once the chromosome is properly aligned, CUL3/KLHL22 ubiquitinates K492 at PBD of PLK1 and disassociates PLK1 from kinetochores, thus satisfies the spindle assembly checkpoint (SAC) and promotes mitotic progression (61). Most importantly, PLK1's expression and activity maintain high in the early mitosis, however, PLK1 has to go through proteolysis in anaphase to ensure successful cytokinesis and proper mitotic exit (62). It is well established that APC/C, an E3 ligase of diverse mitotic proteins, also contributes to the proteolysis of PLK1 in anaphase (62, 63). Cdc20 binds with APC/C to initiate mitotic exit by targeting mitotic proteins containing a destruction box (D box), such as securin (64, 65). Hereafter, Cdc20 is degraded by itself and substituted by Cdh1, through which APC/C gains a broader specificity toward mitotic protein (63, 65). PLK1 contains a conserved RxxL D-box-like motif that could be recognized and ubiquitinated by APC/C^{Cdh1}. Subsequently, PLK1 goes through proteasome degradation to achieve a proper mitotic exit eventually (62, 66). Moreover, CHIP (C-terminal Hsc70-interacting protein) is also reported as an E3 ligase to modulate PLK1's homeostasis during mitosis in prostate cancer (67).

Recently, innovative post-translational modifications of PLK1, other than phosphorylation and ubiquitination, have also been revealed. After phosphorylation and activation by CDK1/cyclin B1, SUMO-conjugating enzyme UBC9 interacts with PLK1 to conjugates SUMOs (small ubiquitin-like modifiers) (68). This SUMOylation of PLK1 enhances its nuclear translocation and prevents it from proteasome degradation (68). Besides, SUMO-1 could regulate PLK1in microtubules and the spindle pore, while SUMO-2/3 is related to PLK1's localization on kinetochores, as reported recently (69). Moreover, monomethylation at K209 by methyltransferase G9a silences PLK1 through antagonizing T210 phosphorylation under DNA damage stress (70). PLK1 with methyl-deficient K209A mutant results in defects in DNA damage repair and DNA replication, whereas cells with methyl-mimic K209M mutant PLK1 exhibit prolonged metaphase-to-anaphase transition due to the improper separation of the chromosome (70). Furthermore, SET7/9 could

suppress PLK1 kinase activity through methylation of PLK1 at K191 in early mitosis, promoting a dynamic attachment of KT-MT for error correction (71).

1.3 PLK1's Biological Function

1.3.1 PLK1 in cell cycle

PLK1 is a well-known cell cycle regulating kinase and plays a vital role in regulating cell division. Collective data have demonstrated that PLK1 is critical for the early development of mouse embryos, the complete depletion of which causes extensive mitotic aberrations and embryonic lethal (72, 73). Pre-clinical studies have revealed that PLK1 participates in multiple cell-cycle related processes, involving mitotic entry, centrosome maturation, spindle assembly, chromosome aggregation, and cytokinesis (74).

1.3.1.1 *PLK1 with CDK1/cyclin B1*

It is well established that the activity of the CDK1/cyclin B1 complex is crucial for the G2/M transition and is precisely mediated by a protein network to ensure the appropriate commitment to a mitotic state (75). Intriguingly, CDK1-mediated phosphorylation can not only directly regulate the stability and activity of its substrate but may provide a docking site of PBD to prime the further phosphorylation by PLK1 (76, 77). At the onset of mitosis, Wee1, the CDK1 inhibitory kinase, could be phosphorylated by CDK1 and PLK1 at S123 and S53 separately to generate a phosphor-degron (78). As a consequence, Wee 1 is recognized and ubiquitinated by β-TrCP to degradation, leading to the rapid activation of CDK1 (78). Similarly, the Myt1-mediated inhibition toward CDK1 would diminish once dual-phosphorylated by CDK1 and PLK1 (79, 80). In parallel, PLK1-dependent phosphorylation of Cdc25c enhances its translocation to the nucleus, thus dephosphorylating and activating in CDK1 during the prophase (81). Besides, PLK1 phosphorylates cyclin B1 during prophase to stimulate its rapid nuclear entry (82, 83). Moreover, FOXM1, function as a master transcriptional factor of multiple mitotic genes including cyclin B1 and PLK1 itself, is also demonstrated as a substrate of PLK1, which would dramatically enhance its transcriptional activity and promote mitotic progression (84).

1.3.1.2 *PLK1* at *centrosomes*

In the G2 phase, PLK1 is recruited by Gravin to localize at the centrosomes, a prerequisite for the formation of mature centrosomes (85, 86). Henceforward, the pericentriolar matrix (PCM) of centrosomes undergoes a dramatic expansion to organize spindle microtubules in advance of the formation of a bipolar spindle (87). Ninein-like protein (NLP) plays a crucial role in microtubule organization and interacts with γ-tubulin ring complexes (γ-TuRCs) to stimulate microtubule nucleation (88). Once phosphorylated by PLK1, NLP fails to associate with either centrosomes or γ-tubulin, thus grants the proper establishment of the mitotic spindle (88). In parallel, PLK1 phosphorylates Pericentrin (PCNT) to initiate the centrosomes maturation, enhance recruitment of centrosomal proteins, and ensure fidelity of centriole separation as well (89, 90). Recently, Sas-4 is identified as a novel PLK1 substrate in *Drosophila*, related to the expansion of PCM (91). At the onset of mitosis, the phosphorylation of PLK1 is essential for Sas-4 to recruit γ-tubulin and Cnn and enable its localization to expand outward from the centrosome (91).

Except for centrosome maturation, PLK1 also participates in the centrosome disjunction and separation during late G2/prophase (6). PLK1-dependent phosphorylation of Mst2 could enhance the activity of its downstream Nek2A to remove C-Nap1 and Rootletin from centrioles, consequently activating centrosome disjunction (92, 93). In addition, Kinesin family member 11 (KIF11), a key factor to drive apart duplicated centrosomes, is activated indirectly by PLK1 through Nek9 and Nek6/7 kinase cascade (94). Once centrosomes are separated, PLK1 contributes to the nuclear envelope breakdown (NEBD) via phosphorylating p150[Glued], to allow the interplay between chromosome and spindle (95). Furthermore, centrosomal PLK1 is a mediator of switching dynein/dynactin through regulating dynactin members and NuMA (nuclear mitotic apparatus protein 1) to establish a dictated mitotic spindle (96). Last but not least, the sequential phosphorylation of Aurora A and PLK1 stabilizes 53BP1 (p53-binding protein 1) to facilitate the maintenance of centrosome integrity (97).

1.3.1.3 *PLK1 at kinetochores*

Except for centrosomes, PLK1 locates at kinetochores and plays a crucial role in the regulation of KT-MT attachment (98). In the interphase and early mitosis, PLK1 binds with PBIB1 via PBD

and subsequently could be recruited to kinetochores (99). Intriguingly, PLK1 phosphorylates PBIB1 at T78 to induce its degradation at kinetochores, thereby enabling PLK1 to associate with other components (99). To maintain localization and function in kinetochores, PLK1 interacts with several scaffold proteins after PBIB1 degradation, including INCENP (inner centromere protein), BUB1 (benzimidazole 1), BUBR1, and RSF1 (100-103). BUBR1 could be phosphorylated by PLK1 during prometaphase, thus promotes the enrichment of PP2A/B56α phosphatase by BUBR1 at kinetochores (102, 104). PP2A/B56α complex mediates the dephosphorylation of Aurora B to counter its activity on the outer kinetochores, leading to the stability of MT-KT attachment (104). Interestingly, PLK1 could also phosphorylate BRCA2 and facilitate it to form a complex with BUBR1 and PP2A, to establish a stable KT-MT interaction and ensure the proper chromosome alignment (105, 106). Besides, PLK1 could promote the establishment of proper KT-MT attachment by phosphorylating CLIP-170 (107). The knockdown of CLIP-170 results in the defects of KT-MT attachment in human cells and leads to mitotic arrest (108). CK2 (Casein kinase 2)-induced phosphorylation of CLIP-170 is essential for its dynein/dynactin-dependent kinetochore localization, the process of which is facilitated and enhanced by PLK1 (107). Moreover, Tex14 (testis expressed protein 14) is recruited to kinetochores by PLK1 to regulate the KT-MT attachment during early mitosis (109). Hereafter, the PLK1-mediated phosphorylation of Tex14 also results in its ubiquitination by APC/C and subsequent degradation, to guarantee the proper transition from metaphase to anaphase (109). Also, PLK1 phosphorylates MDC1 to promote prometaphase-metaphase transition and maintain genomic stability, independent of MDC1's role in DNA damage repair (110). Furthermore, PLK1 positively regulates Sgt1 and enhances its association with MIS12 complex at kinetochores, thereby promotes the recruitment of NDC80 and promises efficient microtubule-binding sites (111). Above all, both unstable KT-MT attachment and centromere disintegration are demonstrated as the mechanisms of chromosome alignment defects induced by PLK1 inhibition, suggesting PLK1's essential function in both centrosome and kinetochores during mitosis (112).

1.3.1.4 *PLK1 in spindle formation and chromosome segregation*

For accurate chromosome segregation, the formation of KT-MT attachment is tightly controlled and under the surveillance of the spindle assembly checkpoint (113). Monopolar spindle 1 (MPS1) is the principal organizer of the SAC signaling cascade, which could bind to the unattached

kinetochores and recruit SAC-related proteins, thus prevents the activation of APC/C and exit of mitosis (113). It has been well established that PLK1 cooperates with MPS1 to initiate, maintain, and regulate the activity of SAC (114-117). PLK1 directly phosphorylates MPS1 to enhance its catalytic activity and initiate SAC signaling (117). Meanwhile, PLK1-phosphorylated BUB1 and KNL1 facilitate the recruitment of other SAC components to kinetochores (115-117). Besides, PLK1 is necessary for the localization and activity of Aurora B at kinetochores during SAC (114) but also contributes to its removal after KT-MT formation as previously described (104).

Once SAC is satisfied, mitotic checkpoint complex (118), the inhibitory machinery of APC/C, is disassembled due to PLK1's negative regulation of p31^{comet} (119). Significantly, PLK1 initiates the E3 ligase activity of APC/C through dual phosphorylation along with CDK1/cyclin B1, leading to the degradation of cyclins and other mitotic regulators (120). In parallel, PLK1 controls the destruction of APC/C inhibitor EMI1 (early mitotic inhibitor 1) as well, inducing rapid activation of APC/C and entry to anaphase (121). In addition, sister chromatids experience segregation and have to be distributed equally to different poles in anaphase, the process of which is also mediated by PLK1 (122). Cohesin functions to hold two sister chromatids together since the S phase, the deactivation of which is the fundamental basis for chromatids separation (122). In the prophase and prometaphase, PLK1 phosphorylates the subunits of cohesin, subsequently disassociates cohesin from chromosome arms and enhances its cleavability, contributing to the proper separation of chromosomes (122, 123).

1.3.1.5 *PLK1 in cytokinesis*

After chromosome segregation, cells must undergo cleavage under the guidance of the midzone to achieve a successful cell division (124). During anaphase, PLK1 could translocate from centrosomes and kinetochores to the mitotic midzone with the facilitation of PRC1 (protein regulator of cytokinesis 1) (125). CDK1 involves in the PRC1 regulation and acts as an inhibitor toward the interaction between PRC1 and PLK1 before anaphase, as previously reported (125). However, another study proposes that PLK1 is the dominant regulator of PRC1's activity in both pre-anaphase and post-anaphase, instead of CDK1 (124). The phosphorylation of PLK1 could inhibit PRC1's activity in organizing the midzone complex, preventing the pre-mature of the midzone for cells in metaphase (124). Another well studied target of PLK1 during cytokinesis is

22

RhoA signaling. In late mitosis, RhoGEF ECT2 is recruited and activated by HsCyk-4 to the central spindle, thus facilitating the targeting and activation of RhoA GTPase, which is crucial for the maintenance of cortical contractility and the specification of cleavage plane (126). Significantly, PLK1 promotes the central spindle recruitment of ECT2 through phosphorylation, triggering the initiation of cytokinesis and the integration of cleavage furrow (126, 127). As a consequence, the inhibition of PLK1 abolishes the localization of RhoA GTPase at the equatorial cortex, eventually fails cytokinesis (128-130). Besides, PLK1 and RhoA function together to maximize the activity of ROCK2 kinase, thus promoting the contraction of actomyosin during cleavage (131). In the meantime, PLK1 also associates with other proteins located at the central spindle, including MKLP2 (mitotic kinesin-like protein2), NUDC (nuclear distribution gene C), SVIL (supervillin), and CEP55 (centrosomal protein of 55 kDa), to ensure appropriate cytokinesis (132-135).

1.3.2 PLK1 in DNA Damage

Due to its crucial role in cell cycle regulation, it is not surprising that PLK1 is inactivated and subjected to degradation after DNA damage in G2 and mitosis (30, 136). Once DNA damage repair is completed, PLK1 is also responsible for shutting down the DNA damage checkpoint and promoting mitotic progression (6).

As previously mentioned, Aurora A and Bora phosphorylate PLK1 at T210 to enhance its activity and promote mitotic entry (44). Under DNA double-strand break in the G2 phase, Bora is phosphorylated at T501 by ATM/ATR directly, then ubiquitinated by E3-ligase SCF-β-TrCP and degraded (137). As a consequence, the degradation of Bora finally leads to the inhibition of PLK1, which would be further enhanced by phosphatase PP2A/B55α (57, 137). In parallel, G9A monomethylates PLK1 at Y209 to antagonize the T210 phosphorylation and contributes to the PLK1 inhibition as well. (70). Meanwhile, in response to DNA damage in the G2 phase, Cdc14B translocates to the nucleoplasm and activates E3 ligase APC/C^{Cdh1} to degrade PLK1 and induce arrest (136). Recently, a study has shown that ATM spreads all over the chromatin and prevents mitotic progression under DNA damage, but its inhibition toward PLK1 could counteract by chromatin-bound phosphatase Wip1 (138). Wip1 antagonizes ATM's activity to re-active PLK1 and allows the cell cycle to restart even though ATM is still present at DNA lesions (138). Besides,

Claspin is stabilized and activated dependent on ATR/CHK1 activity, triggering the DNA damage checkpoint (139, 140). Once PLK1's activity recuperates, PLK1 phosphorylates Claspin, thus promotes its degradation via E3-ligase SCF-β-TrCP, to recover from the DNA damage checkpoint and move forward to mitosis (140). Moreover, PLK1 and CK2 sequentially phosphorylate Rad51 to enhance its recruitment to the damage site and promote DNA damage repair through HR (homologous recombination) (141). Also, PLK1 phosphorylates Mre11, a component of MRN (Mre11/Rad50/Nbs1), to prevent the loading of the MRN complex to damaged DNA and subsequently inhibit DNA damage repair (142). Furthermore, under DNA replication stress, PLK1 suppresses DNA damage checkpoint through its interaction with RAD9 (143). Recently, it has also been indicated that PLK1 cooperates with CDK1/cyclin B1 in targeting CtIP to induce the error-prone microhomology-mediated end joining and recover from the G2/M checkpoint (144).

In addition to the DNA damage signaling cascade, PLK1 also involves in the regulation of p53, a key mediator of DNA damage checkpoint (145). Upon DNA damage, p53 is activated and stabilized by ATM/ATR and CHK1/CHK2, either inducing the cell cycle arrest or leading to the cell apoptosis (146-148). As previously discussed, p53 and its downstream p21 could inhibit the transcription of PLK1 (33-37, 39, 52), while reactivated PLK1 diminishes p53's activity to enter the mitosis after DNA damage repair. PLK1 co-localizes with and directly phosphorylates p53 in the nucleus, thereby abrogates its transcription activity, facilitates its nuclear export, and induces its degradation (149, 150). Besides, Topors (topoisomerase I-binding protein), function as ubiquitin and SUMO-1 E3 ligase to stabilize p53, is a substrate of PLK1, which would be inhibited and led to degradation by PLK1's phosphorylation (151, 152). Moreover, PLK1 phosphorylates GTSE1 (G2 and S-phase-expressed 1) to induce its nuclear translocation and activity, shuttling p53 out of the nucleus (153). Furthermore, Numb is identified as a novel substrate of PLK1, the phosphorylation of which uncouple Numb from p53 and causes the proteasome degradation of p53 (154).

1.4   Conclusion

PLK1 is the prerequisite in the regulation of multiple cell processes, the functions of which are vital and irreplaceable for cell proliferation and cancer progression. Recently, except for its classical role in cell cycle and DNA damage, plenty of reports also reveal PLK1's role in cancer

cell metabolism, metastasis, and progression, targeting at SREBP1, MTHFR, TSC1, G6PD, PTEN, CRAF, FBW7, etc. (155-161). Consequently, PLK1 appears to be a promising and feasible target for cancer therapy, and the inhibitors aiming at PLK1 are under investigation and clinical trials (74, 162). However, there is still a lot to learn about PLK1's function and regulation in the cell cycle, as well as cancer progression. For instance, epigenetic, immunology, and microenvironment affect gene expression drastically and control tumor development dominantly. PLK1's role in these cellular processes remains unclear and needs further investigation, which is essential for understanding PLK1's role in tumor progression and the application of PLK1 inhibitors. With the development of innovative tools and technologies, such as PLK1 mice models and FRET (Fluorescence Resonance Energy Transfer)-biosensors (163), it is possible to further investigate and understand PLK1's interaction with other molecules within cells.

CHAPTER. 2   MATERIAL AND METHODS

2.1   Cell culture and drugs

LNCaP, 22Rv1, and TRAMP-C2 cells were purchased from ATCC in 2016. C4-2 was obtained from M.D. Anderson Cancer Center. A375 and A375R cells were kindly provided by Dr. Nihal Ahmad from the University of Wisconsin. The human prostate cell lines were cultured in RPMI1640 medium supplemented with 10% (v/v) FBS, 100 Units/mL penicillin, and 10 ug/mL streptomycin at 37°C in 5% CO_2. TRAMP-C2 cell was cultured in DMEM (Dulbecco's modified Eagle's medium) with 0.005 mg/ml bovine insulin, 10 nM dehydroisoandrosterone, 5% fetal bovine serum, 5% Nu-Serum IV, 100 Units/mL penicillin, and 10 ug/mL streptomycin at 37°C in 5% CO_2. The melanoma cell lines were cultured in DMEM with 10% fetal bovine serum, 100 Units/mL penicillin, and 10 ug/mL streptomycin at 37°C in 5% CO_2. All the cells were within 50 passages and Mycoplasma was detected every 3 months using MycoAlert™ PLUS Mycoplasma Detection Kit (Lonza, Cat No. LT07-705). For cell 3D culture, DMEM/F12 medium was used and supplemented with 20 ng/mL EGF, 20 ng/mL bFGF, 10% B27, 0.4% BSA, and 4 ug/mL insulin. The 96-well plate was treated with 50 ul Matrigel (Corning, Cat No. 356234) and incubated in 37°C for 1h. At the same time, the cells were digested into single cells, counted and suspended using DMEM/F12 medium. The cell suspension was then mixed with Matrigel at 1:1 to 100uL in total and seeded into the pre-coated 96-well plates. Finally, 50 ul DMEM/F12 medium will be added in the top and the cells were cultured at 37°C in 5% CO_2.

GSK461364A, JQ1, BI2536, BI6727, and PLX-4032 were purchased from Selleckchem. TanespiMycin was obtained from Medchem Express and Diptoindonesin G was kindly provided by Dr. Wei Xu from the University of Wisconsin.

2.2   Cell viability assay

Cells were seeded with 2×10^3 -1×10^4 per well in 96-well plates, cultured for 12h, and treated with different concentrations of drugs. After 72h of incubation, cells were treated with MTT (3-(4,5-dimethylthiazol-2-yl)-2,5-diphenyltetrazolium bromide) for 4h. Upon resolving the crystal with 100 μL of DMSO, cells were subjected to a plate reader to measure the absorbance at 570

nm. The IC50 values were obtained from the average viability curves generated by four independent measurements of each condition.

2.3   Combination index

The combination index (CI) was calculated with the Chou-Talalay method by using the following equation (164, 165): $CI = \frac{(Am)50}{(As)50} + \frac{(Bm)50}{(Bs)50}$. The IC50 of two drugs was measured respectively and indicated as $(As)_{50}$ and $(Bs)_{50}$. Subsequently, the two drugs were mixed at the $(As)_{50}/(Bs)_{50}$ ratio to treat the cells, to get the parameters of $(Am)_{50}$ and $(Bm)_{50}$ when the mixture achieves a 50% inhibitory effect. Antagonism is indicated when $CI > 1$, $CI = 1$ indicates an additive effect, and CI < 1 indicates synergy.

2.4   Transwell migration and invasion assay

Cells were cultured in the serum-free medium for 24h. For migration assay, cells were suspended in serum-free medium and seeded with 2×10^4 -4×10^4 per well into 24-well transwell insert, then medium containing 10% FBS were added into the receiver well. After 24h incubation, the cells were fixed with 10% formalin for 30 min and stained with 0.5% crystal violet for 30 min. For invasion assay, the Matrigel was diluted with the serum-free medium in the ratio of 1:40. The transwell inserts were treated with the diluted Matrigel for 1h under 37°C. Cells (2×10^4 -4×10^4) in serum-free medium were planted into the Matrigel-treated transwell inserts. The inserts were harvested after 48h, fixed with 10% formalin for 30 min, and stained with 0.5% crystal violet for 30 min (166). The photos were taken with a Nikon microscope.

2.5   Wound healing assay

Cells were seeded into 6-well plates and incubate for 24h to achieve 100% confluence. A 200 uL pipette tip was used to make a vertical wound down through the cell monolayer, and the cell debris was washed out by PBS. Then cells continued to culture in the medium containing 1% serum, with or without drugs. The pictures were taken at 12h or 24h with the Nikon microscope to monitor the wound closure (166).

2.6   Antibodies

Antibodies against SOX 10 and HSP90 were products of Santa Cruz Biotechnology. Anti-PLK1 was obtained from Millipore. Antibodies against Axin2 and Ki67 were purchased from Abcam, whereas antibodies against β-actin and c-Myc were obtained from Sigma. Antibodies against CD45, CD8, Foxp3, PD-L1, CD4, CD25, CD11b, Ly6C, and Ly6G were purchased from Biolegend. All other antibodies were purchased from Cell Signaling Technology.

2.7   Immunoblotting (IB)

Cells were washed by PBS twice after harvest and then re-suspended with TBSN or RIPA buffer with protease inhibitors and phosphatase inhibitors. After sonication, cell lysates were collected, and protein concentrations were measured by using Protein Assay Dye Reagent (Bio-Rad, Cat No. 5000006) or Pierce™ BCA Protein Assay Kit (ThermoFisher, Cat No. 23225). Mix the proteins from each group with SDS-PAGE loading respectively and boil it for 5 min. Upon transferring to polyvinylidene difluoride membranes, proteins were probed with indicated antibodies (167). The primary antibodies were diluted in 5% milk in a 1:1000 ratio and incubated at 4°C overnight. Then the membrane was washed 3 times X 5 min with TBST and incubated with diluted second antibodies (1:3000) in the room temperate for 1 h. Before exposure, the membrane was washed 3 times X 5 min with TBST, and then the signal will be detected with the Clarity Western ECL Substrate (BIO-RAD, Cat No. 1705061).

2.8   RNA isolation and quantitative real-time PCR (qRT-PCR)

Total RNA was extracted from either tissues or cells by using the RNeasy® mini kit (Qiagen) and subsequently subjected to reverse transcription using the QuantiTect Reverse Transcription Kit (Qiagen). The PCR program for the reverse transcription is 42 for 2 min, 42°C for 15 min, and 95°C for 3 min. FastStart Universal SYBR Green Master (130) was used to measure the expression level of indicated mRNA and was normalized to β-actin, respectively. The PCR program for qRT-PCR is 95°C for 10min, and repeat 40 cycles of 95°C for 15 s and 60°C for 30 s. The primers used to detect mouse *Plk1* and *Actb* are listed. *Plk1*-F: CCATCTTCTGGGTCAGCAAGTG; *Plk1*-R: CCGTCATTGTAGAGAATCAGGCG; *Actb*-F: CATTGCTGACAGGATGCAGAAGG; *Actb*-R: TGCTGGAAGGTGGACAGTGAGG

2.9　Histology and H&E staining

Tumors were fixed in 10% neutral buffered formalin, paraffin-embedded, and sectioned to 5 mm by the histology research laboratory of Purdue University. After murine or human paraffin-embedded slides were deparaffinized and rehydrated, the slides were stained with Hematoxylin and Eosin Stain kit (Vector Laboratories, Cat No. H-3502), and the procedures were performed following the protocol of the kit. The pictures were taken with a Nikon microscope.

2.10　Immunofluorescence (IF) and Immunohistochemistry (IHC) staining

After murine or human paraffin-embedded slides were deparaffinized and rehydrated, antigens were retrieved in antigen unmasking solution (Vector Laboratories, Cat No. H-3301-250). Samples were then blocked, incubated with indicated primary antibodies in a 1:200 ratio, followed by incubation with secondary antibodies. For IF staining, the slides were mounted by VECTASHIELD® Antifade Mounting Medium with DAPI (Vector Laboratories, Cat No. H-1200). For IHC staining, the slides were stained with VECTASTAIN® Elite® ABC Universal Plus kit (Vector Laboratories, Cat No. PK-8200). The pictures were taken with a Nikon microscope.

2.11　Colony formation assay

Cells (500-5000/well) were seeded in 6-well plates and cultured in medium alone or containing different drugs for 14 days, with the medium change every 2 days. After culturing, cells were fixed in 10% formalin and stained with 0.5% crystal violet for 30 minutes, followed by counting of colony numbers.

2.12　Annexin V/ PI staining

Cells (5×10^5/well) were seeded in 6-well plates, cultured in medium alone or containing different drugs, and subjected to the procedure using the Annexin V apoptosis kit (BioVision, K101-25), followed by analysis with Flowjo.

2.13   Cell cycle analysis

Cells (5 x 10^5/well) were seeded in 6-well plates, cultured in medium alone or containing different drugs, and harvested. Cells were then fixed in 70% ethanol, stained with 50 mg/mL PI (propidium iodide), and subjected to flow cytometry analysis.

2.14   Flow cytometry analysis

Cells (1 x 10^5/well) were seeded in 12-well plates and cultured in normal medium overnight. For 2-NBDG staining, the cells were washed with PBS twice and incubated with the glucose-free medium containing 100 ug/mL 2-NBDG (Cayman, Cat No. 11046) for 1 h. For MitoSOX (ThermoFishes, Cat No. M36008) and MitoTracker Green FM (Cell signaling Technology, Cat No. 9074), the probes were added into the medium at a final concentration of 5uM for MitoSox and 100nM for MitoTracker Green FM, followed by 15 min incubation. Cells were then harvested, stained with DAPI (ThermoFisher, Cat No. D1306), and subjected to flow cytometry analysis.

2.15   Patient-derived xenograft model

Mice carrying LuCaP35CR tumors were obtained from Dr. Robert Vessella at the University of Washington (168). Tumors were cut into 20-30 mm^3 pieces and then were implanted into pre-castrated NSG mice. When tumors' size reached 250-300 mm^3, mice were randomly separated into four groups for control, two single treatments, and the combination treatment, respectively. The experiment was approved by the Institutional Animal Care and Use Committee (IACUC). The protocol No. is 2018-3023.

2.16   22Rv1-derived mouse xenograft model

22Rv1 cells were transfected with Flag-Axin2-WT and Flag-Axin2-311A plasmids and selected with 500 µg/mL G418 for 4 weeks. Cells (2.5 x 10^5 cells/mouse) were mixed with an equal volume of Matrigel (Corning, Cat No. 356234) and inoculated into the right flank of NSG mice (Harlan Laboratories). One week later, animals were randomized into treatment and control groups with 4 mice each. JQ1 was delivered via gavage, twice a week. Tumor volumes were estimated from the formula: V = L x W^2/2 [V is volume (mm^3); L is length (mm); W is width (mm)]. The experiment

was approved by the Institutional Animal Care and Use Committee (IACUC). The protocol No. is 2018-3023.

2.17 TRAMP-C2-derived mouse allograft model

TRAMP-C2 cells (1×10^5 cells/mouse) were mixed with an equal volume of Matrigel (Collaborative Biomedical Products) and inoculated into the right flank of C57BL/6 wild type mice (Envigo). One week later, animals were randomized for control, GSK461364A alone, JQ1 alone, combination treatment, and BI2536 alone, respectively. Tumor volumes were estimated from the formula: $V = L \times W^2/2$ [V is volume (mm^3); L is length (mm); W is width (mm)]. After 10 days of treatment, mice (5 mice/group) were sacrificed and the tumors were obtained. The proportion of PD-L1$^+$/CD45$^-$ cell, T regulatory cells (T_{reg}, CD4$^+$CD25$^+$FoxP3$^+$), and Myeloid-derived suppressor cells (MDSC, CD45$^+$Gr-1$^+$CD11b$^+$) were analyzed by flow cytometry. The experiment was approved by the Institutional Animal Care and Use Committee (IACUC). The protocol No. is 2018-3023.

2.18 Serum prostate-specific antigen (PSA) measurement

After blood was collected from tumor-carrying mice twice per week, serum PSA levels were measured by using a PSA ELISA kit (Abnova, Cat No. KA0208) (25).

2.19 Seahorse analysis

Cells (1×10^4-4×10^4 per well) were seeded in XFe96 cell culture microplates in RPMI 1640 medium or DMEM (10% FBS with antibiotics). After 12h of incubation, cells were treated with the corresponding drug(s) for 24h. Cartridges were hydrated in calibrant buffer in a non-CO$_2$ incubator at 37°C for at least 12h before analysis. Before being subjected to seahorse analysis, cells were washed with the corresponding medium twice and incubated in a non-CO$_2$ incubator for 1 hour. For glycolysis stress test (GST), the GST medium was prepared by supplementing XF base Medium with 2 mM glutamine, and pH was adjusted to 7.4. For mitochondrial stress test (MST), MST medium was prepared by supplementing XF base Medium with 2 mM glutamine, 1 mM pyruvate, and 10 mM glucose, and pH was adjusted to 7.4. The drugs from the XF GST kit and MST kit were diluted with the corresponding medium into designed concentrations and then added

into corresponding ports of the cartridge. After calibration of the cartridge, cells went through GST or MST programs. Data were analyzed by using the Seahorse XF Cell GST Report Generator and Seahorse XF Cell MST Report Generator, respectively.

2.20   Statistical analysis

Data are presented as mean ± standard derivation of the mean (s.d.). Reproducibility was ensured by performing more than three independent experiments. The statistical significance of the results was analyzed by the two-tailed, unpaired Student's t-test. The statistical analysis was performed with StatView (Abacus Concepts Inc.) or Prism 7 (GraphPad). A P value of less than 0.05 indicates statistical significance. The statistical information are presented in each figure legend.

CHAPTER. 3 PLK1 INHIBITION ENHANCES THE EFFICACY OF BRD4 BLOCKADE IN CASTRATION-RESISTANT PROSTATE CANCER

3.1 Introduction

Prostate cancer (PCa) is one of the most frequently diagnosed cancers among men and the leading causes of cancer-related death worldwide (169). According to the American Cancer Society, there will be 191,930 newly diagnosed PCa cases, as well as 47,050 deaths in the United States in 2020 (170). Due to its critical role in PCa development, Androgen receptor (AR) signaling is the dominant target to treat PCa patients initially. Androgen deprivation therapy (ADT) functions effectively and systematically to suppress both local and metastatic PCa, thus is broadly used in the clinical. Unfortunately, most PCa patients eventually gain resistance to ADT and develop into castration-resistant prostate cancer (CRPC), which lacks efficient treatment and significantly shortens the survival period of patients (171, 172). Consequently, it is urgently required for novel therapies to treat CRPC patients in clinical.

Polo-like kinase 1(PLK1), a serine-threonine kinase and essential regulator of mitosis, has been proven as a potential and novel target for cancer therapy (162). PLK1 involves multiple aspects of mitosis, from mitotic entry to cytokinesis (173). Compared to the adjacent normal tissues, PLK1 is highly expressed in the tumors and negatively correlated with the patients' survival (14, 162, 174). Due to its critical role in cell proliferation, several specific inhibitors targeting PLK1 are under investigation and in clinical trials to determine their efficacy and safety profiles (175). GSK461364A (thiophene derivative) is a highly potent PLK1 inhibitor, showing a strong inhibitory effect in multiple cancers, and currently under Phase 1 clinical trial (118, 176-180).

Bromodomain-containing protein 4 (BRD4), the most extensively investigated member of the bromodomain and extraterminal domain (BET) family, functions as an epigenetic reader to regulate transcription (181). It is well established that BRD4 could facilitate RNA polymerase II to initiate the transcription, subsequently promote the expression of multiple oncogenes, including Fos, Jun, and c-Myc (182). Most importantly, BRD4 could directly recruit AR to its target loci and function as a co-activator of AR signaling (183). JQ1 is a highly specific inhibitor for BRD4, which

could bind competitively to the acetyl-lysine recognition motif of BRD4 and disrupts its recruitment during transcription, thus effectively suppresses tumor growth (184, 185).

In this study, we have validated the efficacy of the novel treatment strategy combining PLK1 inhibitor GSK461364A and BRD4 inhibitor JQ1 in two aggressive human CRPC cell lines, 22Rv1 and C4-2, as well as a patient-derived xenograft model. This innovative combination treatment could induce G2/M arrest, promote cell apoptosis, suppress tumor proliferation, and inhibit cellular metabolism both *in vitro* and *in vivo*. Based on the previous publication of our lab, we have shown that PLK1 could regulate the β-catenin pathway through direct phosphorylation of Axin2, which stabilizes the binding between GSK3β and β-catenin, leading to the degradation of β-catenin in the cytoplasm. Conversely, Plk1 inhibition would induce the activation of Wnt/β-catenin signaling, resulting in the expression of c-Myc (175, 186, 187). Meanwhile, PLK1 could enhance AR signaling in prostate cancer (188, 189), while JQ1 could effectively antagonize AR signaling and repress c-Myc transcription through inhibiting BRD4 (183). Therefore, we propose that the observed synergistic effect for GSK461364A and JQ1 is through regulating c-Myc and AR signaling.

3.2   Results

3.2.1   GSK461364A and JQ acts synergistically *in vitro*

To investigate whether GSK461364A and JQ1 could work synergistically in human CRPC cell lines, 22Rv1 and C4-2 cells were under the treatment of either DMSO, GSK461364A, JQ1, or the combination of GSK461364A and JQ1, and then harvested for IB to detect the expression of the apoptotic indicator, cleaved-PAPR (Figures 1A and 1B). As shown in Figure 1A, the treatment of low-dosage JQ1 (100nM) or GSK461364A (lane 2 and 3) only led to a weak apoptotic response in 22Rv1 cells after 48h, whereas combining GSK461364A and JQ1 (lane 5) could robustly induce the cell apoptosis. Similarly, the dramatic elevation of apoptosis also could be observed in C4-2 cells under the combination treatment (Figure 1B). Consistently, the analysis of Annexin V/PI staining also revealed a significant increase in the apoptotic cell population under co-treatment of GSK461364A and JQ1 (Figure 1C), suggesting GSK461364A and JQ1 acts cooperatively in inducing cell apoptosis. Besides, GSK461364A and JQ1 showed a significant synergistic

suppression in cell proliferation and colony formation in 22Rv1 and C4-2 cells (Figures 1D-1G). Furthermore, the cell cycle defects have been monitored by flow cytometry upon drug treatment in 22Rv1 cells. Intriguingly, based on the cell cycle analysis, the presence of JQ1 could dramatically enhance the efficacy of GSK461364A to arrest the cells at the G2/M phase, potentiating JQ-1 related cell death in 22Rv1 cells (Figure 1H). To further confirm the synergy between GSK461364A and JQ1, the combination index (CI) has been calculated through the Chou-Talalay method (163, 164). The IC_{50} value of JQ1 for 22Rv1 and C4-2 was measured to be 400 nmol/L and 300 nmol/L, respectively, while it dramatically reduced to 50 nmol/L and 75 nmol/L under the presence of GSK461364A. Based on the equation, the CI value was calculated as 0.625 and 0.750, respectively, in 22Rv1 and C4-2 cells (Tables 1 and 2), indicating a strong synergistic effect between GSK461364A and JQ1. Above all, we have demonstrated that JQ1 and GSK461364A function cooperatively *in vitro* to inhibit CRPC proliferation and progression.

3.2.2   GSK461364A plus JQ synergistically inhibit the growth of PDX-derived tumors

To confirm the efficacy of this novel combination therapy *in vivo*, we next utilized the LuCaP35CR, a patient-derived xenograft (PDX) mouse model. Compared to the control group, the JQ1-treated group has shown a slight inhibition in the tumor size without significant difference (Figure 2A). However, the efficacy of JQ1 was remarkably elevated after combination with GKS61364A, showing a dramatic decrease in tumor volume and weight in contrast to either the control or mono-treatment group (Figures 2B and 2C). Most importantly, it also could be observed that the apoptotic bodies with condensed cytoplasm and pyknotic notably increased under the co-treatment of GSK461364A and JQ1, based on the histology staining (Figure 3A). Consistent with the previous findings, increasing cleaved-Caspase 3-positive cells could be detected, together with the robust reduction of Ki-67-positive cells in the co-treatment group (Figure 3B). Altogether, we have demonstrated that GSK461364A and JQ1 could function synergistically and effectively both *in vivo* and *in vitro*, providing a novel therapeutic strategy to CRPC patients.

3.2.3   The synergy between PLK1 and BRD4 inhibition is due to the suppression of AR and c-Myc signaling

To further investigate the mechanism underlying this synergy, AR and c-Myc, two critical molecules for CRPC development and progression, were detected by IB under the drug treatment

(Figures 4A and 4B). After combination treatment, the expression of c-Myc, AR full length, AR variants, and AR downstream target PSA significantly reduced in both 22Rv1 and C4-2 cells compared to the single treatment. Interestingly, a previous publication of our lab has demonstrated Axin2, a key regulator of Wnt/β-catenin signaling, as a PLK1's substrate (175). PLK1 could phosphorylate Axin2 at S311 to stabilize the binding between GSK3β and β-catenin, eventually leading to the degradation of β-catenin in prostate cancer cells. As such, the inhibition of PLK1 could prevent β-catenin from degradation and activate its downstream signaling, including the expression of c-Myc (175). Meanwhile, PLK1 could regulate AR to enhance its signaling and promote PCa proliferation (188, 189). BRD4 binds to the promoter region of c-Myc and regulates AR signaling directly, indicating the synergy may due to the regulation of c-Myc and AR signaling. To further understand how JQ1 enhances GSK461364A's efficacy, we constructed the cells expressing different forms of Axin2 (WT or S311A) to compare their responses toward JQ1 treatment. Of note, the Axin2-S311A mutant mimics the condition of PLK1 inhibition, as it is unable to be phosphorylated by PLK1 anymore. Subsequently, 22Rv1 and C4-2 cells, expressing either WT or S311A Axin2, were treated with JQ1 and subjected to IB. Not surprisingly, cells expressing S311A mutant has been more sensitive to the treatment of JQ1 in contrast to cells expressing WT Axin2, showing a dramatic induction in cell apoptosis, as well as a robust decrease in c-Myc and AR signaling (Figures 4C-4E). In summary, these data supported our hypothesis that JQ1 could enhance PLK1's efficacy through targeting AR and c-Myc signaling.

3.2.4   22Rv1-derived tumors expressing Axin2-S311A are more sensitive to JQ1

To further test our hypothesis *in vivo*, 22Rv1 cells stably expressing either Axin2-WT or Axin2-S311A were implanted into NSG mice to test their response to JQ1 treatment. As expected, the 22Rv1 cell expressing Axin2-S311A was more aggressive and showed an elevated proliferative rate compared to the cell expressing Axin2-WT (Figure 5A). Consistently, a low dosage of JQ1 (6.25mg/kg body weight) could remarkably repress tumor proliferation, and a dramatic reduction of tumor volume could be observed (Figures 5A and 5B). Serum PSA levels also dropped significantly in the Axin2-S311A group under JQ1 treatment, indicating the suppression of AR signaling (Figure 5C). Morphologically, increasing apoptotic bodies, as well as reduced Ki-67 and elevated cleaved-Caspase 3, had been observed in Axin2-S311A expressing tumors after JQ1

treatment. Taken together, JQ1 could overcome the side effects of the PLK1 inhibitor, which causes β-catenin nuclear accumulation, thus enhance the efficacy of PLK1 inhibition in CRPC.

3.2.5   Co-treatment of GSK461364A and JQ1 inhibits cell metabolism

Due to the critical role of AR and c-Myc in CRPC development and metabolism regulation, it is possible that the combination treatment of GSK461364A and JQ1 significantly affect cell metabolism and cause severe metabolic defects, finally leading to cell death. Aerobic glycolysis and mitochondrial oxidative phosphorylation are the two major pathways to produce ATP in cells. Consequently, we measured the rate of glycolysis and oxidative phosphorylation under drug treatment in 22Rv1 cells using Seahorse. As shown in Figures 6A and 6B, mono-treatment could slightly inhibit glycolytic ability compared to the non-treated cells. As expected, JQ1 cooperating with GSK461364A further reduced the glycolytic rate, as well as the glycolytic capacity and glycolytic reserve after 24h treatment. Moreover, we have also measured the rate of oxidative phosphorylation in 22Rv1 cells (Figures 6C and 6D), showing the combination treatment of GSK461364A and JQ1 significantly inhibited the basal oxidative phosphorylation and ATP production. Interestingly, there were no appreciable differences in spare respiratory capacity and proton leakage between each group, indicating that neither monotherapy nor combination therapy could influence mitochondrial function. In summary, our data has indicated that GSK461364A and JQ1 could act synergistically in inhibition of both glycolysis and oxidative phosphorylation of CRPC cells.

3.2.6   Combination treatment of GSK461364A and JQ1 has a minor impact on PD-L1 expression

Recently, a study reported BRD4 as a positive regulator of PD-L1 (190). Therefore, we aimed to validate whether the combination therapy has any impact on the expression of PD-L1 expression in PCa cells. TRAMP-C2, an aggressive mouse prostate cell line expressing high-level PD-L1, was utilized to address this question. As shown in Figure 7A, the treatment of interferon-gamma (10 ug/mL) induced the expression of PD-L1. In contrast, both mono- and dual- treatment slightly induced PD-L1 expression, but the co-treatment of the two drugs did not show a synergistic effect. To further evaluate this finding *in vivo*, TRAMP-C2 cells were implanted in C57/B6 wild type mice and treated with vehicle, GSK461364A, JQ1, the combination of GSK461364A and JQ1, or

BI2536. As BI2536 is a dual inhibitor of Plk1 and BRD4 (191), it represented a positive control in this allograft experiment. Compared to the control group, there was no significant difference in tumor volumes in all treated groups (Figure 7B), while tumor weight significantly decreased after the combination treatment (Figures 7C and 7D). Tumors were digested into single cells right after harvest and stained with corresponding antibodies to detect proportions of specific cell populations by flow cytometry. Based on the results, none of the drug treatment showed a significant impact on the PD-L1 expression level in tumor cells (Figure 7E), Myeloid-derived suppressor cells population (Figure 7F), or the percentage of T regulatory cells (Figure 7G). Concisely, our data have indicated that the combination of GSK46164A and JQ1 may have a limited effect on the immune system upon this experimental condition.

3.3   Discussion

BRD4 functions as a critical epigenetic reader, which could directly recruit P-TEFb (positive transcription elongation factor complex b), the mediator complex, and multiple transcription factors to the promoter regions to facilitate functions of RNA polymerase II (192, 193). As a consequence, BRD4 not only marks selected M/G1 genes in mitotic chromatin as transcriptional memory but direct post-mitotic gene transcription, including c-Myc as well (194). Due to the essential role of c-Myc in cancer proliferation and progression, BRD4 is considered a potential and promising target for novel cancer therapies. Based on the previous observation, the efficacy of JQ1, a highly specific inhibitor of BRD4, has been tested in multiple cancer cells, showing acute repression of c-Myc, induction of apoptosis, and inhibition of growth (183, 195). Most importantly, JQ1 could inhibit PCa proliferation in an AR-dependent manner by disrupting the binding between AR and chromatin (183). Herein, we presented a novel therapeutic strategy to combine JQ1 with PLK1 inhibitor GSK461364A, thus significantly increasing the efficiency of JQ1 (Figure 6E).

PLK1 is crucial for cell cycle progression, especially during mitosis, participating in several processes from mitotic entry to cytokinesis. To date, abundant researches have pointed out PLK1 is overexpressed in multiple cancer types and cross-interacts with cancer-associated pathways (74). Emerging evidence supports that PLK1 contributes to the acquisition of drug resistance, suggesting it as a potential target for novel cancer therapies. For example, PLK1 phosphorylates Orc2 to induce continued DNA replication, therefore leading to the gemcitabine resistance in pancreatic

cancer (196). Besides, the PLK1-dependent phosphorylation of CLIP-170 and p150^{Glued} affects the microtubule dynamics, thus resulting in the docetaxel resistance in PCa (107, 197). Furthermore, the inhibition toward PLK1 could enhance the efficiency of metformin and β-catenin inhibitor in CRPC (175, 198). Therefore, PLK1 seems to be a promising target in CRPC treatment.

Herein, we investigated the efficacy of PLK1 inhibitor GSK461364A and BRD4 inhibitor JQ1, as well as the dual treatment combining GSK461364A and JQ1, in human CRPC cells 22Rv1 and C4-2. We have revealed that GSK461364A and JQ1 act synergistically from multiple aspects, including inhibition of proliferation, promotion of apoptosis, and arrest of the cell cycle (Figures 1A-1H). In parallel, GSK461364A could dramatically enhance the efficacy of JQ1 in the LuCaP35CR PDX model, confirming the efficiency of this novel therapeutic strategy *in vivo* (Figures 2A-2C and 3A-3B). Intriguingly, the combination of GSK461364A and JQ1 not only inhibited c-Myc expression but also suppress the expression and function of AR, both full length and variants. Moreover, the dual treatment could further inhibit glycolysis and oxidative phosphorylation in 22Rv1 cells compared to the single treatment. Furthermore, considering that BRD4 is related to the expression of PD-L1 (190), we tested the effects of the combination treatment on the immune system. As indicated in Figure 7A, the combination treatment showed no synergistic effect on the PD-L1 expression in TRAMP-C2 cells *in vitro*. Besides, TRAMP-C2 derived allograft model was treated with indicated drugs, showing that the combination therapy did have synergistic inhibition on tumor growth (Figure 7B) but had a limited effect on the immune system (Figures 7E-7G). However, to further confirm the impacts of combination treatment on the immune system, more experiments are required by using other prostate cancer models.

In summary, our *in vitro* and *in vivo* data suggested the strong synergy between PLK1 inhibitor GSK61364A and BRD4 inhibitor JQ1 in CRPC from two aspects: 1) JQ1 suppresses c-Myc expression, thus decreasing the side effects of PLK1 inhibitor, and 2) PLK1 inhibitor along with BRD4 inhibitor represses AR signaling synergistically. Consequently, this novel therapeutic strategy can be considered for clinical trials to treat CRPC patients.

Table 1 The IC$_{50}$ values of GSK461364A and JQ1 in 22Rv1 cells

Drugs	IC$_{50}$	CI
GSK461364A	12nM	
JQ1	400nM	
GSK461364A (in combination 200nM/L JQ1)	3nM	
JQ1(in combination 6nM/L GSK461364A)	50nM	CI=0.625

Table 2 The IC$_{50}$ values of GSK461364A and JQ1 in C4-2 cells

Drugs	IC$_{50}$	CI
GSK461364A	7nM	
JQ1	300nM	
GSK461364A (in combination 150nM/L JQ1)	2nM	
JQ1(in combination 3.5nM/L GSK461364A)	75nM	CI=0.750

Figure 1. GSK461364A and JQ1 acts synergistically in CRPC cells

(A-B) 22Rv1 cells and C4-2 cells were treated with DMSO, JQ1, GSK461364A, or the combination of JQ1 and GSK461364A, respectively, for 48h, followed by IB to detect the expression of cleaved-PARP. (C) 22Rv1 cells (2.5×10^5) were treated with DMSO, 500nM JQ1, 10 nM GSK461364A, or JQ1 plus GSK461364A, respectively. After 48h, cells were collected, stained with Annexin V/PI for 15 minutes and 2,0000 cells were analyzed per sample by flow cytometry. (D-E) 22Rv1 cells (0.5×10^3) and C4-2 cells (1×10^3) were seeded in 6-well plates and treated with indicated drugs. The fresh medium containing drugs was changed every 3 days for 2 weeks in total, then the cells were fixed with formalin and monitored by crystal violet staining. The experiments shown are representatives of 3 repeats. (F-G) 22Rv1 and C4-2 cells (5×10^3) were seeded in 6-well plates and treated with indicated drugs, followed by the counting of cell numbers for five days. (H) 22Rv1 cells (2.5×10^5) were treated with DMSO, 500 nM JQ1, 10 nM GSK461364A, or JQ1 plus GSK461364A, respectively. After 24h of treatment, cells were collected, fixed with 70% ethanol, stained with PI for 30 minutes, and analyzed with flow cytometry.

Figure 1 continued

A

22Rv1

GSK461364A, nM	-	6	-	-	6	6
JQ1, nM	-	-	100	200	100	200
Cleaved-PARP						
GAPDH						
Cleaved-PARP/GAPDH	1.0	1.32	1.11	1.40	1.89	1.76

B

C4-2

GSK461364A, nM	-	5	-	-	5	5
JQ1, nM	-	-	100	200	100	200
Cleaved-PARP						
GAPDH						
Cleaved-PARP/GAPDH	1.0	6.37	1.48	1.48	8.08	9.93

C

Propidium Iodide

Control — JQ1 — GSK461364A — GSK461364A + JQ1

42
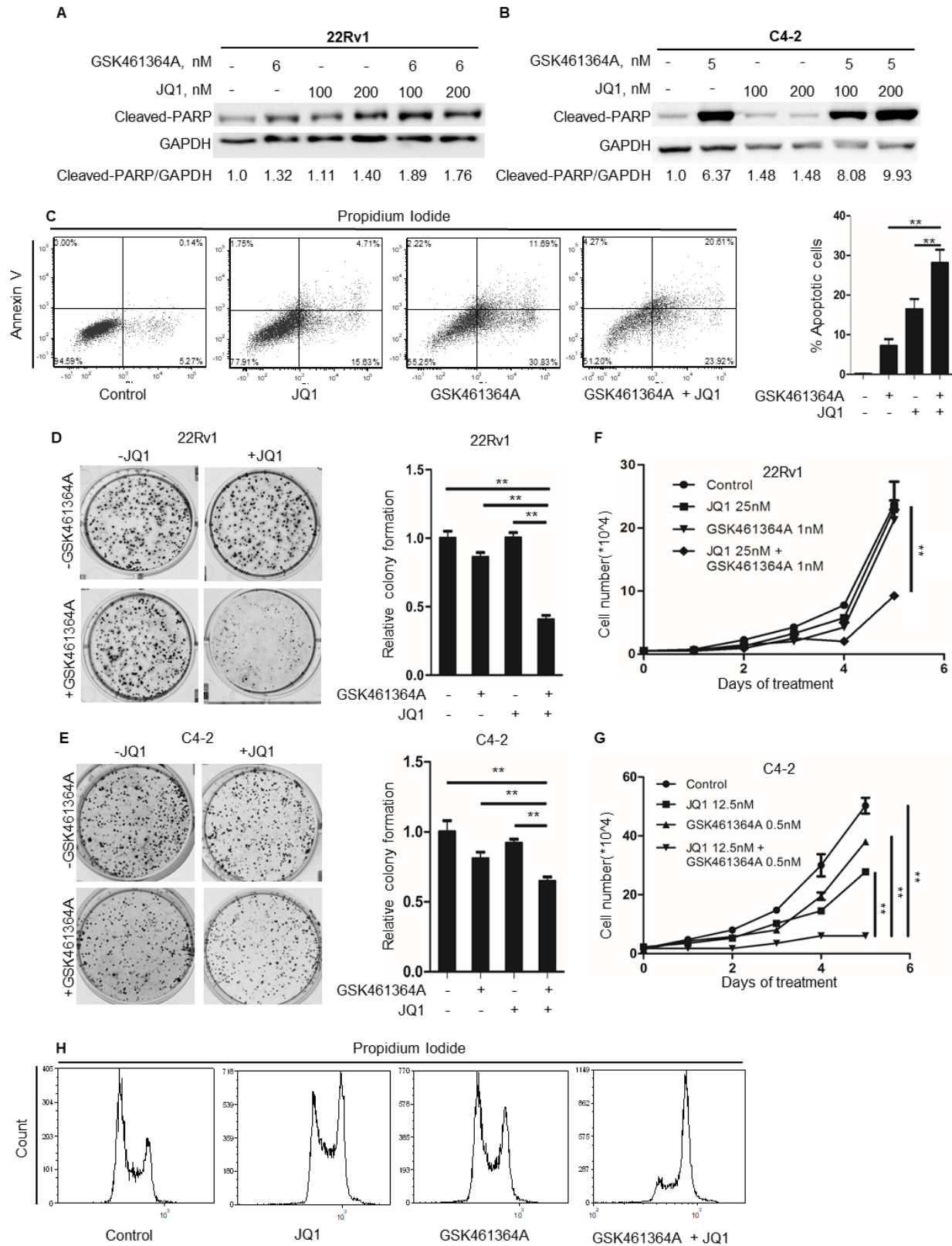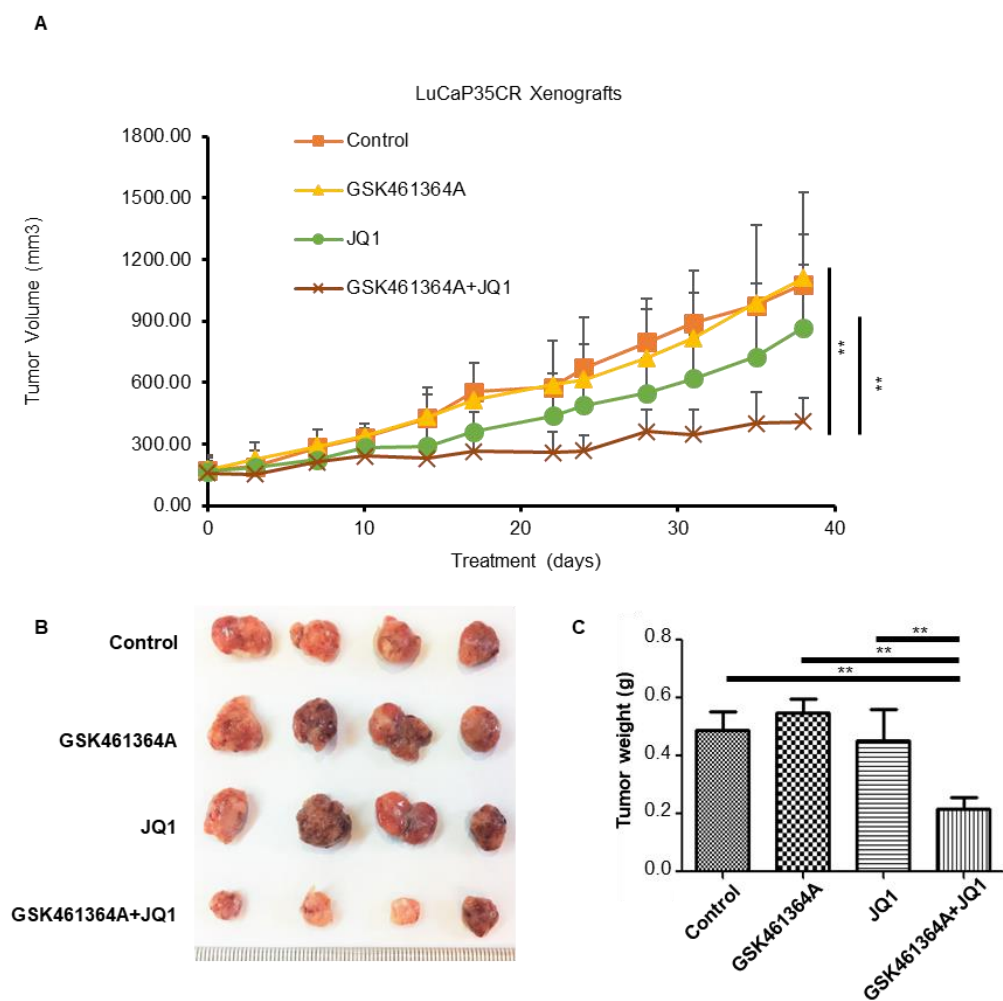
Figure 2. GSK461364A with JQ synergistically inhibits the growth of PDX-derived tumors.

(A) Growth curves of the PDX model. LuCaP35CR tumors were implanted into pre-castrated NSG mice, administered with GSK461364A (12 mg/kg body weight, intravenous injection, twice a week), JQ1 (25 mg/kg body weight, oral gavage, twice a week), or a combination of both drugs. The sizes of the tumors in each group were measured every 3 days (mean ± SEM; n = 4 mice from each experiment group). **, P < 0.01. (B) Representative images of the fresh tumors at the end of the study. (C) Tumor weight was measured after being freshly removed from the bodies. **, P < 0.01.
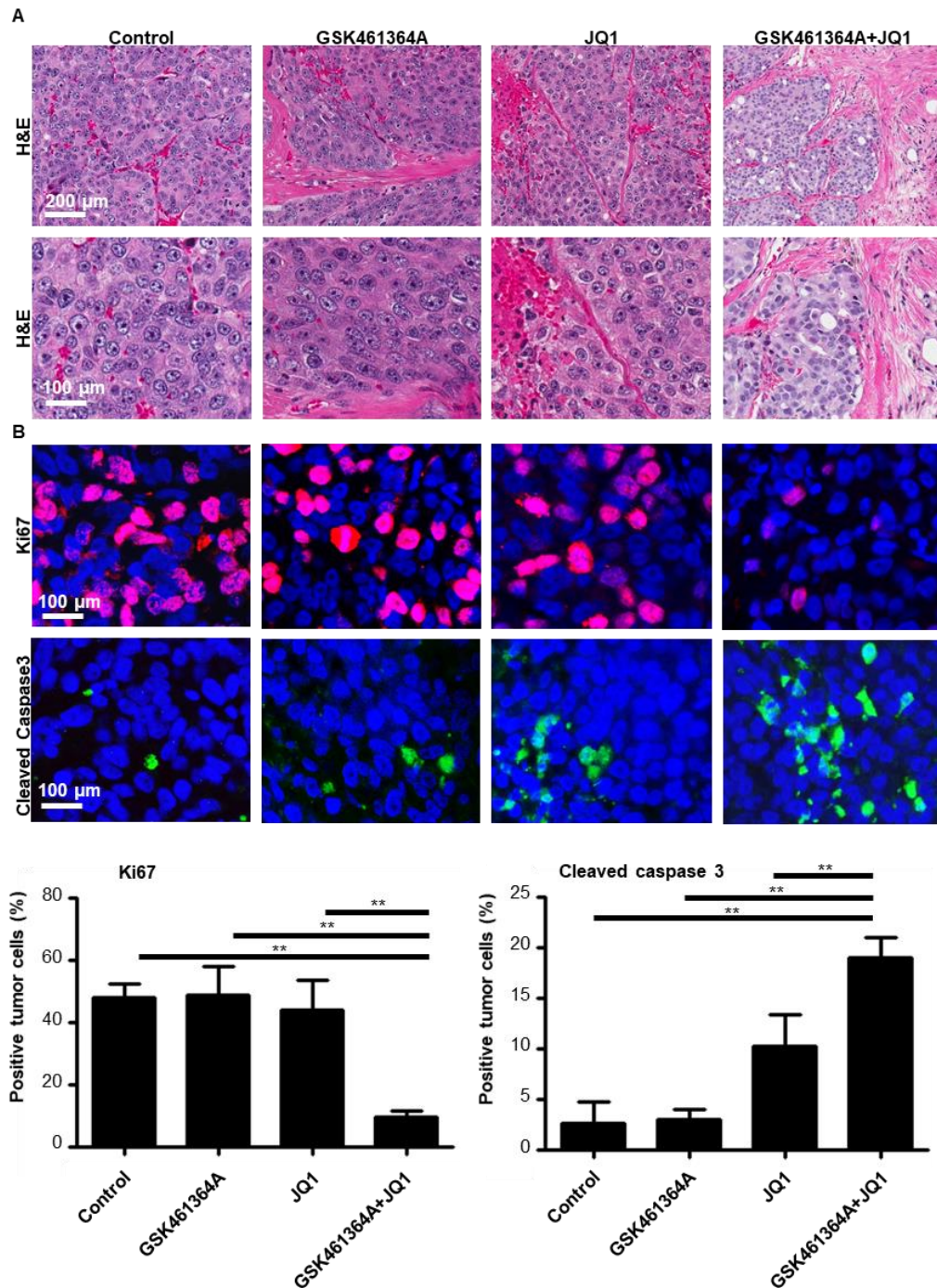
Figure 3. Histologic analysis of LuCaP35CR-derived xenograft tumors.

(A) Representative images of H&E staining on LuCaP35CR tumor sections from different treatment groups. (B) Top: Representative images of IF staining for Ki67 and cleaved caspase 3. Bottom: Quantification of Ki67- or cleaved caspase-3-positive cells within total cells. For quantification, at least 300 cells were scored within each field (x 20 fields, more than 3 sections at different tumor depths/mouse) as the percentages of Ki67- or cleaved caspase 3-positive cells. *, $P < 0.05$; **, $P < 0.01$.

A

22Rv1, 48h

| GSK461364A, nM | – | 6 | – | 6 |
| JQ1, nM | – | – | 200 | 200 |

AR

c-Myc

GAPDH

| AR/GAPDH | 1.00 | 0.73 | 0.68 | 0.39 |
| AR-V/GAPDH | 1.00 | 0.86 | 0.84 | 0.42 |

B

C4-2, 48h

| GSK461364A, nM | – | 5 | – | – | 5 | 5 |
| JQ1, nM | – | – | 100 | 200 | 100 | 200 |

AR

GAPDH

| AR/GAPDH | 1.00 | 0.87 | 1.10 | 1.03 | 0.57 | 0.55 |

c-Myc

PSA

Actin

| c-Myc/GAPDH | 1.00 | 0.45 | 0.56 | 0.33 | 0.35 | 0.19 |
| PSA/GAPDH | 1.00 | 0.68 | 1.04 | 0.87 | 0.67 | 0.44 |

C

22Rv1, 48h

| Flag-Axin2 | WT | S311A | WT | S311A |
| JQ1, nM | 1000 | 1000 | 0 | 0 |

Flag-Axin2

Cleaved-PARP

Actin

D

C4-2, 48h

| Flag-Axin2 | WT | WT | S311A | S311A |
| JQ1, nM | 0 | 500 | 0 | 500 |

Flag-Axin2

Cleaved-PARP

Actin

| Flag-Axin2/Actin | 1.00 | 1.04 | 0.98 | 1.16 |
| Cleaved-PARP/Actin | 1.00 | 2.96 | 0.95 | 3.60 |

AR

c-Myc

PSA

Actin

AR/Actin	1.00	1.08	1.21	0.61
c-Myc/Actin	1.00	0.08	0.99	0.02
PSA/Actin	1.00	0.62	1.04	0.37

E

22Rv1, 48h

| Flag-Axin2 | WT | WT | S311A | S311A |
| JQ1, nM | 0 | 500 | 0 | 500 |

Flag-Axin2

AR

GAPDH

| AR/GAPDH | 1.00 | 0.42 | 0.78 | 0.30 |
| AR-V/GAPDH | 1.00 | 0.46 | 0.82 | 0.36 |

c-Myc

GAPDH

| c-Myc/GAPDH | 1.00 | 0.33 | 0.91 | 0.16 |

Figure 4. The synergistic effect of GSK461364A plus JQ1 in 22Rv1 and C4-2 cells is due to suppression of AR signaling and c-Myc.

(A-B) 22Rv1 cells and C4-2 cells (3 x 10^5) were treated for 48h with indicated drugs, followed by IB to detect AR, c-Myc, and PSA. (C-E) 22Rv1 cells (3 x 10^5) and C4-2 cells (2 x 10^5) were transfected with Flag-Axin2 plasmids (WT or S311A) and treated with 500 nM JQ1 for 48h, followed by IB to detect the levels of Flag, cleaved PARP, AR, c-Myc, and PSA.
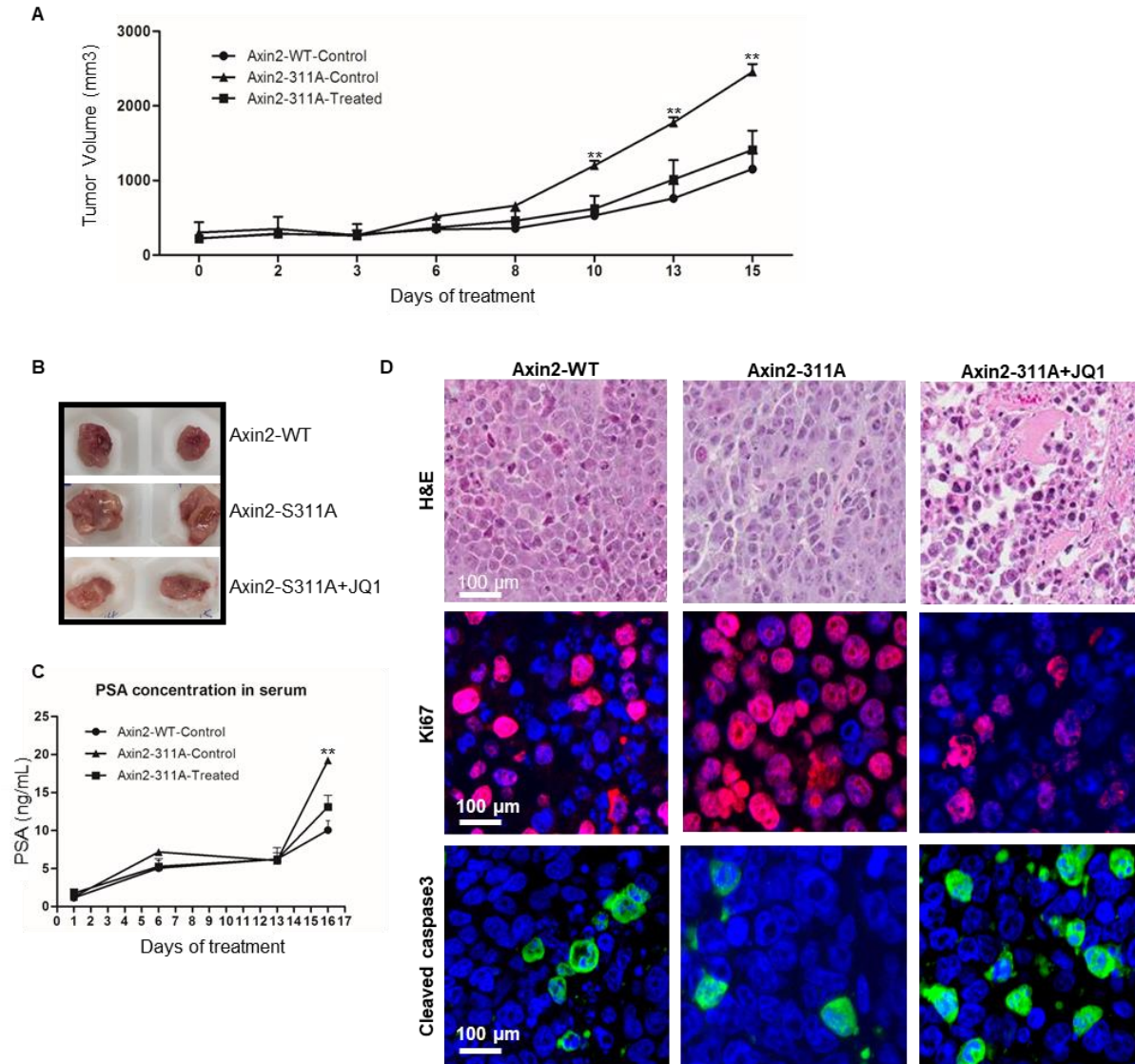
Figure 5. Xenograft tumors derived from 22Rv1 cells expressing Axin2-S311A mutant are more sensitive to JQ1 treatment than those expressing WT Axin2.

(A) Growth curves of tumors derived from 22Rv1 cells expressing different forms of Axin2 (WT or S311A). 22Rv1 cells (2.5×10^5) expressing either Axin2-WT or Axin2-S311A were implanted into pre-castrated NSG mice for 22 days and administrated with JQ1 (6.25 mg/kg body weight) by oral gavage every 3 days, followed by measurement of tumor sizes (mean $\pm$ SEM; n = 4 mice from each experiment group). **, $P < 0.01$. (B) Representative images of the fresh tumors were taken at the end of the study. (C) Serum PSA levels were measured for tumor-bearing mice using a PSA Elisa Kit (mean $\pm$ SEM; n=4 mice from each experiment group). **, $P < 0.01$. (D) Representative images of H&E staining and IF staining for Ki67 and cleaved caspase-3 on formaldehyde-fixed, paraffin-embedded tumor sections from different treatment groups as in (A).

46
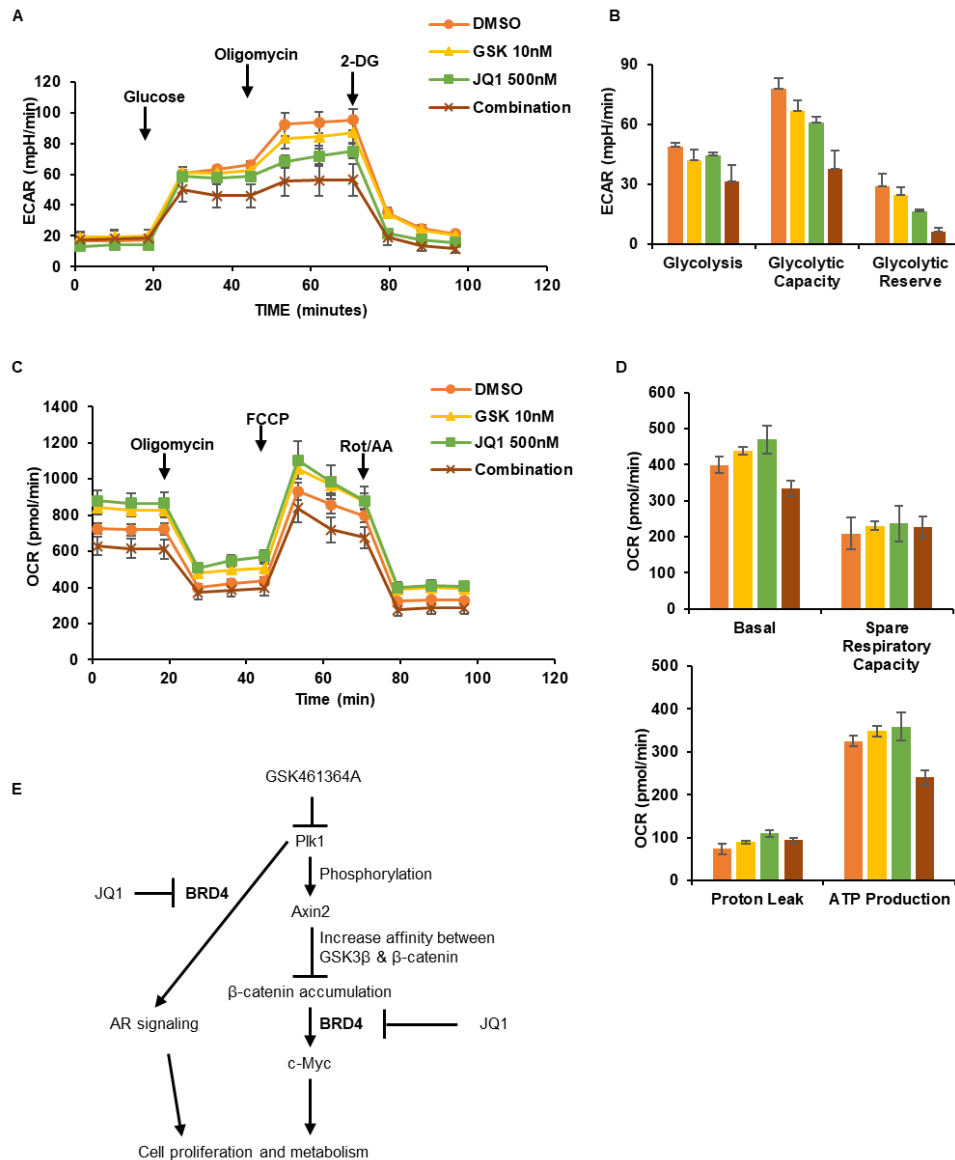
Figure 6. Co-treatment with GSK461364A and JQ1 dramatically inhibits cell metabolism.

(A) Glycolytic rate was measured under single or dual treatment by Seahorse. 22Rv1 cells were treated with indicated drugs for 24h and subjected to the protocol in which glucose, oligoMycin, and 2-deoxyglucose (2-DG) were added at the time points indicated. (B) Calculated glycolysis rates, glycolysis capacity, and glycolytic reserve. The data were normalized by the relative cell number. (C) Oxidative phosphorylation under single or dual treatment was measured by Seahorse. 22Rv1 cells were treated with GSK461364A, JQ1, or both for 24h and subjected to the protocol in which oligoMycin, FCCP, and Rotenone/antiMycin A were added at the time points indicated. (D) Calculated basal respiratory rate, spare respiratory capacity, proton leak, and ATP production. The data were normalized by the relative cell number. (E) Proposed working model for JQ1 and GSK461364A.
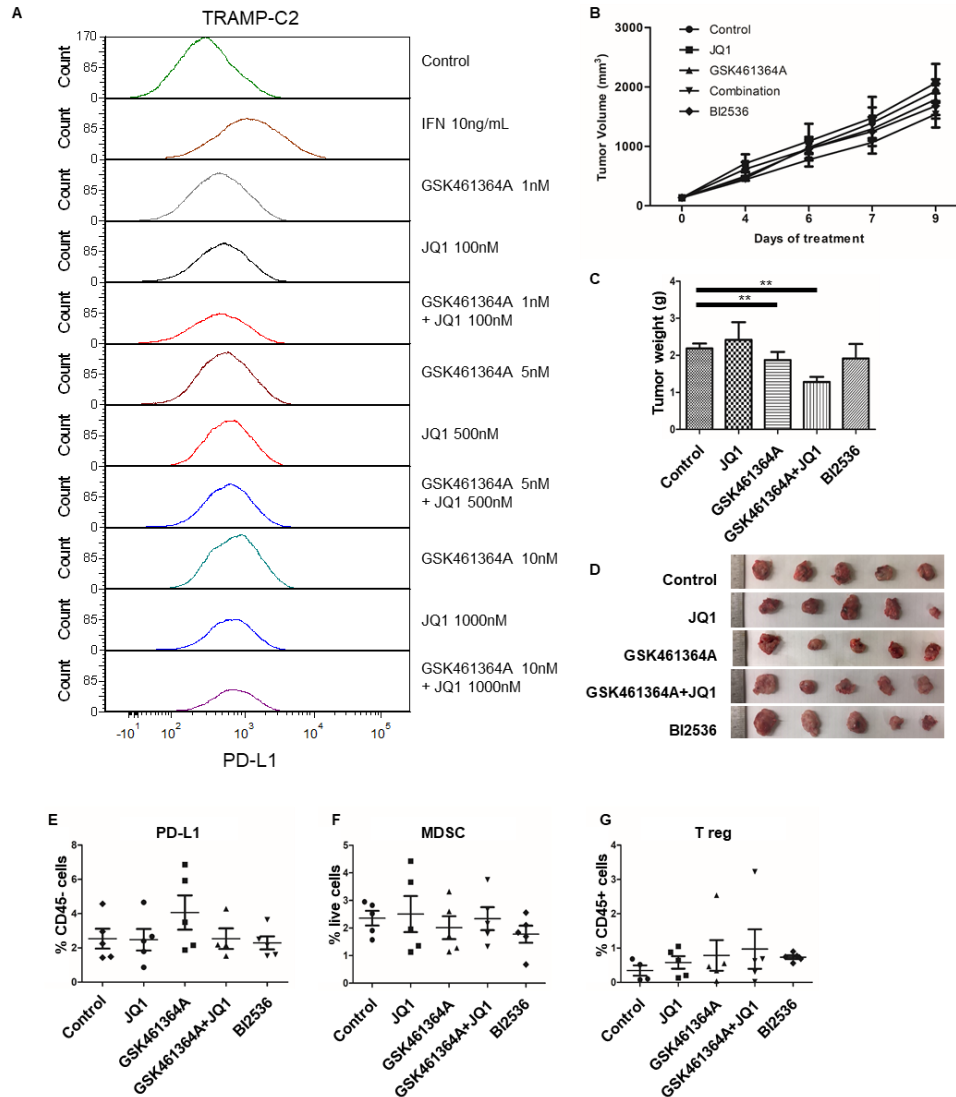
Figure 7. Co-treatment of GSK461364A and JQ1 has a minor effect on PD-L1 expression

(A) TRAMP-C2 cells were treated with indicated drugs for 72h, followed by flow cytometry to detect the PD-L1exrpession level. (B) Growth curve of TRMAP-C2 derived tumors. C57/B6 mice inoculated with TRAMP-C2 cells and randomly assigned into 5 groups, administered with either vehicle, GSK461364A (12 mg/kg body weight, intravenous injection), JQ1 (25 mg/kg body weight, oral gavage), a combination of both drugs, or BI2536 (18 mg/kg body weight, intravenous injection). The sizes of the tumors in each group were measured along with every treatment (mean ± SEM; n = 5 mice from each experiment group). (C) Tumors weighed right after being freshly removed from the bodies. **, P < 0.01. (D) Representative images of the tumors at the end of the study. (E-G) Tumors were digested into single cells after harvest and stained with corresponding antibodies for 30 min. 100,000 cells were analyzed per sample by flow cytometry. E) Quantification of PD-L1-positive cells in cancer cells. F) Quantification of MDSC cells within live cells. G) Quantification of T-reg cells within total immune cells.

CHAPTER. 4   PLK1 FUNCTIONS AS AN ONCOGENE TO PROMOTE THE PROGRESSION AND METASTASIS IN MELANOMA

4.1   Introduction

Melanoma is one of the most frequently diagnosed cancers in the Caucasian population of both genders, representing the most aggressive and deadliest form of skin cancer (199, 200). According to the American Cancer Society, the 5-year-survival rate for localized melanoma patients could achieve as high as 98.7%. In contrast, once melanoma develops into higher grade and metastasizes to distant organs, the patient survival will be exceedingly poor, as low as 27.3% (201, 202). Melanoma arises from the melanocytes carrying genetic mutations (203). As reported, over 50% of patients with advanced melanoma harboring activating mutations in BRAF oncogene (204, 205). Importantly, BRAF V600E is the most common mutation found clinically, resulting in the robust increase of kinase activity and constitutive activation of MAPK (mitogen-activated protein kinase) signaling pathway (206-208). PLX-4032 (Vemurafenib) (209), a specific inhibitor of mutant BRAF, has shown an impressive response in phase 3 clinical trial and has been approved for the treatment of metastatic malignant melanoma by FDA in 2011 (210). However, due to the rapid development of resistance, the duration of response under the single treatment is frequently short (overall ~6 months) (210, 211), highlighting the urgent requirement for the novel therapy in melanoma treatment.

Polo-like kinase 1 (PLK1) has been demonstrated as a novel target in cancer treatment recently (162). PLK1, a crucial cell cycle regulator, participates in multiple mitotic processes, including centrosome maturation, mitotic entry, spindle assembly, sister chromatid segregation, mitotic exit, and cytokinesis (212). Compared to the normal tissues, the expression level of PLK1 is significantly elevated in multiple cancers (174). Most importantly, the expression level of PLK1 negatively correlates with the melanoma patients' survival period based on the TCGA database (213). Furthermore, PLK1 has been identified as an oncogene to promote proliferation, motility, and resistance to various drugs, including doxorubicin, gemcitabine, and taxol, in a variety of cancers (107, 160, 214, 215). Above all, accumulating evidence has indicated PLK1 as a potent and promising target in cancer treatment. Currently, various PLK1 inhibitors are under clinical trials to validate their efficacy and safety profiles in several cancer types (74). BI6727 (volasertib),

a highly potent ATP-competitive inhibitor of PLK1 (216), has been shown to impede cell proliferation, induce cell cycle arrest, and promote cell death (217, 218).

In our study, we have shown a strong synergistic effect in the combined treatment of BI6727 and PLX-4032 in BRAF V600E mutant A375 and PLX-4032-resistant A375R cells. This novel combination therapy has shown an improved efficacy on inhibition of cell proliferation, induction of cell death, and suppression of cell metastasis *in vitro* compared to mono-treatment. Further, it has been validated *in vivo* by the A375R-derived xenograft model. Importantly, overexpression of PLK1 promotes tumor growth and metastasis in $Braf^{CA/+} / Pten^{loxp/loxp}$ mouse model, whereas knocking out PLK1 would dramatically suppress melanoma progression.

4.2 Results

4.2.1 *Plk1* is involved in melanoma progression

It has been well established that higher PLK1 expression is negatively associated with survival prognoses of patients in multiple cancer types (14). Based on the analysis of the TCGA database (14), patients with higher *PLK1* expression showed a dramatic reduction in overall survival period (Figure 8A), as well as disease-free survival, compared to patients with low-*PLK1* expression. To further confirm PLK1's role in melanoma progression, we have crossed the existing melanoma mouse model $Braf^{CA/+} / Pten^{loxp/loxp}$ (219, 220) with either *Plk1-KI* (221) or $Plk1^{loxp/loxp}$ mice (72), respectively. 4-OH-Tamoxifen was applied to the flank region of the female mice at 4 to 6-week-old to induce the expression of transgenes (Figure 8B). Consistent with human patients, overexpression of *Plk1* significantly shortened the survival period in the melanoma mouse model, and the median survival length decreased from 59 d to 44 d compared to $Braf^{CA/+} / Pten^{loxp/loxp}$ mice (Figure 8C). Moreover, the size of primary tumors significantly increased in $Braf^{CA/+} / Pten^{loxp/loxp} / Plk1-KI$ mice (Figure 8D). Meanwhile, the expression level of *Plk1* was dramatically elevated in $Braf^{CA/+} / Pten^{loxp/loxp} / Plk1-KI$ mice in both mRNA (Figure 8E) and protein levels (Figure 8F). On the contrary, although $Braf^{CA/+} / Pten^{loxp/loxp} / Plk1^{loxp/loxp}$ mice could eventually develop tumors, the tumor formation and progression were significantly delayed, as well as prolonged survival period, as indicated in Figures 8G and 8H. Interestingly, one allele knockdown of *Plk1* has shown

no significant effect on tumor formation compared to $Braf^{CA/+}$ / $Pten^{loxp/loxp}$ mice. Overall, the expression level of *Plk1* is tightly related to the progression of melanoma.

4.2.2   *Plk1* induces melanoma metastasis in *Braf*$^{CA/+}$/ *Pten*$^{loxp/loxp}$ mouse model

Previously, abundant researches have demonstrated that PLK1 is related to cancer metastasis in multiple cancers (160, 222, 223). Similarly, *Plk1* promoted metastasis in $Braf^{CA/+}$/ $Pten^{loxp/loxp}$ mice. As indicated in Figures 9A and 9B, a dramatic increase in the metastasis to draining lymph nodes has been observed in mice with higher *Plk1* expression. Besides, the frequency of distant metastasis had elevated upon the overexpression of *Plk1* (Figure 9C). Histologically, robust invasion across the muscle layer under the skin and increasing metastatic loci in lymph nodes were present in $Braf^{CA/+}$ / $Pten^{loxp/loxp}$ / *Plk1-KI* mice compared to $Braf^{CA/+}$ / $Pten^{loxp/loxp}$ mice (Figures 9D and 9E). Intriguingly, Sox10, a melanoma marker to promote melanoma progression (224), was expressed excessively in $Braf^{CA/+}$ / $Pten^{loxp/loxp}$ / *Plk1-KI* mice (Figure 9F).

4.2.3   Plk1 promotes melanoma progression *in vitro*

To further investigate the role and function of *Plk1* in melanoma, the mouse melanoma tumors were digested and cultured *in vitro* to establish mouse melanoma cell lines mMC ($Braf^{CA/+}$ / $Pten^{loxp/loxp}$) and mMPI ($Braf^{CA/+}$ / $Pten^{loxp/loxp}$ / *Plk1-KI*). In contrast to mMC, mMPI showed a higher level of Plk1 expression, as well as a larger cell volume and different morphology (Figures 10A and 10B). Meanwhile, the ability of migration and colony formation has also robustly increased in mMPI cells (Figures 10C and 10D). To assess whether Plk1 impacts sphere formation ability, we cultured mMC and mMPI cells in a 3D environment and found a dramatic elevation in the sphere size upon Plk1 expression (Figures 10E and 10F). Based on previous publications (225, 226), the morphology of tumorspheres could reflect the gene expression profile of distinct cell types. Compared to mass-shaped tumorsphere, the stellate-shape usually indicates a lack of robust cell-cell adhesion and represents an invasive phenotype. Significantly, as high as 75% of mMPI tumorspheres exhibited the stellate shape, 3-fold compared to mMC, suggesting an intensive metastatic capability (Figure 10G) (225). Furthermore, Plk1 also promoted cell invasive ability, as well as drug resistance to PLX-4032 treatment (Figures 10H and 10I).

4.2.4 Plk1 affects the metabolism of mouse melanoma cells

As melanoma metastasis is tightly related to metabolic adaption (227), metabolic activity was evaluated by the use of mMC and mMPI cells. Based on the seahorse analysis, higher Plk1 expression induces both basal and compensatory glycolysis (Figure 11A). However, treatment with 2-NBDG, a fluorescent glucose analog, showed that the glucose uptake was decreased in mMPI cells, suggesting that the portion of glycolysis in glucose utilization increased (Figure 11B). Besides, as indicated by Mitotraker Green, the active mitochondrial mass was significantly decreased in mMPI cells (Figure 11C). Intriguingly, although there was no significant difference in the basal respiration level, the maximal oxidative phosphorylation rate and coupling efficiency were significantly increased in mMPI cells compared to mMC cells (Figures 11D and 11E), arguing that the mitochondrial activity was much higher and more efficient in mMPI cells. Furthermore, a previous publication has demonstrated that oxidative stress could suppress distant metastasis of melanoma (228). In agreement, the percentage of high oxidative stress population was dramatically decreased in mMPI cells as indicated in Figure 11F. In summary, Plk1 overexpression significantly elevates both glycolysis and oxidative phosphorylation in mouse melanoma cells.

4.2.5 PLK1 induces metastasis and drug resistance in human melanoma cells

To further confirm PLK1's role in human melanoma cells, we have first tested the expression of PLK1 in A375 cells and PLX-4032-resistant A375R cells. Compared to A375, there was a significant elevation of PLK1 expression level in A375R cells, as well as the metastatic marker N-Cadherin, as indicated in Figure 12A (comparing lane 1 vs lane 4), suggesting that higher PLK1 may contribute to metastasis and drug resistance. To test such a hypothesis, we manipulated the expression levels of PLK1 in A375 and A375R cells. Knocking down of PLK1 inhibited expression of two metastatic markers N-Cadherin and Vimentin in both mouse melanoma B16-F10 cells and A375 cells (Figures 12B and 12C). Besides, the ability to heal the wound was diminished considerably upon PLK1 knockdown in A375R cells (Figure 12D). Moreover, lower PLK1 expression significantly sensitized the cells toward PLX-4032 treatment in both A375 and A375R cells (Figures 12E and 12F). Remarkably, stably overexpression of PLK1 leads to the increased metastasis and resistance to PLX-4032 in A375 cells, but such an effect was not as

dramatic as A375R cells that have an elevated level of PLk1 to begin with (Figures 12G-12J). In summary, our data has demonstrated that PLK1 could promote metastasis and drug resistance in human melanoma cells.

4.2.6 PLK1 inhibitor acts synergistically with PLX-4032 in human melanoma cells

Because PLK1 overexpression resulted in resistance to PLX-4032 in A375 cells, which carry BRAF V600E mutation, we asked whether inhibition of PLK1 is a new approach to enhance the efficacy of PLX-4032 in melanoma cells. Combination indices of two inhibitors (BI6727 and PLX-4032) were calculated to be 0.667 and 0.750 in A375 and A375R cells, respectively, suggesting a synergistic effect of two inhibitors (Tables 3 and 4). To further assess the efficiency of the combination of BI6727 and PLX-4032, we analyzed cell death induced by drug treatment and showed that the combination treatment could robustly induce cell apoptosis compared to the single drug-treated groups (Figures 13A-13D). Interestingly, the co-treatment induced cell cycle arrest at the G1 phase in A375 cells, whereas it caused the G2/M phase arrest in A375R cells (Figures 13E and 13F), indicating the differences in the cell cycle regulation between A375 and A375R cells. Moreover, even under low drug concentration, BI6727 and PLX-4032 could act cooperatively in the inhibition of cell proliferation (Figures 13G and 13H) and the ability to form colonies as well (Figures 13I and 13J), in comparison to the mono-therapies. To investigate whether the metastatic ability is affected by the combination therapy, we performed wound healing assays and transwell migration assays (Figures 13K and 13L). As expected, metastasis was dramatically diminished in both A375 and A375R cells upon the combination treatment, compared with either the control, PLX-4032-treated, or BI6727-treated group. In conclusion, our *in vitro* experiments have indicated that BI6727 and PLX-4032 could act cooperatively in the treatment of human melanoma cells, leading to the suppression of cell proliferation, induction of apoptosis, arrest of the cell cycle, and repression of metastasis.

4.2.7 BI6727 and PLX-4032 cooperatively inhibit A375R-derived xenograft *in vivo*

To better validate our previous finding *in vitro*, we have evaluated whether BI6727 and PLX-4032 act synergistically *in vivo* by using an A375R-derived xenograft model. Compared to the control group, A375R-derived tumors have exhibited a very limited response toward the single treatment

of PLX-4032, as shown in Figure 14A. Significantly, even though BI6727 itself has shown dramatic suppression, PLX-4032 could further facilitate and greatly enhance the efficiency of BI6727 in the inhibition of cell proliferation and tumor weights (Figures 14A-14C). Furthermore, as a result of the combination treatment of BI6727 and PLX-4032, several key regulators have been significantly repressed compared to either control or single drug-treated groups, including MAPK signaling pathway (p-BRaf and p-ERK), metastatic markers (N-Cadherin and Vimentin), proliferative marker PCNA, and melanoma-related transcription factor SOX10 (Figure 14D). Histologically, the remarkable decrease in cell content and dramatic elevation in apoptotic bodies have been detected in the tumor samples under the treatment of dual inhibitors, in comparison to control and mono-treated groups (Figure 14E). To conclude, it has been well demonstrated that PLK1 inhibitor BI6727 and BRAF V600E inhibitor PLX-4032 cooperatively suppress the growth of the A375R-derived xenograft model *in vivo*.

4.3 Discussion

It has been well documented that PLK1 is tightly related to multiple steps of the cell cycle and participates in the regulation of various cancer-related signaling pathways (74). Accumulating evidence has shown that PLK1 is highly expressed in multiple cancer types and negatively correlated with the patients' survival (14). To evaluate Plk1's role and function in melanoma progression, we have crossed the existing melanoma mouse model $Braf^{CA/+} / Pten^{loxp/loxp}$ with either *Plk1-KI* or *Plk1$^{loxp/loxp}$* mice (219, 220), followed by the monitoring of melanoma progression as indicated in Figure 8B. Significantly, in comparison to $Braf^{CA/+} / Pten^{loxp/loxp}$ mice, overexpression of *Plk1* accelerated melanoma progression and metastasis (Figures 8C, 8D, and 9A-9F), whereas knocking out of *Plk1* significantly improved the overall survival (Figures 8G and 8H). Moreover, mMPI cells, derived from $Braf^{CA/+} / Pten^{loxp/loxp} / Plk1-KI$ mice, showed a robust increase in the metastatic capability, as well as resistance to PLX-4032, compared to mMC cells derived from $Braf^{CA/+} / Pten^{loxp/loxp}$ mice in both 2D and 3D culture (Figures 10A-10I). Intriguingly, a higher expression level of *Plk1* also contributes to the metabolic reprogramming, not only promoting glycolysis but also elevating the capacity and efficiency of oxidative phosphorylation (Figures 11A-11E). In parallel, oxidative stress also has been dramatically suppressed in mMPI cells compared to mMC cells, suggesting a potential mechanism for the *Plk1*-induced metastasis (Figure

11F). Overall, *Plk1* functions as an oncogene to induce the progression and metastasis of mouse melanoma, likely via regulating energy metabolism.

PLX-4032 (Vemurafenib), a well-established and FDA-approved drug, has been the most effective therapy to treat the malignant melanoma patients harboring BRAF V600E mutation (210). Due to the fast emergence of resistance, a novel therapeutic strategy is urgently needed in the treatment of localized and metastatic melanoma. In our study, compared to parental A375 cells, PLX-4032-resistant A375R cells exhibit a higher expression level of PLK1, indicating that PLK1 may contribute to the drug resistance of PLX-4032 (Figure 12A). To validate our hypothesis, we compared responses to PLX-4032 in isogenic melanoma cells with different levels of PLK1. We found that PLK1 depletion inhibited the metastasis and sensitized the cells to PLX-4032 and that overexpression of PLK1 significantly increased the expression level of metastatic markers and rendered the cells to be resistant to PLX-4032 (Figures 12G and 12J). Further, we have demonstrated that PLK1 inhibitor BI6727 could cooperate with PLX-4032 to treat melanoma (Figure 13). The combination of BI6727 and PLX-4032 could act synergistically from multiple aspects, including proliferation, apoptosis, cell cycle arrest, and metastasis. Moreover, the efficacy of BI6727 and PLX-4032 has been further confirmed in the A375R-derived xenograft model (Figure 14), showing the inhibition of tumor growth, induction of apoptosis, and suppression of cancer-associated signaling pathway. In conclusion, our *in vitro* and *in vivo* data had demonstrated that BI6727 could robustly enhance the efficacy of PLX-4032 in both sensitive and resistant human melanoma cells.

To summarize, our data has indicated that PLK1 functions as a critical regulator to promote progression, metastasis, and drug resistance in melanoma, making it a potential and promising target to be further tested and applied in clinical.

Table 3. The IC$_{50}$ values of BI6727 and PLX-4032 in A375 cells

Drugs	IC$_{50}$	CI
BI6727	6nM	
PLX-4032	100nM	
BI6727 (in combination 50nM/L PLX-4032)	1nM	CI=0.667

Table 4. The IC$_{50}$ values of BI6727 and PLX-4032 in A375R cells

Drugs	IC$_{50}$	CI
BI6727	11nM	
PLX-4032	10uM	
BI6727 (in combination 2.5uM/L PLX-4032)	5.5nM	CI=0.750

Figure 8. Plk1 involves in mouse melanoma progression

(A) Plk1 expression is negatively correlated to human melanoma patient survival. The plot was generated by OncoLnc based on the TCGA survival data (213). (B) Schematic showing the breeding strategy and inducing method. (C) The survival curve of $Braf^{CA/+}$ / $Pten^{loxp/loxp}$ / $Plk1$-KI mice versus $Braf^{CA/+}$ / $Pten^{loxp/loxp}$ mice. The mice were euthanized when the tumor diameters reached 15mm. The median survival period is 44 and 59, respectively, in $Braf^{CA/+}$ / $Pten^{loxp/loxp}$ / $Plk1$-KI mice and $Braf^{CA/+}$ / $Pten^{loxp/loxp}$ mice. (D) After 40d of localized induction, the mice were euthanized and tumor diameter was measured. (E) The mRNA level of $Plk1$ in melanoma was harvested from mice with indicated genotypes. (F) Representative IHC staining for Plk1in the locally induced melanoma. (G) The survival curve of $Braf^{CA/+}$ / $Pten^{loxp/loxp}$ mice versus $Braf^{CA/+}$ / $Pten^{loxp/loxp}$ / $Plk1^{loxp/-}$ mice versus $Braf^{CA/+}$ / $Pten^{loxp/loxp}$ / $Plk1^{loxp/loxp}$ mice. The mice were euthanized when the tumor diameters reached 15mm. The median survival period is 59, 62, and 131 respectively. (H) Representative images of localized melanoma tumors formed in $Braf^{CA/+}$ / $Pten^{loxp/loxp}$ / $Plk1^{loxp/-}$ mouse and $Braf^{CA/+}$ / $Pten^{loxp/loxp}$ / $Plk1^{loxp/loxp}$ mouse after 59d and 129d induction, respectively. $P>0.05$, N.S.; $P<0.05$, *; $P<0.01$, ** by student t-test.

Figure 8 continued

A

B

C
Survival curve

— $Braf^{CA/+} / Pten^{loxp/loxp}$
— $Braf^{CA/+} / Pten^{loxp/loxp} / Plk1\text{-}KI$

Gehan-Breslow-Wilcoxon Test
P=0.0150

1 ul 20 mM 4-OH-Tamaxifen was applied to skin to induce localized tumor

D
Tumor size

P=0.0258

E
$Plk1$

P<0.0001

F

$Braf^{CA/+} / Pten^{loxp/loxp}$ $Braf^{CA/+} / Pten^{loxp/loxp} / Plk1\text{-}KI$

Plk1

G
Survival curve

— $Braf^{CA/+} / Pten^{loxp/loxp}$
— $Braf^{CA/+} / Pten^{loxp/loxp} / Plk1^{loxp/-}$
— $Braf^{CA/+} / Pten^{loxp/loxp} / Plk1^{loxp/loxp}$

H

Day 59
$Braf^{CA/+}$
$Pten^{loxp/loxp}$
$Plk1^{loxp/-}$

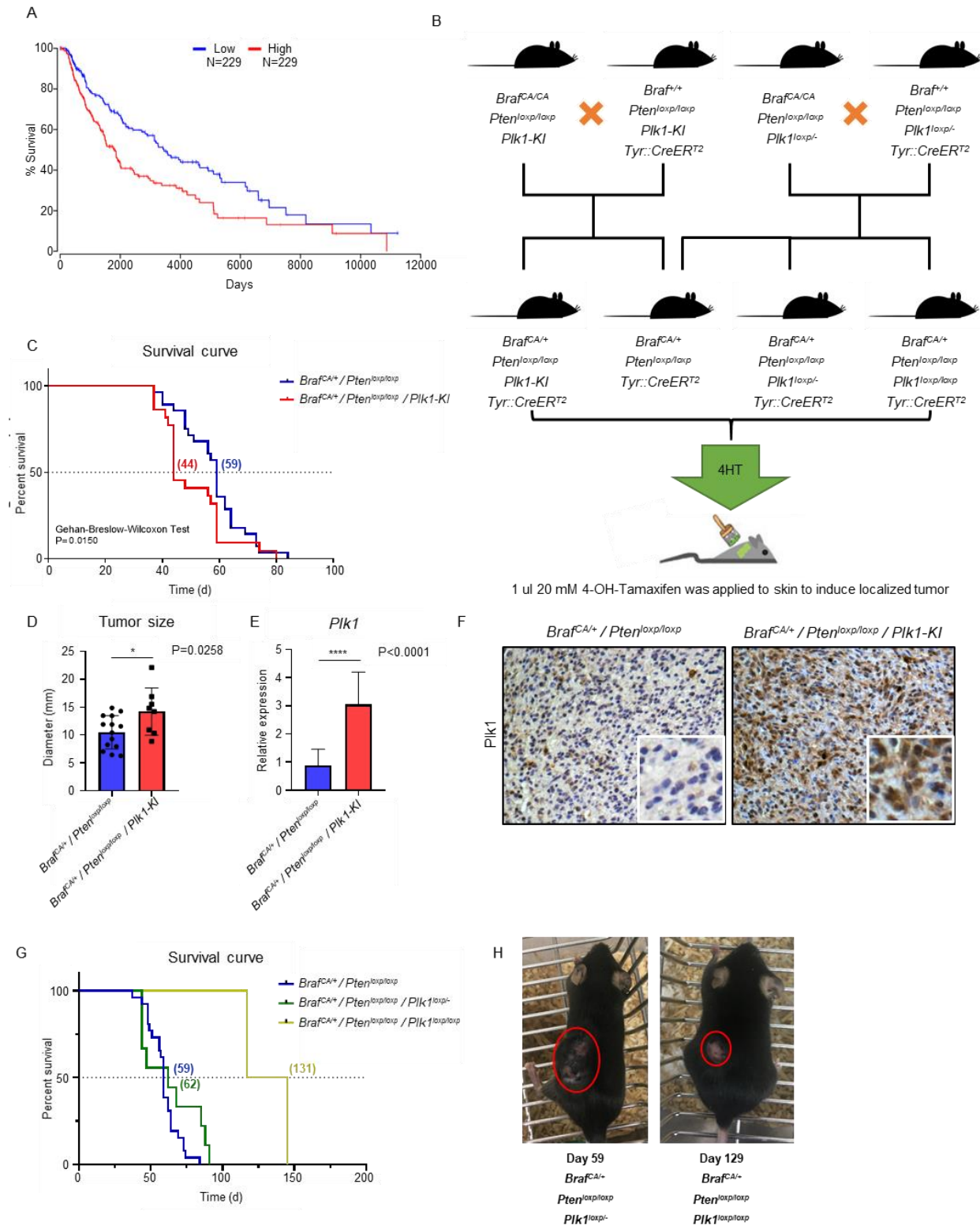Day 129
$Braf^{CA/-}$
$Pten^{loxp/loxp}$
$Plk1^{loxp/loxp}$

Figure 9. Plk1 induces metastasis in $Braf^{CA/+} / Pten^{loxp/loxp}$ mouse model

(A) Representative images of lymph nodes exhibiting the different extent of metastatic melanoma loci. (B) Quantification of metastasis to lymph nodes in $Braf^{CA/+} / Pten^{loxp/loxp}$ and $Braf^{CA/+} / Pten^{loxp/loxp} / Plk1$-$KI$ mice. The localized tumors were induced in the mice with indicated genotype. After 40d, the mice were sacrificed and the lymph nodes were harvested for histology staining. (C) Representative images and quantification of distant metastasis found in indicated mice. (D) H&E stained sections of locally induced tumors from a $Braf^{CA/+} / Pten^{loxp/loxp}$ mice and a $Braf^{CA/+} / Pten^{loxp/loxp} / Plk1$-$KI$ mouse. The Blue arrow indicates the muscle layer. Compared to the $Braf^{CA/+} / Pten^{loxp/loxp}$ mouse, melanoma cells had crossed the muscle layer and showed an elevated invasive ability in PLK1 overexpressed mice. (E) Representative images of H&E stained tumor-draining lymph node from a $Braf^{CA/+} / Pten^{loxp/loxp}$ mouse and a $Braf^{CA/+} / Pten^{loxp/loxp} / Plk1$-$KI$ mouse. (F) Representative images of IHC staining for Sox10 of primary tumor from a $Braf^{CA/+} / Pten^{loxp/loxp}$ mouse and a $Braf^{CA/+} / Pten^{loxp/loxp} / Plk1$-$KI$ mouse. $P>0.05$, N.S.; $P<0.05$, *; $P<0.01$, ** by student t-test.

Figure 9 continued

A

Naïve   Micro-metastasis   Macro-metastasis

B

LN metastasis

$Braf^{CA/+}/Pten^{loxp/loxp}$

$Braf^{CA/+}/Pten^{loxp/loxp}/Plk1-KI$

P=0.0605 N.S.

P=0.0031 **

C

Percentage of GEM mice with distant metastases

Genotype	#	(%)
$Braf^{CA/+}/Pten^{loxp/loxp}$	2/22	9.09
$Braf^{CA/+}/Pten^{loxp/loxp}/Plk1-KI$	4/19	21.05

D

$Braf^{CA/+}/Pten^{loxp/loxp}$ $Braf^{CA/+}/Pten^{loxp/loxp}/Plk1-KI$

E

$Braf^{CA/+}/Pten^{loxp/loxp}$ $Braf^{CA/+}/Pten^{loxp/loxp}/Plk1-KI$

F

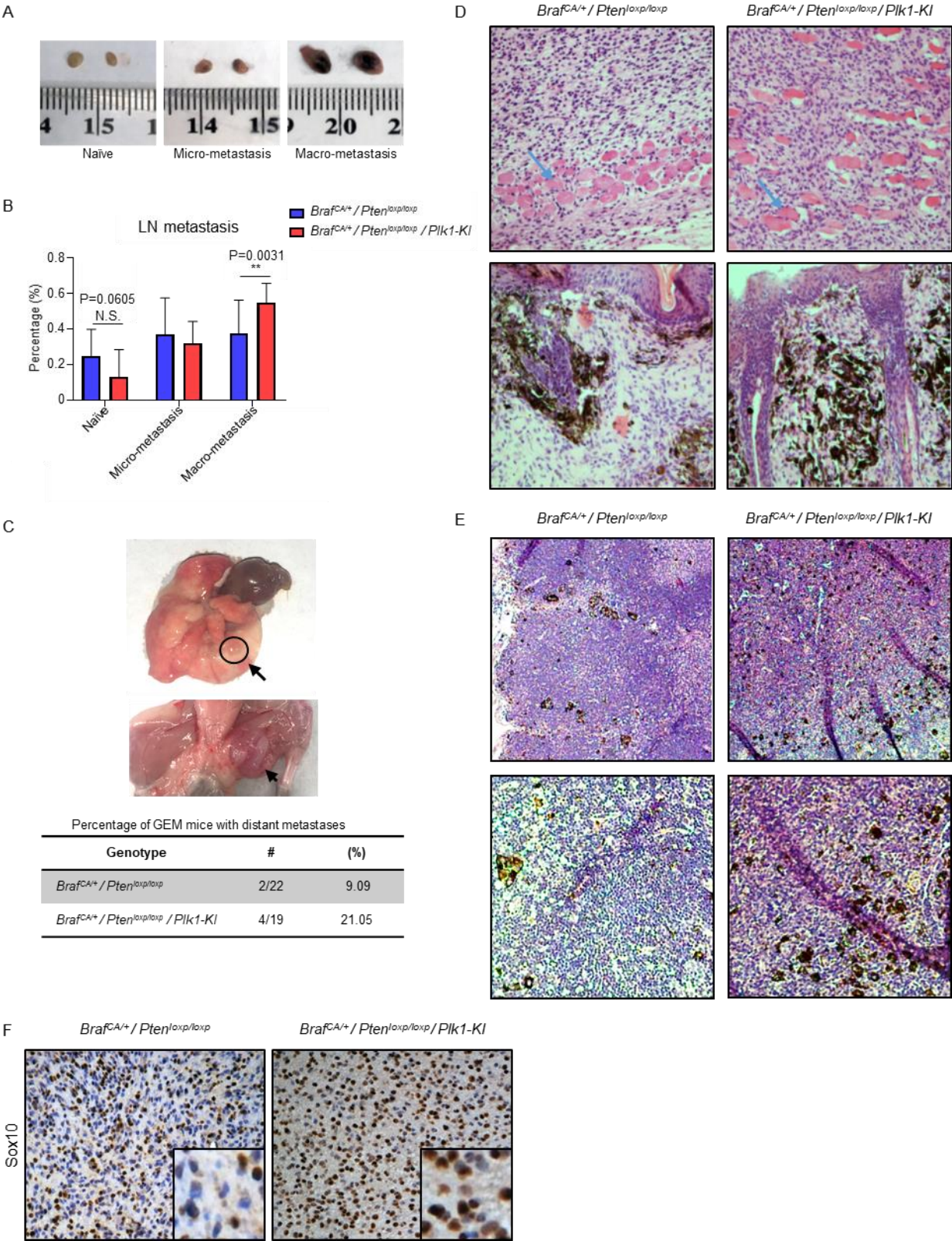$Braf^{CA/+}/Pten^{loxp/loxp}$ $Braf^{CA/+}/Pten^{loxp/loxp}/Plk1-KI$

Sox10

60

Figure 10. Plk1 promotes mouse melanoma progression *in vitro*

(A) Western blots showing the Plk1 expression level of mMC (derived from $Braf^{CA/+}$ / $Pten^{loxp/loxp}$ mouse) and mMPI (derived from $Braf^{CA/+}$ / $Pten^{loxp/loxp}$ / *Plk1-KI* mouse). (B) Representative images of the morphology of mMC and mMPI. (C) Representative images of transwell migration assay to analyze the metastatic ability using mMC and mMPI cells. (D) Representative images (Left) and quantification (Right) of colony formation assay using mMC and mMPI cells. (E and F) Representative images (Left) and quantification (Right) of sphere formation in the 3D matrix using mMC and mMPI cells in day 3 (E) or day 5 (F), respectively. (G) Quantification of sphere morphology formed in the 3D matrix. (H) Representative images of transwell invasion assay to assess the metastatic ability using mMC and mMPI cells. (I) Relative cell viability under the treatment of PLX-4032 at different concentrations in mMC and mMPI cells. $P>0.05$, N.S.; $P<0.05$, *; $P<0.01$, ** by student t-test.
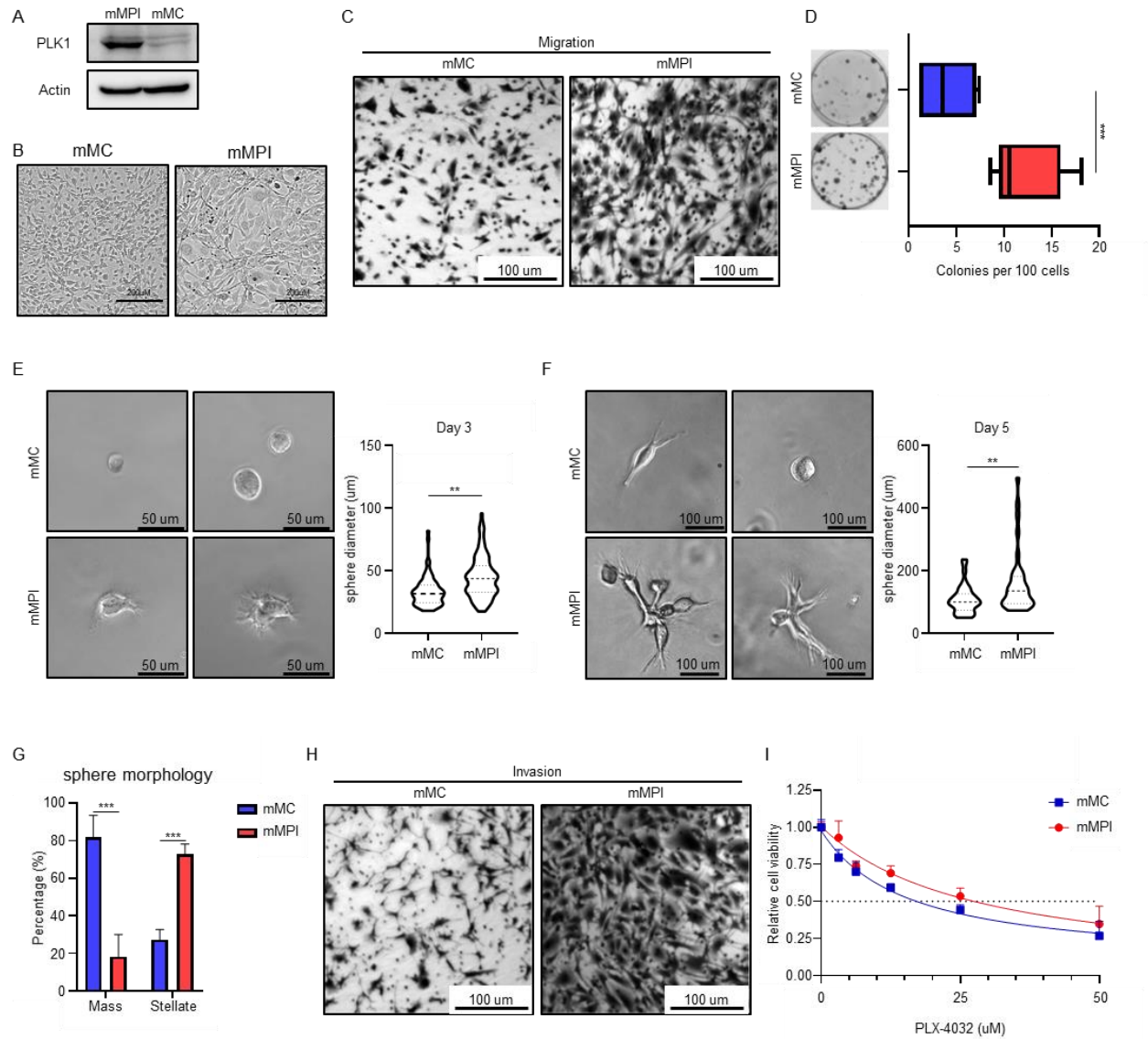
Figure 10 continued

Figure 11. Plk1 impacts the metabolism of mouse melanoma cells

(A)   Glycolytic rate of mMC and mMPI cells was measured by seahorse. (B) Glucose uptake was measured using the 2-NBDG probe in mMC and mMPI cells by flow cytometry. (C) Mitochondria mass was measured using MitoTrakcer Green FM dye in mMC and mMPI cells by flow cytometry. (D) Mitochondrial oxidative phosphorylation was measure by seahorse. (E) Calculated values for respiratory parameters in the indicated cells. (F) Mitochondria oxidative stress of mMC and mMPI was measured using the MitoSOX superoxide indicator by flow cytometry. Left: MitoSOX signal detected by flow cytometry; Right: percentage of MitoSOX-high population among all the cells.
$P > 0.05$, N.S.; $P < 0.05$, *; $P < 0.01$, ** by student t-test.
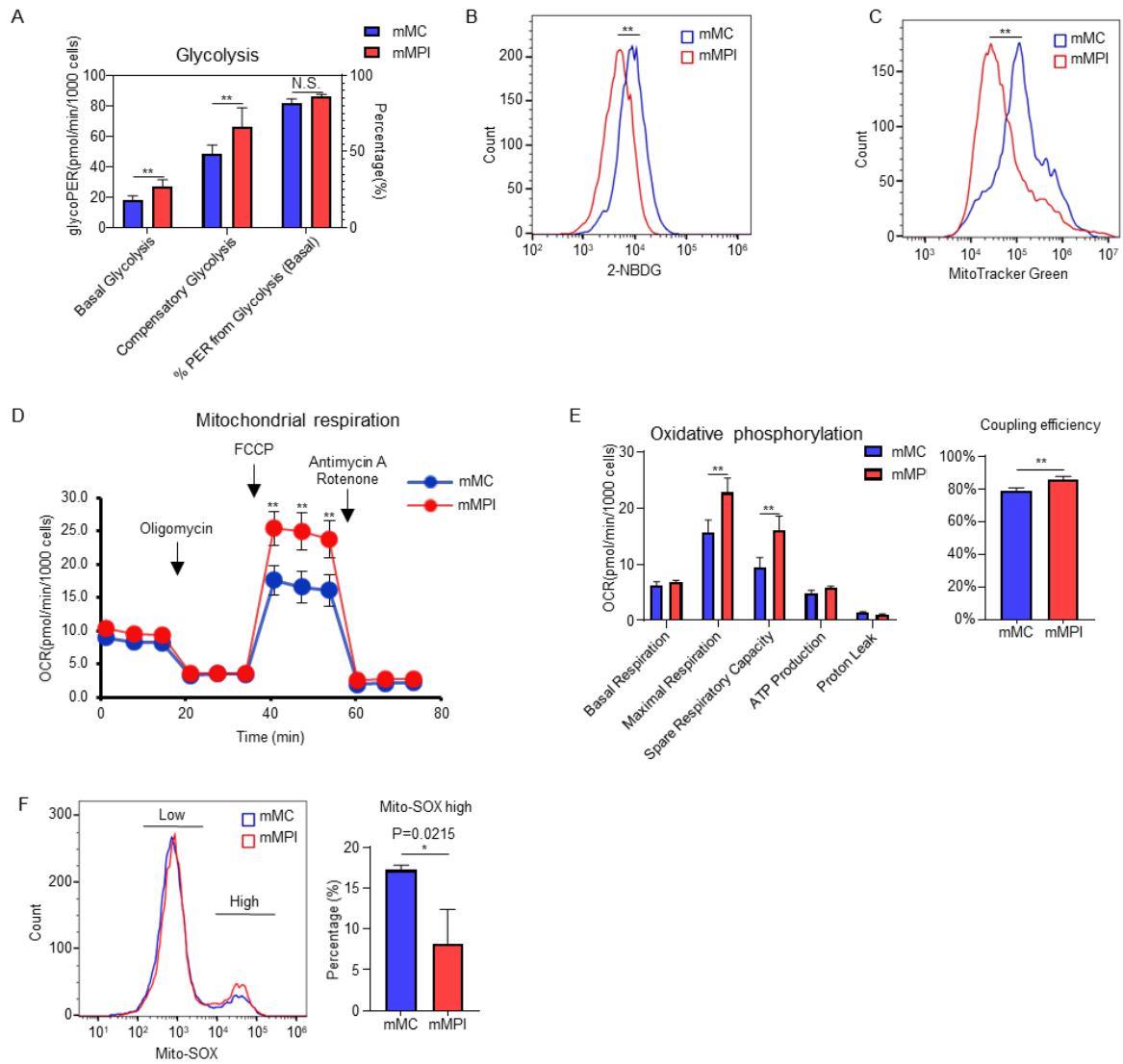
Figure 11 continued

Figure 12. PLK1 overexpression promotes metastasis and PLX-4032 resistance in human melanoma cell lines

(A) Western analysis of PLK1 and N-cadherin expression level in A375 and A375R cells after 24 h treatment of either DMSO or BI6727. (B) The Plk1 was stably knocked down in mouse melanoma cell line B16-F10, in which PLK1 and N-cadherin expression levels were detected by western blot. (C) A375 cells either stabling expressing shCtrl or shPLK1 were treated with indicated PLX-4032 for 72h, then the PLK1 and Vimentin were measured by western. (D) The wound healing assay was conducted using A375R-shCtrl and A375R-shPLK1 cells. The relative distance was measured and quantified after 12h. (E-F) The relative cell viability of A375 (E) and A375R (F), expressing either shCtrl or shPLK1, was measured under the 72h treatment of PLX-4032 with various drug concentrations. (G-H) PLK1 was stably overexpressed in A375 cells and then subjected to either western analysis of Vimentin (G), or measurement of cell viability (H), under the treatment of PLX-4032. (I-J) A375R cells expressing either empty vector (Control) or PLK1 (PLK1-OE) were treated with the indicated concentrations of PLX-4032, then subjected to either western blot to detect the expression of the indicated proteins (I) or MTT assay to evaluate its sensitivity toward PLX-4032 treatment (J). $P > 0.05$, N.S.; $P < 0.05$, *; $P < 0.01$, ** by student t-test.

Figure 12 continued

A

A375   A375R
Bl6727,nM   -   10   20   -   20
PLK1
N-cadherin
Actin

B

B16-F10
shCtrl   shPlk1-1 shPlk1-2
N-cadherin
PLK1
ERK

C

A375, 72h
shPLK1   -   -   -   +   +   +
PLX-4032, uM -   0.1 0.25 -   0.1 0.25
Vimentin
PLK1
Actin

D

A375R
Relative distance

E

A375

F

A375R

G

A375, 72h
PLK1-OE   -   -   -   +   +   +
PLX-4032, uM -   0.1 0.25 -   0.1 0.25
Vimentin
PLK1
Actin

H

A375

I

A375R, 96h
PLK1-OE   -   +   -   +   -   +
PLX-4032, uM -   2.5   10   -   2.5   10
Vimentin
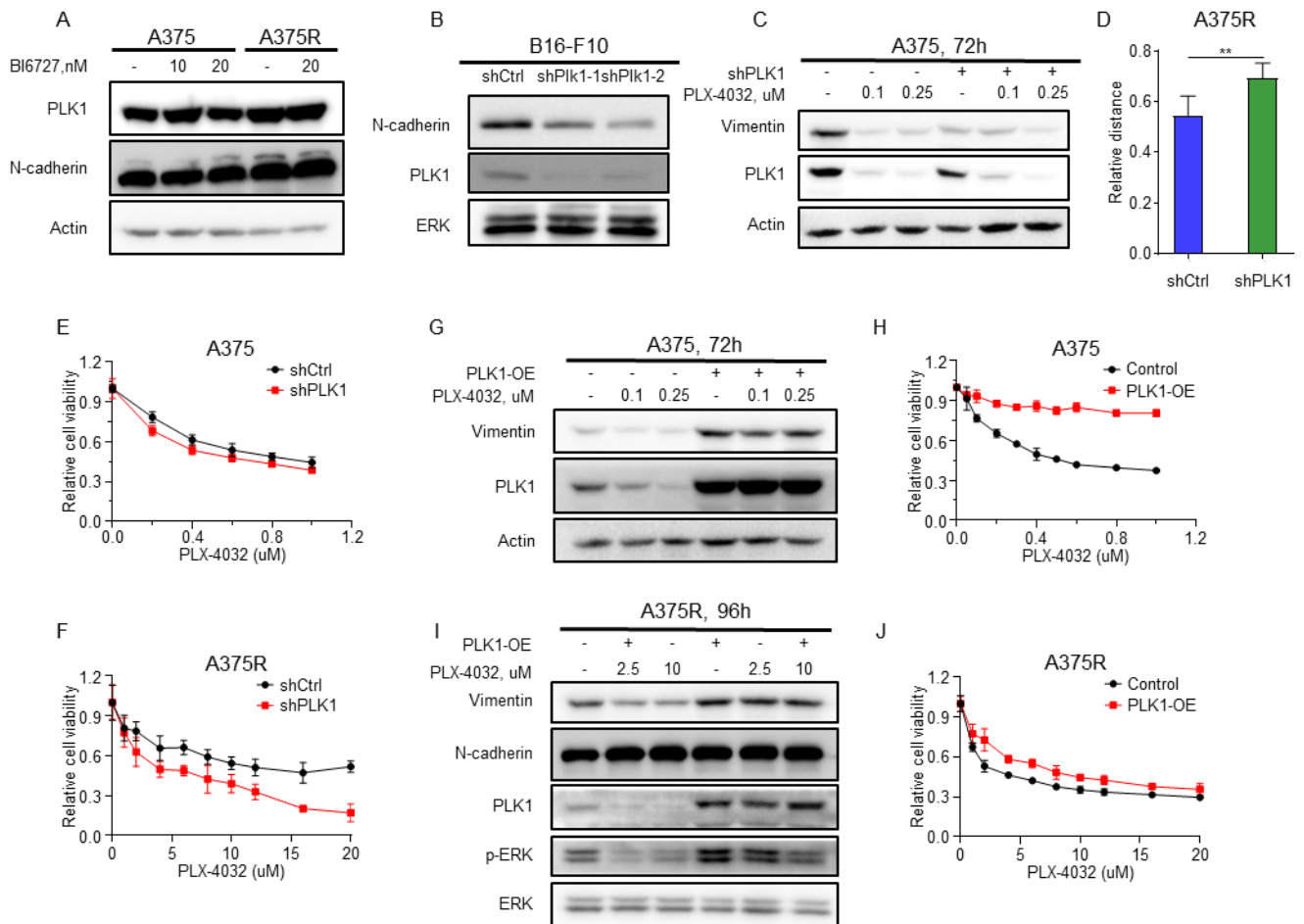N-cadherin
PLK1
p-ERK
ERK

J

A375R

Figure 13. BI6727 and PLX-4032 acts synergistically in human melanoma cell lines

(A-B) A375 (A) and A375R (B) cells were treated with PLX-4032 and BI6727 at the indicated concentrations for 48h and harvested for western blot, respectively, to measure cleaved-PARP level. (C-D) The quantification of apoptotic cell percentage measured by Annexin V/PI assay. A375(C) and A375R (D) cells were treated with DMSO, PLX-4032, BI 6727 or both at the indicated concentrations for 24h, collected and stained with Annexin V and PI, followed by flow cytometry to detect cell apoptotic population (**, P<0.01; n = 3 independent experiments). (E-F) A375 (E) and A375R (F) were treated with indicated drugs, respectively, for 24h. Then, cells were collected, fixed with 70% ethanol, stained with PI for 30 minutes, and then the cell cycle was analyzed with flow cytometry (n = 3 independent experiments). (G-H) A375 (G) and A375R (H) cells were treated with indicated drugs, followed by measurement of cell numbers for six days. (I and J) A375 (I) and A375R (J) cells were treated with DMSO, BI6727, PLX-4032or a combination of the two drugs, respectively. After changing fresh media containing drug(s) every 3 days for two weeks, cells were fixed with formalin, and colony formation was monitored by crystal violet staining. The experiments shown are representatives of 3 repeats. (K) A375 and A375R cells were seeded in the 6-well plate. Once reaches 100% confluence, a wound was made in the attached cells and its closure was monitored under the microscope upon the treatment of indicated drugs. Left: the quantification of relative gap distance in 24h post scratch (**, P<0.01; n = 3 independent experiments); Right: the representative images of 3 repeats. (L) A375 and A375R cells were seeded into the transwell chamber of a 24-well plate and treated with DMSO, BI 6727, PLX-4032, or both at the indicated concentrations in RPMI-1640 without FBS. The lower chambers were filled with RPMI-1640 containing 10% FBS. After 24h, the cells were fixed with methanol and stained with crystal violet. Photos were taken by the Nikon microscope.
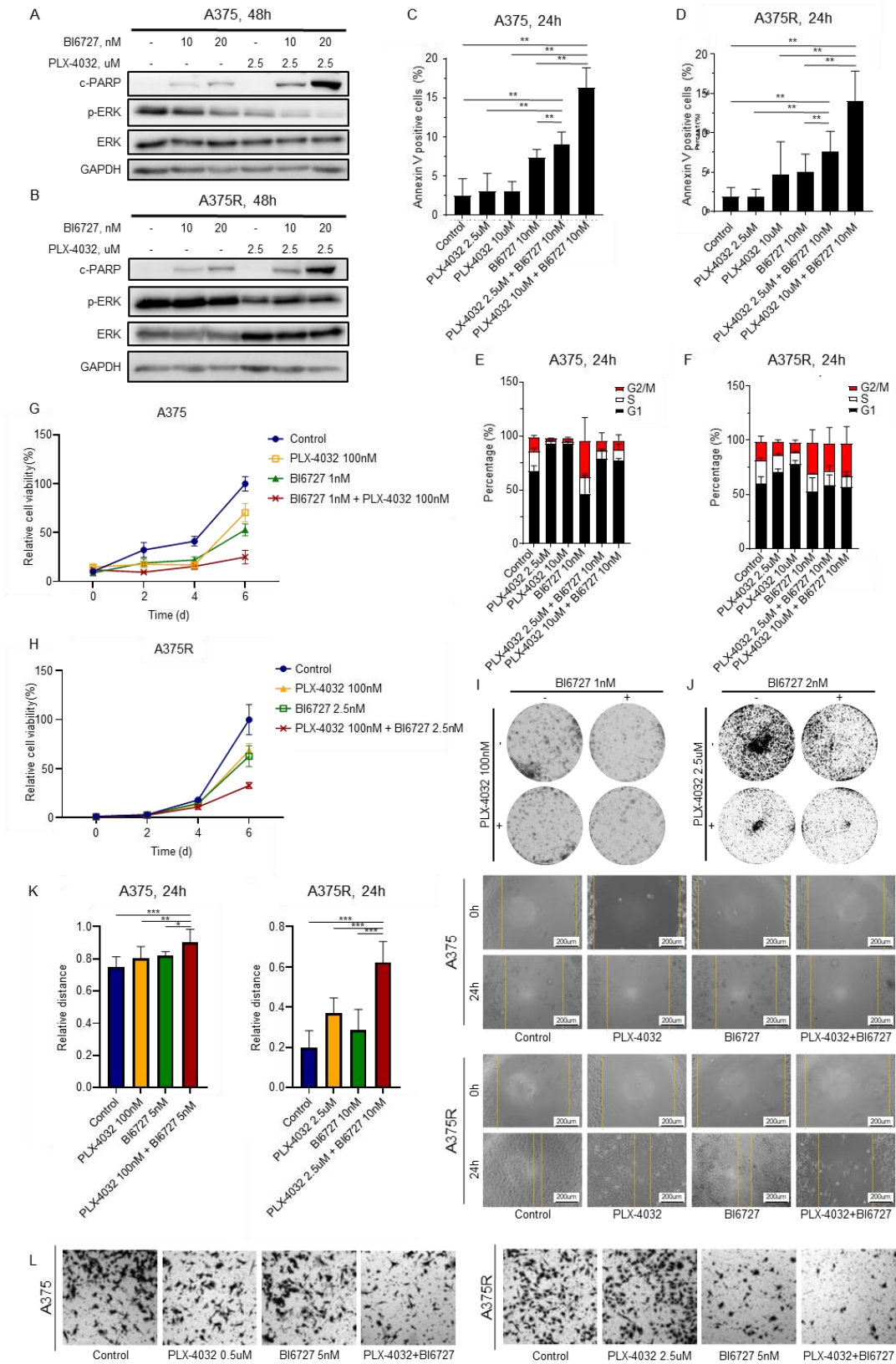
Figure 13 continued

Figure 14. BI6727 and PLX-4032 cooperatively inhibit tumor growth in A375R-derived xenograft

(A) Growth curves of A375R-derived tumors. Female nude mice were inoculated with A375R cells (2×10^6) and administered with PLX-4032 (50 mg/kg body weight, oral gavage, once daily), BI6727 (10 mg/kg body weight, intraperitoneal injection, every two days), or a combination of both drugs. The sizes of the tumors in each group were measured every 2 days (mean ± SEM; n = 4 mice from each experiment group). (B) Tumor weight measurement right after being freshly removed from the bodies. (C) Representative images of the tumors at the end of the study. (D) A375R-derived tumors from each group were collected and subjected to western blot to detect the expression of indicated proteins. (E) The representative images of H&E staining to show the pathologic structure of A375R-derived tumors from each group. $P>0.05$, N.S.; $P<0.05$, *; $P<0.01$, **; $P<0.001$, *** by student t-test.

Figure 14 continued
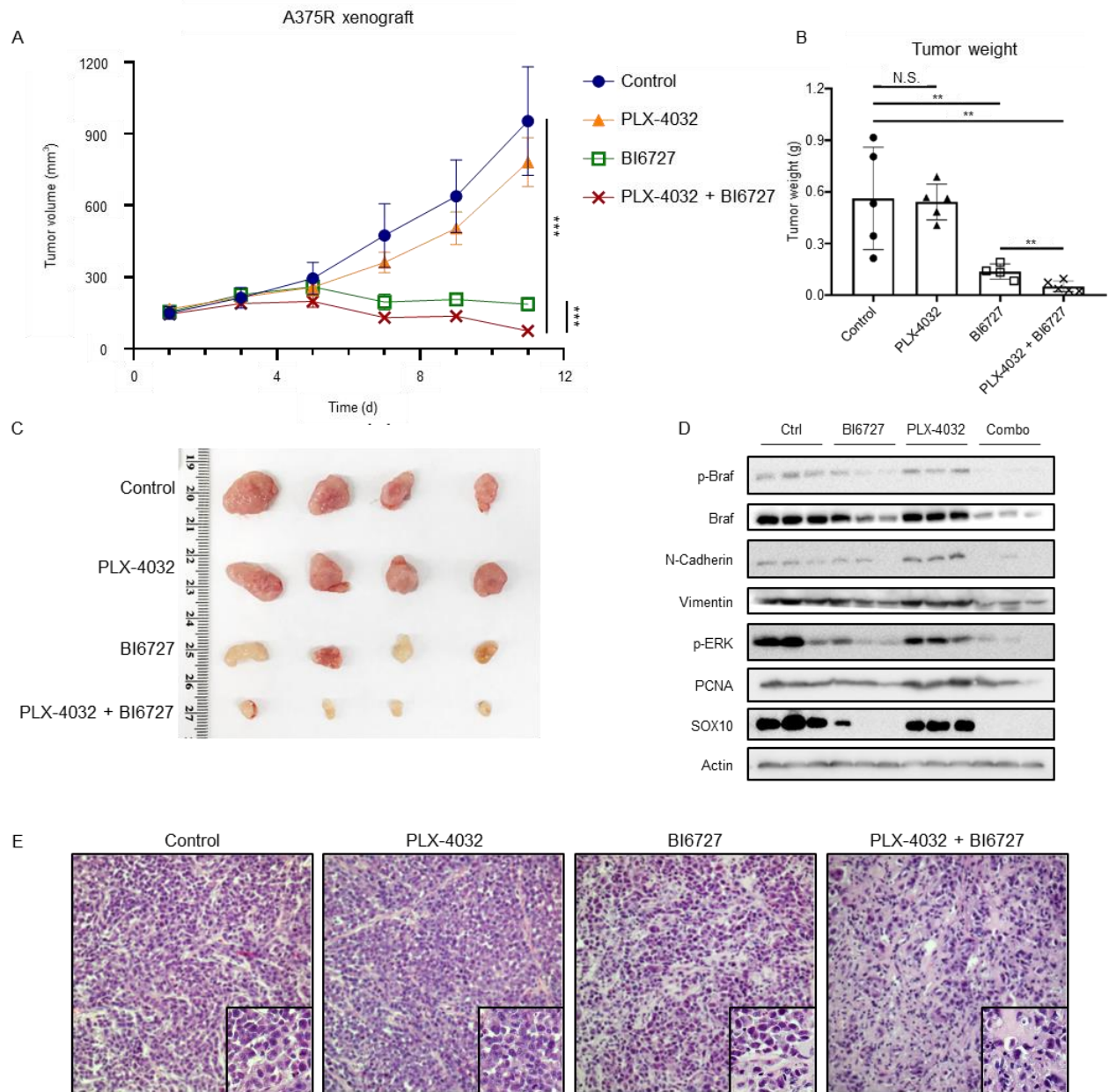
CHAPTER. 5   SUMMARY AND FUTURE DIRECTIONS

5.1   Improved treatment of PCa

Due to the critical role of AR in PCa, blocking the function of the AR signaling pathway is the major therapeutic strategy to treat either primary or metastatic PCa patients in the clinic (171). Consequently, ADT has been widely used to treat the early stage PCa patient for decades due to its strong efficiency, whereas patients would develop into CRPC eventually (171). Based on the current circumstance, it is urgently required for the novel therapy to improve the life span and quality of CRPC patients. In this study, we have developed an effective combination strategy to treat CRPC and confirmed its efficacy using *in vitro* cell culture and *in vivo* xenograft models. In conclusion, PLK1 inhibitor GSK461364A and BRD4 inhibitor JQ1 act cooperatively from various aspects to inhibit the progression of human CRPC, including proliferation and apoptosis. Mechanistically, PLK1 could active the Wnt/β-Catenin signaling through phosphorylating Axin2. Thus, the inhibition of PLK1 could elevate β-Catenin and induce the expression of c-Myc, which could sensitize cells to the treatment of JQ1, as BRD4 is the direct regulator of c-Myc. Moreover, GSK461364A and JQ1 cooperate to suppress AR signaling, further enhancing the efficacy of combining GSK461364A and JQ1. Interestingly, we do find that the combination treatment could inhibit both glycolysis and oxidative phosphorylation, while the underlying mechanism remains elusive. It requires further investigation to figure out whether the treatment could affect the metabolism directly through regulating metabolic enzymes or indirectly by targeting metabolic-related transcription factors. On the other hand, the immune system participates in cancer treatment and influences the efficacy of drug treatment to a large degree. Consequently, it is necessary to evaluate the role of the immune system in the treatment of GSK461364A and JQ1. In our study, we utilized the TRAMP-C2-derived allograft model to investigate the efficacy of co-treatment and evaluate its influence on the immune system as well. However, due to the limitation of experimental settings, we could not draw a confident conclusion to address these questions, and more experiments must be conducted to confirm the response of the immune system to the dual treatment. To accomplish this goal, the TRAMP mice will be treated with the novel combination therapy, and the tumor progression will be tightly monitored as well.

5.2   PLK's role in melanoma

Malignant melanoma is the most aggressive and dangerous form of skin cancers, frequently diagnosed among whites than any other racial group. Due to its strong metastatic ability, the five-year survival rates of distant melanoma is as low as 27.3% in the US (170, 202). Over half of the patients contain BRAF mutations, particularly BRAF V600E, to cause the constitutive activation of the MAPK signaling pathway, thus making BRAF a primary therapeutic target in clinical (204). PLX-4032 is an FDA-approved drug to treat melanoma patients with BRAF V600E mutation, exhibiting a profound therapeutic efficiency only for a relatively short period. Consequently, it is worthwhile to identify a novel target in the treatment of melanoma to enhance the efficacy of PLX-4032 in clinical.

PLK1, beyond its well-documented roles in the cell cycle, is overexpressed in cancers and negatively correlated with patient survival (14). To investigate its role in melanoma, we have generated mouse melanoma models, either overexpressing or knocking out *Plk1*. Significantly, *Plk1* could promote the progression and metastasis of melanoma but also contribute to the metabolic remodeling and drug resistance to PLX-4032 as well in the $Braf^{CA/+}$ / $Pten^{loxp/loxp}$ mouse model. In parallel, the expression of PLK1 is much higher in the PLX-4032-resistant A375R cells compared to its parental sensitive A375 cells. Manipulating PLK1 in A375 and A375R cells significantly impact their sensitivity to PLX-4032 and the ability of metastasis. Moreover, PLK1 inhibitor BI6727 could act cooperatively with PLX-4032 to suppress melanoma progression and metastasis *in vitro* and *in vivo*. To summarize, PLK1 has been regarded as an oncogene in the progression of melanoma, as well as a promising therapeutic target in clinical.

However, the mechanisms of how PLK1 functions in melanoma development are still unclear. To address this question, we will harvest the mouse tumors from $Braf^{CA/+}$ / $Pten^{loxp/loxp}$ mice and $Braf^{CA/+}$ / $Pten^{loxp/loxp}$ / $Plk1$-KI mice, respectively, for the RNA-Seq to analyze the alterations of the cancer-related signaling. Subsequently, we will perform experiments to validate the role of molecules or signaling pathways that are tightly related to the phenotype. Most importantly, how PLK1 regulated these key molecules will be deeply investigated. Moreover, the efficacy of the dual treatment, BI6727 and PLX-4032, would be further validated using the transgenic mouse model.

REFERENCES

1.   Sunkel CE, Glover DM. polo, a mitotic mutant of Drosophila displaying abnormal spindle poles. J Cell Sci. 1988;89 (Pt 1):25-38.

2.   Llamazares S, Moreira A, Tavares A, Girdham C, Spruce BA, Gonzalez C, et al. polo encodes a protein kinase homolog required for mitosis in Drosophila. Genes Dev. 1991;5(12A):2153-65.

3.   van de Weerdt BC, Medema RH. Polo-like kinases: a team in control of the division. Cell Cycle. 2006;5(8):853-64.

4.   Andrysik Z, Bernstein WZ, Deng L, Myer DL, Li YQ, Tischfield JA, et al. The novel mouse Polo-like kinase 5 responds to DNA damage and localizes in the nucleolus. Nucleic Acids Res. 2010;38(9):2931-43.

5.   Petronczki M, Lenart P, Peters JM. Polo on the Rise-from Mitotic Entry to Cytokinesis with Plk1. Dev Cell. 2008;14(5):646-59.

6.   Bruinsma W, Raaijmakers JA, Medema RH. Switching Polo-like kinase-1 on and off in time and space. Trends Biochem Sci. 2012;37(12):534-42.

7.   van de Weerdt BC, Littler DR, Klompmaker R, Huseinovic A, Fish A, Perrakis A, et al. Polo-box domains confer target specificity to the Polo-like kinase family. Biochim Biophys Acta. 2008;1783(6):1015-22.

8.   Lee KS, Grenfell TZ, Yarm FR, Erikson RL. Mutation of the polo-box disrupts localization and mitotic functions of the mammalian polo kinase Plk. Proc Natl Acad Sci U S A. 1998;95(16):9301-6.

9.   Jang YJ, Ma S, Terada Y, Erikson RL. Phosphorylation of threonine 210 and the role of serine 137 in the regulation of mammalian polo-like kinase. J Biol Chem. 2002;277(46):44115-20.

10.   Fenton B, Glover DM. A conserved mitotic kinase active at late anaphase—telophase in syncytial Drosophila embryos. Nature. 1993;363(6430):637-40.

11.   Lee KS, Yuan YL, Kuriyama R, Erikson RL. Plk is an M-phase-specific protein kinase and interacts with a kinesin-like protein, CHO1/MKLP-1. Molecular and cellular biology. 1995;15(12):7143-51.

12.   Lake RJ, Jelinek WR. Cell cycle- and terminal differentiation-associated regulation of the mouse mRNA encoding a conserved mitotic protein kinase. Molecular and cellular biology. 1993;13(12):7793-801.

13.   Martin BT, Strebhardt K. Polo-like kinase 1: target and regulator of transcriptional control. Cell Cycle. 2006;5(24):2881-5.

14.   Liu Z, Sun Q, Wang X. PLK1, A Potential Target for Cancer Therapy. Translational oncology. 2017;10(1):22-32.

15.   Bräuninger A, Strebhardt K, Rübsamen-Waigmann H. Identification and functional characterization of the human and murine polo-like kinase (Plk) promoter. Oncogene. 1995;11(9):1793-800.

16.   Uchiumi T, Longo DL, Ferris DK. Cell cycle regulation of the human polo-like kinase (PLK) promoter. J Biol Chem. 1997;272(14):9166-74.

17.   Tategu M, Nakagawa H, Sasaki K, Yamauchi R, Sekimachi S, Suita Y, et al. Transcriptional regulation of human polo-like kinases and early mitotic inhibitor. Journal of genetics and genomics = Yi chuan xue bao. 2008;35(4):215-24.

18.   Olsson AY, Feber A, Edwards S, Te Poele R, Giddings I, Merson S, et al. Role of E2F3 expression in modulating cellular proliferation rate in human bladder and prostate cancer cells. Oncogene. 2007;26(7):1028-37.

19.   Alvarez B, Martinez AC, Burgering BM, Carrera AC. Forkhead transcription factors contribute to execution of the mitotic programme in mammals. Nature. 2001;413(6857):744-7.

20.   Laoukili J, Kooistra MR, Bras A, Kauw J, Kerkhoven RM, Morrison A, et al. FoxM1 is required for execution of the mitotic programme and chromosome stability. Nature cell biology. 2005;7(2):126-36.

21.   Liu X, Erikson RL. Activation of Cdc2/cyclin B and inhibition of centrosome amplification in cells depleted of Plk1 by siRNA. Proc Natl Acad Sci U S A. 2002;99(13):8672-6.

22.   Zwicker J, Lucibello FC, Wolfraim LA, Gross C, Truss M, Engeland K, et al. Cell cycle regulation of the cyclin A, cdc25C and cdc2 genes is based on a common mechanism of transcriptional repression. EMBO J. 1995;14(18):4514-22.

23.   Lucibello FC, Truss M, Zwicker J, Ehlert F, Beato M, Muller R. Periodic cdc25C transcription is mediated by a novel cell cycle-regulated repressor element (CDE). EMBO J. 1995;14(1):132-42.

24.   Zwicker J, Lucibello FC, Jerome V, Brusselbach S, Muller R. CDF-1 mediated repression of cell cycle genes targets a specific subset of transactivators. Nucleic Acids Res. 1998;26(4):4926-32.

25.   Muller GA, Quaas M, Schumann M, Krause E, Padi M, Fischer M, et al. The CHR promoter element controls cell cycle-dependent gene transcription and binds the DREAM and MMB complexes. Nucleic Acids Res. 2012;40(4):1561-78.

26. Gunawardena RW, Siddiqui H, Solomon DA, Mayhew CN, Held J, Angus SP, et al. Hierarchical requirement of SWI/SNF in retinoblastoma tumor suppressor-mediated repression of Plk1. J Biol Chem. 2004;279(28):29278-85.

27. Bakkenist CJ, Kastan MB. DNA damage activates ATM through intermolecular autophosphorylation and dimer dissociation. Nature. 2003;421(6922):499-506.

28. Matsuoka S, Huang M, Elledge SJ. Linkage of ATM to cell cycle regulation by the Chk2 protein kinase. Science. 1998;282(5395):1893-7.

29. Yarden RI, Pardo-Reoyo S, Sgagias M, Cowan KH, Brody LC. BRCA1 regulates the G2/M checkpoint by activating Chk1 kinase upon DNA damage. Nat Genet. 2002;30(3):285-9.

30. Smits VA, Klompmaker R, Arnaud L, Rijksen G, Nigg EA, Medema RH. Polo-like kinase-1 is a target of the DNA damage checkpoint. Nature cell biology. 2000;2(9):672-6.

31. van Vugt MA, Smits VA, Klompmaker R, Medema RH. Inhibition of Polo-like kinase-1 by DNA damage occurs in an ATM- or ATR-dependent fashion. J Biol Chem. 2001;276(45):41656-60.

32. Ree AH, Bratland A, Nome RV, Stokke T, Fodstad O. Repression of mRNA for the PLK cell cycle gene after DNA damage requires BRCA1. Oncogene. 2003;22(55):8952-5.

33. McKenzie L, King S, Marcar L, Nicol S, Dias SS, Schumm K, et al. p53-dependent repression of polo-like kinase-1 (PLK1). Cell Cycle. 2010;9(20):4200-12.

34. Fischer M, Quaas M, Steiner L, Engeland K. The p53-p21-DREAM-CDE/CHR pathway regulates G2/M cell cycle genes. Nucleic Acids Res. 2016;44(1):164-74.

35. Quaas M, Muller GA, Engeland K. p53 can repress transcription of cell cycle genes through a p21(WAF1/CIP1)-dependent switch from MMB to DREAM protein complex binding at CHR promoter elements. Cell Cycle. 2012;11(24):4661-72.

36. Zhou Z, Cao JX, Li SY, An GS, Ni JH, Jia HT. p53 Suppresses E2F1-dependent PLK1 expression upon DNA damage by forming p53-E2F1-DNA complex. Exp Cell Res. 2013;319(20):3104-15.

37. Pandit B, Halasi M, Gartel AL. p53 negatively regulates expression of FoxM1. Cell Cycle. 2009;8(20):3425-7.

38. Li X. Epigenetics and cell cycle regulation in cystogenesis. Cell Signal. 2020;68:109509.

39. Ward A, Hudson JW. p53-Dependent and cell specific epigenetic regulation of the polo-like kinases under oxidative stress. PLoS One. 2014;9(1):e87918.

40. Ward A, Sivakumar G, Kanjeekal S, Hamm C, Labute BC, Shum D, et al. The deregulated promoter methylation of the Polo-like kinases as a potential biomarker in hematological malignancies. Leuk Lymphoma. 2015;56(7):2123-33.

41. Mundt KE, Golsteyn RM, Lane HA, Nigg EA. On the regulation and function of human polo-like kinase 1 (PLK1): effects of overexpression on cell cycle progression. Biochem Biophys Res Commun. 1997;239(2):377-85.

42. Jang YJ, Lin CY, Ma S, Erikson RL. Functional studies on the role of the C-terminal domain of mammalian polo-like kinase. Proc Natl Acad Sci U S A. 2002;99(4):1984-9.

43. Xu J, Shen C, Wang T, Quan J. Structural basis for the inhibition of Polo-like kinase 1. Nat Struct Mol Biol. 2013;20(9):1047-53.

44. Seki A, Coppinger JA, Jang CY, Yates JR, Fang G. Bora and the kinase Aurora a cooperatively activate the kinase Plk1 and control mitotic entry. Science. 2008;320(5883):1655-8.

45. Macurek L, Lindqvist A, Lim D, Lampson MA, Klompmaker R, Freire R, et al. Polo-like kinase-1 is activated by aurora A to promote checkpoint recovery. Nature. 2008;455(7209):119-23.

46. Daub H, Olsen JV, Bairlein M, Gnad F, Oppermann FS, Korner R, et al. Kinase-selective enrichment enables quantitative phosphoproteomics of the kinome across the cell cycle. Mol Cell. 2008;31(3):438-48.

47. Lee KS, Erikson RL. Plk is a functional homolog of Saccharomyces cerevisiae Cdc5, and elevated Plk activity induces multiple septation structures. Molecular and cellular biology. 1997;17(6):3408-17.

48. Paschal CR, Maciejowski J, Jallepalli PV. A stringent requirement for Plk1 T210 phosphorylation during K-fiber assembly and chromosome congression. Chromosoma. 2012;121(6):565-72.

49. Bruinsma W, Macurek L, Freire R, Lindqvist A, Medema RH. Bora and Aurora-A continue to activate Plk1 in mitosis. J Cell Sci. 2014;127(Pt 4):801-11.

50. Seki A, Coppinger JA, Du H, Jang CY, Yates JR, 3rd, Fang G. Plk1- and beta-TrCP-dependent degradation of Bora controls mitotic progression. J Cell Biol. 2008;181(1):65-78.

51. van de Weerdt BC, van Vugt MA, Lindon C, Kauw JJ, Rozendaal MJ, Klompmaker R, et al. Uncoupling anaphase-promoting complex/cyclosome activity from spindle assembly checkpoint control by deregulating polo-like kinase 1. Molecular and cellular biology. 2005;25(5):2031-44.

52. Maroto B, Ye MB, von Lohneysen K, Schnelzer A, Knaus UG. P21-activated kinase is required for mitotic progression and regulates Plk1. Oncogene. 2008;27(36):4900-8.

53. Yamashiro S, Yamakita Y, Totsukawa G, Goto H, Kaibuchi K, Ito M, et al. Myosin phosphatase-targeting subunit 1 regulates mitosis by antagonizing polo-like kinase 1. Dev Cell. 2008;14(5):787-97.

54. Kachaner D, Filipe J, Laplantine E, Bauch A, Bennett KL, Superti-Furga G, et al. Plk1-dependent phosphorylation of optineurin provides a negative feedback mechanism for mitotic progression. Mol Cell. 2012;45(4):553-66.

55. Dumitru AMG, Rusin SF, Clark AEM, Kettenbach AN, Compton DA. Cyclin A/Cdk1 modulates Plk1 activity in prometaphase to regulate kinetochore-microtubule attachment stability. eLife. 2017;6.

56. Foley EA, Maldonado M, Kapoor TM. Formation of stable attachments between kinetochores and microtubules depends on the B56-PP2A phosphatase. Nature cell biology. 2011;13(10):1265-71.

57. Wang L, Guo Q, Fisher LA, Liu D, Peng A. Regulation of polo-like kinase 1 by DNA damage and PP2A/B55alpha. 2015;14(1):157-66.

58. Liu J, Zhang C. The equilibrium of ubiquitination and deubiquitination at PLK1 regulates sister chromatid separation. Cell Mol Life Sci. 2017;74(12):2127-34.

59. Kang D, Chen J, Wong J, Fang G. The checkpoint protein Chfr is a ligase that ubiquitinates Plk1 and inhibits Cdc2 at the G2 to M transition. J Cell Biol. 2002;156(2):249-59.

60. Zhuo X, Guo X, Zhang X, Jing G, Wang Y, Chen Q, et al. Usp16 regulates kinetochore localization of Plk1 to promote proper chromosome alignment in mitosis. J Cell Biol. 2015;210(5):727-35.

61. Beck J, Maerki S, Posch M, Metzger T, Persaud A, Scheel H, et al. Ubiquitylation-dependent localization of PLK1 in mitosis. Nature cell biology. 2013;15(4):430-9.

62. Lindon C, Pines J. Ordered proteolysis in anaphase inactivates Plk1 to contribute to proper mitotic exit in human cells. J Cell Biol. 2004;164(2):233-41.

63. Wasch R, Engelbert D. Anaphase-promoting complex-dependent proteolysis of cell cycle regulators and genomic instability of cancer cells. Oncogene. 2005;24(1):1-10.

64. Morgan DO. Regulation of the APC and the exit from mitosis. Nature cell biology. 1999;1(2):E47-53.

65. Eckerdt F, Strebhardt K. Polo-like kinase 1: target and regulator of anaphase-promoting complex/cyclosome-dependent proteolysis. Cancer Res. 2006;66(14):6895-8.

66. Glotzer M, Murray AW, Kirschner MW. Cyclin is degraded by the ubiquitin pathway. Nature. 1991;349(6305):132-8.

67. Chen L, Li J, Farah E, Sarkar S, Ahmad N, Gupta S, et al. Cotargeting HSP90 and Its Client Proteins for Treatment of Prostate Cancer. Mol Cancer Ther. 2016;15(9):2107-18.

68. Wen D, Wu J, Wang L, Fu Z. SUMOylation Promotes Nuclear Import and Stabilization of Polo-like Kinase 1 to Support Its Mitotic Function. Cell Rep. 2017;21(8):2147-59.

69. Feitosa WB, Hwang K, Morris PL. Temporal and SUMO-specific SUMOylation contribute to the dynamics of Polo-like kinase 1 (PLK1) and spindle integrity during mouse oocyte meiosis. Dev Biol. 2018;434(2):278-91.

70. Li W, Wang HY, Zhao X, Duan H, Cheng B, Liu Y, et al. A methylation-phosphorylation switch determines Plk1 kinase activity and function in DNA damage repair. Sci Adv. 2019;5(3):eaau7566.

71. Yu R, Wu H, Ismail H, Du S, Cao J, Wang J, et al. Methylation of PLK1 by SET7/9 ensures accurate kinetochore-microtubule dynamics. J Mol Cell Biol. 2020;12(6):462-76.

72. Wachowicz P, Fernandez-Miranda G, Marugan C, Escobar B, de Carcer G. Genetic depletion of Polo-like kinase 1 leads to embryonic lethality due to mitotic aberrancies. Bioessays. 2016;38 Suppl 1:S96-S106.

73. Lu LY, Wood JL, Minter-Dykhouse K, Ye L, Saunders TL, Yu X, et al. Polo-like kinase 1 is essential for early embryonic development and tumor suppression. Molecular and cellular biology. 2008;28(22):6870-6.

74. Liu X. Targeting Polo-Like Kinases: A Promising Therapeutic Approach for Cancer Treatment. Translational oncology. 2015;8(3):185-95.

75. Lindqvist A, Rodriguez-Bravo V, Medema RH. The decision to enter mitosis: feedback and redundancy in the mitotic entry network. J Cell Biol. 2009;185(2):193-202.

76. Elia AE, Cantley LC, Yaffe MB. Proteomic screen finds pSer/pThr-binding domain localizing Plk1 to mitotic substrates. Science. 2003;299(5610):1228-31.

77. Elia AE, Rellos P, Haire LF, Chao JW, Ivins FJ, Hoepker K, et al. The molecular basis for phosphodependent substrate targeting and regulation of Plks by the Polo-box domain. Cell. 2003;115(1):83-95.

78. Watanabe N, Arai H, Nishihara Y, Taniguchi M, Watanabe N, Hunter T, et al. M-phase kinases induce phospho-dependent ubiquitination of somatic Wee1 by SCFbeta-TrCP. Proc Natl Acad Sci U S A. 2004;101(13):4419-24.

79. Booher RN, Holman PS, Fattaey A. Human Myt1 is a cell cycle-regulated kinase that inhibits Cdc2 but not Cdk2 activity. J Biol Chem. 1997;272(35):22300-6.

80. Nakajima H, Toyoshima-Morimoto F, Taniguchi E, Nishida E. Identification of a consensus motif for Plk (Polo-like kinase) phosphorylation reveals Myt1 as a Plk1 substrate. J Biol Chem. 2003;278(28):25277-80.

81. Toyoshima-Morimoto F, Taniguchi E, Nishida E. Plk1 promotes nuclear translocation of human Cdc25C during prophase. EMBO Rep. 2002;3(4):341-8.

82.   Toyoshima-Morimoto F, Taniguchi E, Shinya N, Iwamatsu A, Nishida E. Polo-like kinase 1 phosphorylates cyclin B1 and targets it to the nucleus during prophase. Nature. 2001;410(6825):215-20.

83.   Yuan J, Eckerdt F, Bereiter-Hahn J, Kurunci-Csacsko E, Kaufmann M, Strebhardt K. Cooperative phosphorylation including the activity of polo-like kinase 1 regulates the subcellular localization of cyclin B1. Oncogene. 2002;21(54):8282-92.

84.   Fu Z, Malureanu L, Huang J, Wang W, Li H, van Deursen JM, et al. Plk1-dependent phosphorylation of FoxM1 regulates a transcriptional programme required for mitotic progression. Nature cell biology. 2008;10(9):1076-82.

85.   Lane HA, Nigg EA. Antibody microinjection reveals an essential role for human polo-like kinase 1 (Plk1) in the functional maturation of mitotic centrosomes. J Cell Biol. 1996;135(6 Pt 2):1701-13.

86.   Canton DA, Keene CD, Swinney K, Langeberg LK, Nguyen V, Pelletier L, et al. Gravin is a transitory effector of polo-like kinase 1 during cell division. Mol Cell. 2012;48(4):547-59.

87.   Job D, Valiron O, Oakley B. Microtubule nucleation. Curr Opin Cell Biol. 2003;15(1):111-7.

88.   Casenghi M, Meraldi P, Weinhart U, Duncan PI, Korner R, Nigg EA. Polo-like kinase 1 regulates Nlp, a centrosome protein involved in microtubule nucleation. Dev Cell. 2003;5(1):113-25.

89.   Kim J, Lee K, Rhee K. PLK1 regulation of PCNT cleavage ensures fidelity of centriole separation during mitotic exit. Nat Commun. 2015;6:10076.

90.   Lee K, Rhee K. PLK1 phosphorylation of pericentrin initiates centrosome maturation at the onset of mitosis. J Cell Biol. 2011;195(7):1093-101.

91.   Ramani A, Mariappan A, Gottardo M, Mandad S, Urlaub H, Avidor-Reiss T, et al. Plk1/Polo Phosphorylates Sas-4 at the Onset of Mitosis for an Efficient Recruitment of Pericentriolar Material to Centrosomes. Cell Rep. 2018;25(13):3618-30 e6.

92.   Mardin BR, Agircan FG, Lange C, Schiebel E. Plk1 controls the Nek2A-PP1gamma antagonism in centrosome disjunction. Curr Biol. 2011;21(13):1145-51.

93.   Bahe S, Stierhof YD, Wilkinson CJ, Leiss F, Nigg EA. Rootletin forms centriole-associated filaments and functions in centrosome cohesion. J Cell Biol. 2005;171(1):27-33.

94.   Bertran MT, Sdelci S, Regue L, Avruch J, Caelles C, Roig J. Nek9 is a Plk1-activated kinase that controls early centrosome separation through Nek6/7 and Eg5. EMBO J. 2011;30(13):2634-47.

95. Li H, Liu XS, Yang X, Song B, Wang Y, Liu X. Polo-like kinase 1 phosphorylation of p150Glued facilitates nuclear envelope breakdown during prophase. Proc Natl Acad Sci U S A. 2010;107(33):14633-8.

96. Kiyomitsu T, Cheeseman IM. Chromosome- and spindle-pole-derived signals generate an intrinsic code for spindle position and orientation. Nature cell biology. 2012;14(3):311-7.

97. Yim H, Shin SB, Woo SU, Lee PC, Erikson RL. Plk1-mediated stabilization of 53BP1 through USP7 regulates centrosome positioning to maintain bipolarity. Oncogene. 2017;36(7):966-78.

98. Lenart P, Petronczki M, Steegmaier M, Di Fiore B, Lipp JJ, Hoffmann M, et al. The small-molecule inhibitor BI 2536 reveals novel insights into mitotic roles of polo-like kinase 1. Curr Biol. 2007;17(4):304-15.

99. Kang YH, Park JE, Yu LR, Soung NK, Yun SM, Bang JK, et al. Self-regulated Plk1 recruitment to kinetochores by the Plk1-PBIP1 interaction is critical for proper chromosome segregation. Mol Cell. 2006;24(3):409-22.

100. Goto H, Kiyono T, Tomono Y, Kawajiri A, Urano T, Furukawa K, et al. Complex formation of Plk1 and INCENP required for metaphase-anaphase transition. Nature cell biology. 2006;8(2):180-7.

101. Qi W, Tang Z, Yu H. Phosphorylation- and polo-box-dependent binding of Plk1 to Bub1 is required for the kinetochore localization of Plk1. Mol Biol Cell. 2006;17(8):3705-16.

102. Elowe S, Hummer S, Uldschmid A, Li X, Nigg EA. Tension-sensitive Plk1 phosphorylation on BubR1 regulates the stability of kinetochore microtubule interactions. Genes Dev. 2007;21(17):2205-19.

103. Lee HS, Park YY, Cho MY, Chae S, Yoo YS, Kwon MH, et al. The chromatin remodeller RSF1 is essential for PLK1 deposition and function at mitotic kinetochores. Nat Commun. 2015;6:7904.

104. Suijkerbuijk SJ, Vleugel M, Teixeira A, Kops GJ. Integration of kinase and phosphatase activities by BUBR1 ensures formation of stable kinetochore-microtubule attachments. Dev Cell. 2012;23(4):745-55.

105. Ehlen A, Martin C, Miron S, Julien M, Theillet FX, Ropars V, et al. Proper chromosome alignment depends on BRCA2 phosphorylation by PLK1. Nat Commun. 2020;11(1):1819.

106. Lee M, Daniels MJ, Venkitaraman AR. Phosphorylation of BRCA2 by the Polo-like kinase Plk1 is regulated by DNA damage and mitotic progression. Oncogene. 2004;23(4):865-72.

107. Li H, Liu XS, Yang X, Wang Y, Wang Y, Turner JR, et al. Phosphorylation of CLIP-170 by Plk1 and CK2 promotes timely formation of kinetochore-microtubule attachments. EMBO J. 2010;29(17):2953-65.

108. Tanenbaum ME, Galjart N, van Vugt MA, Medema RH. CLIP-170 facilitates the formation of kinetochore-microtubule attachments. EMBO J. 2006;25(1):45-57.

109. Mondal G, Ohashi A, Yang L, Rowley M, Couch FJ. Tex14, a Plk1-regulated protein, is required for kinetochore-microtubule attachment and regulation of the spindle assembly checkpoint. Mol Cell. 2012;45(5):680-95.

110. Li Z, Shao C, Kong Y, Carlock C, Ahmad N, Liu X. DNA Damage Response-Independent Role for MDC1 in Maintaining Genomic Stability. Molecular and cellular biology. 2017;37(9).

111. Liu XS, Song B, Tang J, Liu W, Kuang S, Liu X. Plk1 phosphorylates Sgt1 at the kinetochores to promote timely kinetochore-microtubule attachment. Molecular and cellular biology. 2012;32(19):4053-67.

112. Addis Jones O, Tiwari A, Olukoga T, Herbert A, Chan KL. PLK1 facilitates chromosome biorientation by suppressing centromere disintegration driven by BLM-mediated unwinding and spindle pulling. Nat Commun. 2019;10(1):2861.

113. Hayward D, Alfonso-Perez T, Gruneberg U. Orchestration of the spindle assembly checkpoint by CDK1-cyclin B1. FEBS letters. 2019;593(20):2889-907.

114. O'Connor A, Maffini S, Rainey MD, Kaczmarczyk A, Gaboriau D, Musacchio A, et al. Requirement for PLK1 kinase activity in the maintenance of a robust spindle assembly checkpoint. Biol Open. 2015;5(1):11-9.

115. Espeut J, Lara-Gonzalez P, Sassine M, Shiau AK, Desai A, Abrieu A. Natural Loss of Mps1 Kinase in Nematodes Uncovers a Role for Polo-like Kinase 1 in Spindle Checkpoint Initiation. Cell Rep. 2015;12(1):58-65.

116. Ikeda M, Tanaka K. Plk1 bound to Bub1 contributes to spindle assembly checkpoint activity during mitosis. Sci Rep. 2017;7(1):8794.

117. von Schubert C, Cubizolles F, Bracher JM, Sliedrecht T, Kops G, Nigg EA. Plk1 and Mps1 Cooperatively Regulate the Spindle Assembly Checkpoint in Human Cells. Cell Rep. 2015;12(1):66-78.

118. Kuntz K, Salovich J, Mook R, Emmitte K, Chamberlain S, Rheault T, et al. Identification of GSK461364, a novel small molecule polo-like kinase 1 inhibitor for the treatment of cancer. Cancer Research. 2007;67(9 Supplement):4171-.

119. Kaisari S, Shomer P, Ziv T, Sitry-Shevah D, Miniowitz-Shemtov S, Teichner A, et al. Role of Polo-like kinase 1 in the regulation of the action of p31(comet) in the disassembly of mitotic checkpoint complexes. Proc Natl Acad Sci U S A. 2019;116(24):11725-30.

120. Golan A, Yudkovsky Y, Hershko A. The cyclin-ubiquitin ligase activity of cyclosome/APC is jointly activated by protein kinases Cdk1-cyclin B and Plk. J Biol Chem. 2002;277(18):15552-7.

121. Hansen DV, Loktev AV, Ban KH, Jackson PK. Plk1 regulates activation of the anaphase promoting complex by phosphorylating and triggering SCFbetaTrCP-dependent destruction of the APC Inhibitor Emi1. Mol Biol Cell. 2004;15(12):5623-34.

122. Hauf S, Roitinger E, Koch B, Dittrich CM, Mechtler K, Peters JM. Dissociation of cohesin from chromosome arms and loss of arm cohesion during early mitosis depends on phosphorylation of SA2. PLoS Biol. 2005;3(3):e69.

123. Sumara I, Vorlaufer E, Stukenberg PT, Kelm O, Redemann N, Nigg EA, et al. The dissociation of cohesin from chromosomes in prophase is regulated by Polo-like kinase. Mol Cell. 2002;9(3):515-25.

124. Hu CK, Ozlu N, Coughlin M, Steen JJ, Mitchison TJ. Plk1 negatively regulates PRC1 to prevent premature midzone formation before cytokinesis. Mol Biol Cell. 2012;23(14):2702-11.

125. Neef R, Gruneberg U, Kopajtich R, Li X, Nigg EA, Sillje H, et al. Choice of Plk1 docking partners during mitosis and cytokinesis is controlled by the activation state of Cdk1. Nature cell biology. 2007;9(4):436-44.

126. Wolfe BA, Takaki T, Petronczki M, Glotzer M. Polo-like kinase 1 directs assembly of the HsCyk-4 RhoGAP/Ect2 RhoGEF complex to initiate cleavage furrow formation. PLoS Biol. 2009;7(5):e1000110.

127. Petronczki M, Glotzer M, Kraut N, Peters JM. Polo-like kinase 1 triggers the initiation of cytokinesis in human cells by promoting recruitment of the RhoGEF Ect2 to the central spindle. Dev Cell. 2007;12(5):713-25.

128. Santamaria A, Neef R, Eberspacher U, Eis K, Husemann M, Mumberg D, et al. Use of the novel Plk1 inhibitor ZK-thiazolidinone to elucidate functions of Plk1 in early and late stages of mitosis. Mol Biol Cell. 2007;18(10):4024-36.

129. Brennan IM, Peters U, Kapoor TM, Straight AF. Polo-like kinase controls vertebrate spindle elongation and cytokinesis. PLoS One. 2007;2(5):e409.

130. Burkard ME, Randall CL, Larochelle S, Zhang C, Shokat KM, Fisher RP, et al. Chemical genetics reveals the requirement for Polo-like kinase 1 activity in positioning RhoA and triggering cytokinesis in human cells. Proc Natl Acad Sci U S A. 2007;104(11):4383-8.

131. Lowery DM, Clauser KR, Hjerrild M, Lim D, Alexander J, Kishi K, et al. Proteomic screen defines the Polo-box domain interactome and identifies Rock2 as a Plk1 substrate. EMBO J. 2007;26(9):2262-73.

132. Neef R, Preisinger C, Sutcliffe J, Kopajtich R, Nigg EA, Mayer TU, et al. Phosphorylation of mitotic kinesin-like protein 2 by polo-like kinase 1 is required for cytokinesis. J Cell Biol. 2003;162(5):863-75.

133. Zhou T, Aumais JP, Liu X, Yu-Lee LY, Erikson RL. A role for Plk1 phosphorylation of NudC in cytokinesis. Dev Cell. 2003;5(1):127-38.

134. Bastos RN, Barr FA. Plk1 negatively regulates Cep55 recruitment to the midbody to ensure orderly abscission. J Cell Biol. 2010;191(4):751-60.

135. Hasegawa H, Hyodo T, Asano E, Ito S, Maeda M, Kuribayashi H, et al. The role of PLK1-phosphorylated SVIL in myosin II activation and cytokinetic furrowing. J Cell Sci. 2013;126(Pt 16):3627-37.

136. Bassermann F, Frescas D, Guardavaccaro D, Busino L, Peschiaroli A, Pagano M. The Cdc14B-Cdh1-Plk1 axis controls the G2 DNA-damage-response checkpoint. Cell. 2008;134(2):256-67.

137. Qin B, Gao B, Yu J, Yuan J, Lou Z. Ataxia telangiectasia-mutated- and Rad3-related protein regulates the DNA damage-induced G2/M checkpoint through the Aurora A cofactor Bora protein. J Biol Chem. 2013;288(22):16139-44.

138. Jaiswal H, Benada J, Mullers E, Akopyan K, Burdova K, Koolmeister T, et al. ATM/Wip1 activities at chromatin control Plk1 re-activation to determine G2 checkpoint duration. EMBO J. 2017;36(14):2161-76.

139. Kumagai A, Dunphy WG. Claspin, a novel protein required for the activation of Chk1 during a DNA replication checkpoint response in Xenopus egg extracts. Mol Cell. 2000;6(4):839-49.

140. Mamely I, van Vugt MA, Smits VA, Semple JI, Lemmens B, Perrakis A, et al. Polo-like kinase-1 controls proteasome-dependent degradation of Claspin during checkpoint recovery. Curr Biol. 2006;16(19):1950-5.

141. Yata K, Lloyd J, Maslen S, Bleuyard JY, Skehel M, Smerdon SJ, et al. Plk1 and CK2 act in concert to regulate Rad51 during DNA double strand break repair. Mol Cell. 2012;45(3):371-83.

142. Li Z, Li J, Kong Y, Yan S, Ahmad N, Liu X. Plk1 Phosphorylation of Mre11 Antagonizes the DNA Damage Response. Cancer Res. 2017;77(12):3169-80.

143. Wakida T, Ikura M, Kuriya K, Ito S, Shiroiwa Y, Habu T, et al. The CDK-PLK1 axis targets the DNA damage checkpoint sensor protein RAD9 to promote cell proliferation and tolerance to genotoxic stress. eLife. 2017;6.

144. Wang H, Qiu Z, Liu B, Wu Y, Ren J, Liu Y, et al. PLK1 targets CtIP to promote microhomology-mediated end joining. Nucleic Acids Res. 2018;46(20):10724-39.

145. Riley T, Sontag E, Chen P, Levine A. Transcriptional control of human p53-regulated genes. Nat Rev Mol Cell Biol. 2008;9(5):402-12.

146. Shieh SY, Ahn J, Tamai K, Taya Y, Prives C. The human homologs of checkpoint kinases Chk1 and Cds1 (Chk2) phosphorylate p53 at multiple DNA damage-inducible sites. Genes Dev. 2000;14(3):289-300.

147. Cheng Q, Chen J. Mechanism of p53 stabilization by ATM after DNA damage. Cell Cycle. 2010;9(3):472-8.

148. Chehab NH, Malikzay A, Appel M, Halazonetis TD. Chk2/hCds1 functions as a DNA damage checkpoint in G(1) by stabilizing p53. Genes Dev. 2000;14(3):278-88.

149. Ando K, Ozaki T, Yamamoto H, Furuya K, Hosoda M, Hayashi S, et al. Polo-like kinase 1 (Plk1) inhibits p53 function by physical interaction and phosphorylation. J Biol Chem. 2004;279(24):25549-61.

150. Chen J, Dai G, Wang YQ, Wang S, Pan FY, Xue B, et al. Polo-like kinase 1 regulates mitotic arrest after UV irradiation through dephosphorylation of p53 and inducing p53 degradation. FEBS letters. 2006;580(15):3624-30.

151. Yang X, Li H, Zhou Z, Wang WH, Deng A, Andrisani O, et al. Plk1-mediated phosphorylation of Topors regulates p53 stability. J Biol Chem. 2009;284(28):18588-92.

152. Yang X, Li H, Deng A, Liu X. Plk1 phosphorylation of Topors is involved in its degradation. Mol Biol Rep. 2010;37(6):3023-8.

153. Liu XS, Li H, Song B, Liu X. Polo-like kinase 1 phosphorylation of G2 and S-phase-expressed 1 protein is essential for p53 inactivation during G2 checkpoint recovery. EMBO Rep. 2010;11(8):626-32.

154. Shao C, Chien SJ, Farah E, Li Z, Ahmad N, Liu X. Plk1 phosphorylation of Numb leads to impaired DNA damage response. Oncogene. 2018;37(6):810-20.

155. Ma X, Wang L, Huang, Li Y, Yang D, Li T, et al. Polo-like kinase 1 coordinates biosynthesis during cell cycle progression by directly activating pentose phosphate pathway. Nat Commun. 2017;8(1):1506.

156. Li Z, Kong Y, Song L, Luo Q, Liu J, Shao C, et al. Plk1-Mediated Phosphorylation of TSC1 Enhances the Efficacy of Rapamycin. Cancer Res. 2018;78(11):2864-75.

157. Li X, Nai S, Ding Y, Geng Q, Zhu B, Yu K, et al. Polo-like kinase 1 (PLK1)-dependent phosphorylation of methylenetetrahydrofolate reductase (MTHFR) regulates replication via histone methylation. Cell Cycle. 2017;16(20):1933-42.

158. Bengoechea-Alonso MT, Ericsson J. The phosphorylation-dependent regulation of nuclear SREBP1 during mitosis links lipid metabolism and cell growth. Cell Cycle. 2016;15(20):2753-65.

159. Xiao D, Yue M, Su H, Ren P, Jiang J, Li F, et al. Polo-like Kinase-1 Regulates Myc Stabilization and Activates a Feedforward Circuit Promoting Tumor Cell Survival. Mol Cell. 2016;64(3):493-506.

160. Wu J, Ivanov AI, Fisher PB, Fu Z. Polo-like kinase 1 induces epithelial-to-mesenchymal transition and promotes epithelial cell motility by activating CRAF/ERK signaling. eLife. 2016;5.

161. Li Z, Li J, Bi P, Lu Y, Burcham G, Elzey BD, et al. Plk1 phosphorylation of PTEN causes a tumor-promoting metabolic state. Molecular and cellular biology. 2014;34(19):3642-61.

162. Strebhardt K. Multifaceted polo-like kinases: drug targets and antitargets for cancer therapy. Nat Rev Drug Discov. 2010;9(8):643-60.

163. Colicino EG, Hehnly H. Regulating a key mitotic regulator, polo-like kinase 1 (PLK1). Cytoskeleton (Hoboken). 2018;75(11):481-94.

164. Dai D, Holmes AM, Nguyen T, Davies S, Theele DP, Verschraegen C, et al. A potential synergistic anticancer effect of paclitaxel and amifostine on endometrial cancer. Cancer Res. 2005;65(20):9517-24.

165. Chou TC. Drug combination studies and their synergy quantification using the Chou-Talalay method. Cancer Res. 2010;70(2):440-6.

166. Justus CR, Leffler N, Ruiz-Echevarria M, Yang LV. In vitro cell migration and invasion assays. J Vis Exp. 2014(88).

167. Wu ZQ, Yang X, Weber G, Liu X. Plk1 phosphorylation of TRF1 is essential for its binding to telomeres. J Biol Chem. 2008;283(37):25503-13.

168. Corey E, Quinn JE, Buhler KR, Nelson PS, Macoska JA, True LD, et al. LuCaP 35: a new model of prostate cancer progression to androgen independence. The Prostate. 2003;55(4):239-46.

169. Torre LA, Bray F, Siegel RL, Ferlay J, Lortet-Tieulent J, Jemal A. Global cancer statistics, 2012. CA: a cancer journal for clinicians. 2015;65(2):87-108.

170. Siegel RL, Miller KD, Jemal A. Cancer statistics, 2020. CA: a cancer journal for clinicians. 2020;70(1):7-30.

171. Harris WP, Mostaghel EA, Nelson PS, Montgomery B. Androgen deprivation therapy: progress in understanding mechanisms of resistance and optimizing androgen depletion. Nature clinical practice Urology. 2009;6(2):76-85.

172. Chandrasekar T, Yang JC, Gao AC, Evans CP. Mechanisms of resistance in castration-resistant prostate cancer (CRPC). Translational andrology and urology. 2015;4(3):365-80.

173. Combes G, Alharbi I, Braga LG, Elowe S. Playing polo during mitosis: PLK1 takes the lead. Oncogene. 2017;36(34):4819-27.

174. Cholewa BD, Liu XQ, Ahmad N. The Role of Polo-like Kinase 1 in Carcinogenesis: Cause or Consequence? Cancer Research. 2013;73(23):6848-55.

175. Li J, Karki A, Hodges KB, Ahmad N, Zoubeidi A, Strebhardt K, et al. Cotargeting Polo-Like Kinase 1 and the Wnt/beta-Catenin Signaling Pathway in Castration-Resistant Prostate Cancer. Molecular and cellular biology. 2015;35(24):4185-98.

176. Erskine S, Madden L, Hassler D, Smith G, Copeland R, Gontarek R. Biochemical characterization of GSK461364: A novel, potent, and selective inhibitor of Polo-like kinase-1 (Plk1). Cancer Research. 2007;67(9 Supplement):3257-.

177. Gilmartin AG, Bleam MR, Richter MC, Erskine SG, Kruger RG, Madden L, et al. Distinct concentration-dependent effects of the polo-like kinase 1-specific inhibitor GSK461364A, including differential effect on apoptosis. Cancer Res. 2009;69(17):6969-77.

178. Sutton D, Diamond M, Faucette L, Giardiniere M, Zhang S, Gilmartin A, et al. Efficacy of GSK461364, a selective Plk1 inhibitor, in human tumor xenograft models. Cancer Research. 2007;67(9 Supplement):5388-.

179. Laquerre S, Sung C-M, Gilmartin A, Courtney M, Ho M, Salovich J, et al. A potent and selective Polo-like kinase 1 (Plk1) Inhibitor (GSK461364) induces cell cycle arrest and growth inhibition of cancer cell. Cancer Research. 2007;67(9 Supplement):5389-.

180. Olmos D, Barker D, Sharma R, Brunetto AT, Yap TA, Taegtmeyer AB, et al. Phase I study of GSK461364, a specific and competitive Polo-like kinase 1 inhibitor, in patients with advanced solid malignancies. Clin Cancer Res. 2011;17(10):3420-30.

181. Devaiah BN, Gegonne A, Singer DS. Bromodomain 4: a cellular Swiss army knife. Journal of leukocyte biology. 2016;100(4):679-86.

182. Adelman K, Lis JT. Promoter-proximal pausing of RNA polymerase II: emerging roles in metazoans. Nature reviews Genetics. 2012;13(10):720-31.

183. Asangani IA, Dommeti VL, Wang X, Malik R, Cieslik M, Yang R, et al. Therapeutic targeting of BET bromodomain proteins in castration-resistant prostate cancer. Nature. 2014;510(7504):278-82.

184. Ferri E, Petosa C, McKenna CE. Bromodomains: Structure, function and pharmacology of inhibition. Biochem Pharmacol. 2016;106:1-18.

185. Filippakopoulos P, Qi J, Picaud S, Shen Y, Smith WB, Fedorov O, et al. Selective inhibition of BET bromodomains. Nature. 2010;468(7327):1067-73.

186. Momota H, Shih AH, Edgar MA, Holland EC. c-Myc and beta-catenin cooperate with loss of p53 to generate multiple members of the primitive neuroectodermal tumor family in mice. Oncogene. 2008;27(32):4392-401.

187. Wang G, Wang J, Sadar MD. Crosstalk between the Androgen Receptor and beta-Catenin in Castrate-Resistant Prostate Cancer. Cancer Research. 2008;68(23):9918-27.

188. Zhang Z, Chen L, Wang H, Ahmad N, Liu X. Inhibition of Plk1 represses androgen signaling pathway in castration-resistant prostate cancer. Cell Cycle. 2015;14(13):2142-8.

189. Zhang Z, Hou X, Shao C, Li J, Cheng JX, Kuang S, et al. Plk1 inhibition enhances the efficacy of androgen signaling blockade in castration-resistant prostate cancer. Cancer Res. 2014;74(22):6635-47.

190. Hogg SJ, Vervoort SJ, Deswal S, Ott CJ, Li J, Cluse LA, et al. BET-Bromodomain Inhibitors Engage the Host Immune System and Regulate Expression of the Immune Checkpoint Ligand PD-L1. Cell Rep. 2017;18(9):2162-74.

191. Ciceri P, Muller S, O'Mahony A, Fedorov O, Filippakopoulos P, Hunt JP, et al. Dual kinase-bromodomain inhibitors for rationally designed polypharmacology. Nature chemical biology. 2014;10(4):305-12.

192. Bisgrove DA, Mahmoudi T, Henklein P, Verdin E. Conserved P-TEFb-interacting domain of BRD4 inhibits HIV transcription. Proc Natl Acad Sci U S A. 2007;104(34):13690-5.

193. Donati B, Lorenzini E, Ciarrocchi A. BRD4 and Cancer: going beyond transcriptional regulation. Mol Cancer. 2018;17(1):164.

194. Dey A, Nishiyama A, Karpova T, McNally J, Ozato K. Brd4 marks select genes on mitotic chromatin and directs postmitotic transcription. Mol Biol Cell. 2009;20(23):4899-909.

195. Rathert P, Roth M, Neumann T, Muerdter F, Roe JS, Muhar M, et al. Transcriptional plasticity promotes primary and acquired resistance to BET inhibition. Nature. 2015;525(7570):543-7.

196. Song B, Liu XS, Rice SJ, Kuang S, Elzey BD, Konieczny SF, et al. Plk1 phosphorylation of orc2 and hbo1 contributes to gemcitabine resistance in pancreatic cancer. Mol Cancer Ther. 2013;12(1):58-68.

197. Hou X, Li Z, Huang W, Li J, Staiger C, Kuang S, et al. Plk1-dependent microtubule dynamics promotes androgen receptor signaling in prostate cancer. The Prostate. 2013;73(12):1352-63.

198. Shao C, Ahmad N, Hodges K, Kuang S, Ratliff T, Liu X. Inhibition of polo-like kinase 1 (Plk1) enhances the antineoplastic activity of metformin in prostate cancer. J Biol Chem. 2015;290(4):2024-33.

199. Domingues B, Lopes JM, Soares P, Populo H. Melanoma treatment in review. Immunotargets Ther. 2018;7:35-49.

200. Ferlay J, Soerjomataram I, Dikshit R, Eser S, Mathers C, Rebelo M, et al. Cancer incidence and mortality worldwide: sources, methods and major patterns in GLOBOCAN 2012. Int J Cancer. 2015;136(5):E359-86.

201. Bombelli FB, Webster CA, Moncrieff M, Sherwood V. The scope of nanoparticle therapies for future metastatic melanoma treatment. Lancet Oncol. 2014;15(1):e22-32.

202. Howlader N NA, Krapcho M, Miller D, Brest A, Yu M, Ruhl J, Tatalovich Z, Mariotto A, Lewis DR, Chen HS, Feuer EJ, Cronin KA. SEER Cancer Statistics Review, 1975-2016, National Cancer Institute. 2019.

203. Gray-Schopfer V, Wellbrock C, Marais R. Melanoma biology and new targeted therapy. Nature. 2007;445(7130):851-7.

204. Hodis E, Watson IR, Kryukov GV, Arold ST, Imielinski M, Theurillat JP, et al. A landscape of driver mutations in melanoma. Cell. 2012;150(2):251-63.

205. Cancer Genome Atlas N. Genomic Classification of Cutaneous Melanoma. Cell. 2015;161(7):1681-96.

206. Fiskus W, Mitsiades N. B-Raf Inhibition in the Clinic: Present and Future. Annu Rev Med. 2016;67:29-43.

207. Dankner M, Rose AAN, Rajkumar S, Siegel PM, Watson IR. Classifying BRAF alterations in cancer: new rational therapeutic strategies for actionable mutations. Oncogene. 2018;37(24):3183-99.

208. Chong H, Lee J, Guan KL. Positive and negative regulation of Raf kinase activity and function by phosphorylation. EMBO J. 2001;20(14):3716-27.

209. Song B, Liu XS, Davis K, Liu X. Plk1 phosphorylation of Orc2 promotes DNA replication under conditions of stress. Molecular and cellular biology. 2011;31(23):4844-56.

210. Chapman PB, Hauschild A, Robert C, Haanen JB, Ascierto P, Larkin J, et al. Improved survival with vemurafenib in melanoma with BRAF V600E mutation. N Engl J Med. 2011;364(26):2507-16.

211. Sun C, Wang L, Huang S, Heynen GJ, Prahallad A, Robert C, et al. Reversible and adaptive resistance to BRAF(V600E) inhibition in melanoma. Nature. 2014;508(7494):118-22.

212. Barr FA, Sillje HH, Nigg EA. Polo-like kinases and the orchestration of cell division. Nat Rev Mol Cell Biol. 2004;5(6):429-40.

213. Anaya J. OncoLnc: linking TCGA survival data to mRNAs, miRNAs, and lncRNAs. PeerJ computer science. 2016.

214. Gutteridge RE, Ndiaye MA, Liu X, Ahmad N. Plk1 Inhibitors in Cancer Therapy: From Laboratory to Clinics. Mol Cancer Ther. 2016;15(7):1427-35.

215. Rivankar S. An overview of doxorubicin formulations in cancer therapy. J Cancer Res Ther. 2014;10(4):853-8.

216. Rudolph D, Steegmaier M, Hoffmann M, Grauert M, Baum A, Quant J, et al. BI 6727, a Polo-like kinase inhibitor with improved pharmacokinetic profile and broad antitumor activity. Clin Cancer Res. 2009;15(9):3094-102.

217. Brassesco MS, Pezuk JA, Morales AG, de Oliveira JC, Roberto GM, da Silva GN, et al. In vitro targeting of Polo-like kinase 1 in bladder carcinoma: comparative effects of four potent inhibitors. Cancer Biol Ther. 2013;14(7):648-57.

218. Rudolph D, Impagnatiello MA, Blaukopf C, Sommer C, Gerlich DW, Roth M, et al. Efficacy and mechanism of action of volasertib, a potent and selective inhibitor of Polo-like kinases, in preclinical models of acute myeloid leukemia. J Pharmacol Exp Ther. 2015;352(3):579-89.

219. Dankort D, Curley DP, Cartlidge RA, Nelson B, Karnezis AN, Damsky WE, Jr., et al. Braf(V600E) cooperates with Pten loss to induce metastatic melanoma. Nat Genet. 2009;41(5):544-52.

220. Damsky WE, Curley DP, Santhanakrishnan M, Rosenbaum LE, Platt JT, Gould Rothberg BE, et al. beta-catenin signaling controls metastasis in Braf-activated Pten-deficient melanomas. Cancer Cell. 2011;20(6):741-54.

221. Li Z, Liu J, Li J, Kong Y, Sandusky G, Rao X, et al. Polo-like kinase 1 (Plk1) overexpression enhances ionizing radiation-induced cancer formation in mice. The Journal of biological chemistry. 2017;292(42):17461-72.

222. Fu Z, Wen D. The Emerging Role of Polo-Like Kinase 1 in Epithelial-Mesenchymal Transition and Tumor Metastasis. Cancers (Basel). 2017;9(10).

223. Shin SB, Jang HR, Xu R, Won JY, Yim H. Active PLK1-driven metastasis is amplified by TGF-beta signaling that forms a positive feedback loop in non-small cell lung cancer. Oncogene. 2020;39(4):767-85.

224. Tudrej KB, Czepielewska E, Kozlowska-Wojciechowska M. SOX10-MITF pathway activity in melanoma cells. Arch Med Sci. 2017;13(6):1493-503.

225. Edmondson R, Broglie JJ, Adcock AF, Yang L. Three-dimensional cell culture systems and their applications in drug discovery and cell-based biosensors. Assay Drug Dev Technol. 2014;12(4):207-18.

226. Kenny PA, Lee GY, Myers CA, Neve RM, Semeiks JR, Spellman PT, et al. The morphologies of breast cancer cell lines in three-dimensional assays correlate with their profiles of gene expression. Molecular oncology. 2007;1(1):84-96.

227. Lee CK, Jeong SH, Jang C, Bae H, Kim YH, Park I, et al. Tumor metastasis to lymph nodes requires YAP-dependent metabolic adaptation. Science. 2019;363(6427):644-9.

228. Piskounova E, Agathocleous M, Murphy MM, Hu Z, Huddlestun SE, Zhao Z, et al. Oxidative stress inhibits distant metastasis by human melanoma cells. Nature. 2015;527(7577):186-91.

Academic Record

B.A.	Sep. 2011 to Jul. 2015	College of Animal Sciences, Zhejiang University, China Program: Animal Sciences; GPA: 3.57/4.00; Academic Ranking: Top 4 out of 45
R.A.	Sep. 2015 to Jul. 2016	The Institute of Medicinal Plant Development, Chinese Academy of Medical Sciences and Peking Union Medical College, China
Graduate	Aug. 2016 to now	Department of Animal Sciences, Purdue University, USA Program: Ph.D. of Animal Sciences; Major Professor: Dr. Xiaoqi Liu and Dr. Shihuan Kuang GPA: 3.63/4.00

Publications

1) **Mao, F.***, Li, J.*, Luo, Q., Wang, R., Kong, Y., Carlock, C., Liu, Z., Elzey, B. D., & Liu, X. (2018). Plk1 Inhibition Enhances the Efficacy of BET Epigenetic Reader Blockade in Castration-Resistant Prostate Cancer. Molecular cancer therapeutics, 17(7), 1554–1565. https://doi.org/10.1158/1535-7163.MCT-17-0945 (* co-first author)

2) Kong, Y., Cheng, L., **Mao, F.**, Zhang, Z., Zhang, Y., Farah, E., Bosler, J., Bai, Y., Ahmad, N., Kuang, S., Li, L., & Liu, X. (2018). Inhibition of cholesterol biosynthesis overcomes enzalutamide resistance in castration-resistant prostate cancer (CRPC). The Journal of biological chemistry, 293(37), 14328–14341. https://doi.org/10.1074/jbc.RA118.004442

3) Xiong, Y., Wu, Z., Zhang, B., Wang, C., **Mao, F**., Liu, X., Hu, K., Sun, X., Jin, W. and Kuang, S. (2019), Fndc5 loss-of-function attenuates exercise-induced browning of white adipose tissue in mice. The FASEB Journal, 33: 5876-5886. DOI:10.1096/fj.201801754RR

4) Li, C., Lanman, N. A., Kong, Y., He, D., **Mao, F.**, Farah, E., Zhang, Y., Liu, J., Wang, C., Wei, Q., & Liu, X. (2020). Inhibition of the erythropoietin-producing receptor EPHB4 antagonizes androgen receptor overexpression and reduces enzalutamide resistance. The Journal of biological chemistry, 295(16), 5470–5483. https://doi.org/10.1074/jbc.RA119.011385

Honors and Awards

Common Award of Professional Scholarship	2012
The Excellent Communist Youth League Member of Yunfeng Academy	2013
Second-Class Scholarship for Outstanding Merits	2013
Second-Class Scholarship for Outstanding Students	2013
Yiduoli Award	2013
Excellent Award of Professional Scholarship	2013
The Excellent Communist Youth League Member of ZJU	2014
Youth Volunteer Service Award honors a Star of ZJU	2014
Excellent Award of Professional Scholarship	2014
Second-Class Scholarship for Outstanding Merits	2014
Second-Class Scholarship for Outstanding Students	2014
Outstanding Undergraduate Thesis (Design) of ZJU	2015
Henry Moses Award	2018

Teaching experiences

T.A.	BCHM561	Fall 2017
T.A.	BCHM307	Spring 2018